Adeno-associated viral vectors for gene delivery to the non-human primate brain

Thesis by

Miguel Roberto Estella Chuapoco

In Partial Fulfillment of the Requirements

for the Degree of

Doctor of Philosophy

CALIFORNIA INSTITUTE OF TECHNOLOGY

Pasadena, California

2023

(Defended May 5, 2023)

Miguel Roberto Estella Chuapoco
ORCID: 0000-0001-5397-996X

ACKNOWLEDGEMENTS

To paraphrase an old proverb, “It takes a village to train a graduate student.” A PhD may be one of the most unique experiences to choose to do in your 20s and 30s. It requires ingenuity. It requires dedication. It requires resolve. It requires discipline. It requires resourcefulness. I could go on. But by far, it—most importantly—requires the support and contributions from the infinite number of friends, alumni, mentors, collaborators, and peers to help a young scientist realize their goals and grow into a slightly-older-and-more-independent scientist ready to face the uncertainties of life—whether it be scientifically, professionally, or personally.

First and foremost, I’d like to thank Dr. Viviana Gradinaru, my awesome advisor who’s always fostered a prosperous research environment for me to realize my true potential as a scientist and as an individual. My PhD truly felt like an intellectual playground, in large part due to Viviana’s philosophy and positive reinforcement. She always pushed me to the best version of myself (both at the bench and as a human being), never let me accept anything less of my hardest effort, and never placed me in a box to bound my abilities and growth. Viviana was truly a force when it came to her drive and ability to push on in the face of adversity, failure, and even tragedy, and I will always look to her work ethic and positive attitude for inspiration. And yet, this drive and dedication to growth is also supplemented with a healthy dose of realism. From “What’s the worst that can happen?” to “Be sure to make time for the things and people that are important” Viviana will always be a model on how to balance excellence and empathy as a scientist and leader.

Now, it goes without saying that my PhD experience would not have been whole without The Nicks. Anyone who knows Dr. Nick Goeden and Dr. Nick Flytzanis knows that they make science fun and invigorating. Not only was every day a new surprise with their ingenuity and groundbreaking results, but every day working with them was filled with a new story or core memory filled with laughs and unique humor. They were the ones who inspired and taught me how to do capsid engineering and showed me how to embrace and enjoy the sometimes-long and chaotic days that come with doing science—no matter how ridiculous the situation or how unfortunate the mistake. It’s entirely possible that my willingness to witness and be a part of (maybe even cause?) this scientific chaos was the sole reason they gave me the opportunity to become a Scientist when they started Capsida Biotherapeutics. Those eight months were a turning point in my PhD for many reasons, the largest being that when I returned to graduate school, I had a new project that is the main focus of this dissertation.

The only constant in life is change, and there is no better example of change than the turnover in lab members throughout the course of a single PhD. Throughout the course of G-Lab, there have been—and will continue to be—different “generations of G-Lab members,” with each generation having a unique set of shared experiences (much like the

set of shared experiences that connect the Millennial generation or the Baby Boomer generation). From my frame of reference as a member of G-Lab, each generation has had a unique impact on how I've grown as a scientist. In my earliest days in the lab, I learned from the "lab elders" Dr. Collin Challis, Dr. Rose Challis, Dr. Jenny Treweek, Dr. Ryan Cho, Dr. Alon Greenbaum, Dr. Claire Bedbrook, Dr. Elliot Robinson, Dr. Michael Altermatt, Dr. Ken Chan, and Dr. Ben Deverman. I was a young impressionable graduate student, and these bright scientists were the exemplars on how to carry myself and be successful in G-Lab. During my "coming of age" in the lab, I grew up working closely with Dr. Priya Kumar, Dr. David Brown, Dr. Tatyana Dobreva, Dr. Xinhong Chen, Dr. Xiaozhe Ding, Dr. David Goertsen, Acacia Mayfield, Dr. Máté Borsos, Dr. Tim Shay, Dr. Anat Kahan, Dr. Min Jang, and Gerry Coughlin. The bulk of my PhD overlapped with these individuals, and I was very fortunate to work with such a passionate group that was never afraid of rigorous or challenging science. Throughout my PhD, each of these awesome colleagues had some amount of influence on my work. Now, the newest generation of G-Lab scientists (Dr. Changfan Lin, Dr. Seongmin Jang, Dr. Cynthia Arokiaraj, Dr. Sayan Dutta, Dr. Jonathan Hoang, Dr. Yujie Fan, Alex Chung, Cameron Jackson, Karan Mahe, and Tyler Brittain) have brought a renewed invigoration and passion for science to the lab. Thank you for breathing new life into the lab, and for your keen interest and rigorous approach to science. Last but certainly not least, I will always be eternally grateful to the amazing support staff from G-Lab and CLOVER over the years: Zhe Qu, YP Lei, Elisha Mackey, Pat Anguiano, Erin Sullivan, Damien Wolfe, and Nathan Appling. Thank you for all your hard work in keeping the lab running! You all at one point or another had a hand in helping my PhD.

Most, if not all, of the experiments that make up the bulk of this dissertation were truly a Herculean, collaborative effort between multiple labs spanning several years—and even predating my time as a graduate student. So in addition to all the contributions from fellow lab members on these projects, there are SO many parts of this work that simply would not have happened without our great external collaborators. Prof. Andrew S. Fox at UC Davis, his trainees Lillian Campos and Dr. Carly Drzewicki, and the entire veterinary staff at the California National Primate Research Center enabled so many of the awesome work that we were able to do. Drew has gone above and beyond on more than one occasion to make these macaque experiments a reality. Prof. Lin Tian and her team also deserve recognition for their scientific advice and their commitment to making the recording experiments a reality. Drew and Lin were involved in the CAP-Mac project from the very beginning, and it's incredible to look back at the progress we've made over the course of 3+ years.

While the majority of my training took place at Caltech, I would not be doing research if not for the wonderful friends and colleagues from my previous labs at Stanford University. Prof. Kalanit Grill-Spector, Prof. Kevin S. Weiner, Dr. Nathan Witthoft: thank you for giving me the first opportunity to become a scientist and giving me the confidence that I could succeed as a scientist. To the many Lee Lab members (Dr. ManKin Choy, Dr.

Ben Duffy, Dr. Andrew Weitz, and Dr. Hyun Joo Lee to name a few) who were a huge support system for me as I slowly became an independent scientist: thank you for giving me my first real world experience of learning what it meant to be in academia, and how to succeed as a trainee.

Outside the lab, I was fortunate to have many groups that served as my support system. From my middle school and high school friends who have known me the longest and are like brothers to me; to those in San Francisco in my early days that also taught me how to thrive in the chaos of life; to the Stanford in LA crew who were my home away from home as we started a new chapter in LA together; to all the friends from LA that I've made and grown close to while living here: I am eternally grateful for how much you have given me life and made me feel alive with all the stories, adventures, and crazy moments. And of course, to my father, Renato Chuapoco, my mother, Sylvia Chuapoco, my brother, CJ Chuapoco, my cousins (who have acted as my de facto siblings from a young age), and my aunts and uncles who have truly been the proverbial "village" that have raised this child: Thank you for you unwavering support!!!

I'll close this section with a message to any young trainee who is still reading this. Over the past couple of weeks, I've begun taking daily walks to reflect on my time as a graduate student, and during these walks, I've been telling myself to look up more—both figuratively and literally. Look up at the sky. Look up at the tree line. Look up at where the top of buildings meet the sky. A PhD is your time to challenge yourself. A period of 5-7 years (or more) for you to realize what is it you want from your life and scientific career. And as you're looking up, think about how much you want to grow. You may feel moments of inadequacy, you may feel lost, and you may even feel scared. But just remember that those feelings are normal—and it's okay to feel them, especially if you're scared of heights. Because by the end of my PhD, I've realized the sky truly is the limit when it comes to my growth, and I hope you too embrace that adventure on your way to fulfilling your dreams!

ABSTRACT

Viral vectors are efficient gene-delivery carriers for somatic cell gene therapy, and replication-deficient vectors are actively being used in the clinic to replace and correct disease-causing genes and mutations. Mirroring their therapeutic effectiveness, viral vectors are also powerful *in vivo* gene-delivery tools in basic research. In the field of neuroscience, adeno-associated viruses (AAVs) in particular have emerged as a major workhorse that enable efficient *in vivo* expression of opsins for optogenetics, designer GPCRs for chemogenetics, and GCaMP for calcium imaging. Recently, AAV engineering efforts by our group and others have expanded the toolbox of AAV vectors to include capsid variants that traverse the blood-brain-barrier (BBB) in rodents. However, not all engineered AAV capsids translate from mice to non-human primates (NHPs). This is especially true for translation to the rhesus macaque (*Macaca mulatta*), an Old World primate that is the predominant NHP model and shares a more recent common ancestor with humans (~25 million years ago) compared to rodents (~75 million years ago) and New World primates, such as the common marmoset (*Callithrix jacchus*; ~35 million years ago). The primary contents of this dissertation will focus on the development of AAV.CAP-Mac as a vector for non-invasive gene-transfer to the NHP brain and demonstrations of its utility to interrogate neuronal morphology and physiology in the macaque central nervous system. We identified and selected CAP-Mac using a multi-species selection strategy in adult marmosets and infant macaques, where it demonstrated improved delivery efficiency compared to AAV9 and other engineered variants. In individual characterization, CAP-Mac was biased towards neurons in two infant Old World primate species, the rhesus macaque and the green monkey (*Chlorocebus sabaeus*). Given this neuronal tropism in Old World primates, we demonstrated how CAP-Mac can be readily used for non-invasive, Brainbow-like labeling of macaque neurons and calcium imaging of GCaMP *ex vivo*. In closing, we describe CAP-Mac tropism across multiple developmental states, species, and routes of administration. Additionally, we present preliminary data on “orphan capsids,” capsid variants that were engineered to be non-infective, but can be readily re-functionalized using known receptor-ligand pairs. Collectively, the work covered in this dissertation disseminates non-invasive, gene-delivery tools for NHP researchers, and lays the groundwork for further development of more specific and efficacious AAVs that access the NHP brain.

PUBLISHED CONTENT AND CONTRIBUTIONS

[1] **Chuapoco MR***, Flytzanis NC*, Goeden N, Octeau J, Roxas K, Chan K, Scherrer J, Winchester J, Blackburn R, Campos L, Man KN, Sun J, Chen X, Lefevre A, Singh V, Arokiaraj C, Miles T, Vendemiatti J, Jang M, Mich J, Bishaw Y, Gore B, Omstead V, Taskin N, Weed N, Levi BP, Ting J, Miller C, Deverman B, Pickel J, Tian L, Fox A, Gradinaru V. Intravenous functional gene transfer throughout the brain of non-human primates using AAV. Nature Nanotechnology. PMID: 36789432. *Authors contributed equally

M.R.C. helped design and perform all experiments, collected and analyzed data for the rhesus macaque and rodent experiments, prepared all the figures, and wrote the manuscript.

[2] Jang MJ, Coughlin GM, Jackson CR, Chen X, **Chuapoco MR**, Vendemiatti JL, Wang AZ, Gradinaru V. Spatial transcriptomics for profiling the tropism of viral vectors in tissues. Nature Biotechnology. 2023 Jan 26; PMID: 36702899

M.R.C. helped design and perform the rhesus macaque experiments.

[3] Goertsen D*, Flytzanis NC*, Goeden N*, **Chuapoco MR**, Cummins A, Chen Y, Fan Y, Zhang Q, Sharma J, Duan Y, Wang L, Feng G, Chen Y, Ip NY, Pickel J, Gradinaru V. AAV capsid variants with brain-wide transgene expression and decreased liver targeting after intravenous delivery in mouse and marmoset. Nature Neuroscience. 2022 Jan 9;25(1):106–115. PMID: 34887588. *Authors contributed equally

M.R.C. helped perform the common marmoset experiments, analyzed the biodistribution data, and helped write the manuscript.

[4] Campos LJ, Arokiaraj CM, **Chuapoco MR**, Chen X, Goeden N, Gradinaru V, Fox AS. Advances in AAV technology for delivering genetically encoded cargo to the nonhuman primate nervous system. Current Research in Neurobiology. 2023 Apr;4:100086.

M.R.C. performed the rhesus macaque experiments.

[5] Challis RC, Ravindra Kumar S, Chen X, Goertsen D, Coughlin GM, Hori AM, **Chuapoco MR**, Otis TS, Miles TF, Gradinaru V. Adeno-Associated Virus Toolkit to Target Diverse Brain Cells. Annual Review of Neuroscience. 2022 Jul 8;45(1):447–469. PMID: 35440143

M.R.C. performed the rhesus macaque experiments and helped write the review.

TABLE OF CONTENTS

LIST OF FIGURES AND TABLES

Number *Page*

Chapter 1

BACKGROUND AND INTRODUCTION

Campos LJ, Arokiaraj CM, **Chuapoco MR**, Chen X, Goeden N, Gradinaru V, Fox AS. Advances in AAV technology for delivering genetically encoded cargo to the nonhuman primate nervous system. Current Research in Neurobiology. 2023 Apr;4:100086.

1.1 Early uses of viral vectors for *in vivo* gene therapy

In its simplest form, gene therapy uses a gene-delivery carrier—such as a virus—to deliver genetic material encoding a gene-of-interest to human cells for a therapeutic purpose—such as an enzyme in a human patient carrying a deleterious mutation in the gene encoding that enzyme. The earliest human gene therapy trial traces its origins to the late 1950s, when Stanfield Rogers extracted rabbit epithelium from topical warts caused by the Shope papilloma virus. He found that the "papilloma tissue invariably had taken up large amounts of arginine," with "no demonstratable uptake of arginine…in the case of normal or hyperplastic [rabbit] skin"[1]. Based on this initial observation, he had deduced that "the presence of the virus in the cells…enables them to synthesize an enzyme new to them, arginase." Over the course of the next decade, Rogers continued his work on the Shope virus, noting that researchers who had worked directly with the Shope virus had an

observable "lowering of the blood arginine," suggesting that these workers were "carrying 'virus information'" and that the Shope virus acted "as a harmless passenger" in humans[2]. Rogers's work on the Shope papilloma virus had led him to believe that the Shope viral genome encoded an arginase enzyme that could be expressed in mammalian cell *in vivo* and that the virus itself was non-pathogenic. As such, Rogers thought he wielded the first clinical gene therapy for *in vivo* gene transfer. He was finally able to test the therapeutic utility of the Shope virus after H.G. Terheggen identified three children with hyperargininemia, which as the name implies is characterized by elevated serum arginine levels[3]. Rogers and Terheggen administered purified Shope virus to two of the three children. While often cited as the first *in vivo* clinical gene therapy trial, the hyperargininemia trial was criticized as "premature"[4], and the biochemical rationale that Shope viral genome encodes an arginase gene was challenged by the scientific community[5,6]. Finally in 1975, nearly 5 years after the children had been treated and nearly 15 years after Rogers's first observations on the Shope papilloma virus, the trial was declared unsuccessful, as Rogers and Terheggen failed to observe measurable changes in serum arginine levels in the treated children[7].

Despite its failure, the hyperargininemia trial marked a pivotal moment in the history of clinical gene therapy, as the scientific community was forced to legitimize the reality of using viral vectors for genetic intervention in humans—and all the ethical questions and technological challenges associated with it. To grapple with the ethical

questions of genetic modification in human cells, many credit the scientific meeting that took place at the Banbury Center at Cold Springs Harbor in 1982 for defining and conceptualizing the path forward for ethical and efficacious gene therapies[8]. Furthermore, with the introduction of recombinant DNA methods in the early 1970s, many of the technical challenges related to repurposing wildtype viral capsids for therapeutic purposes could now be addressed. By 1990, just 15 years after Rogers and Terheggen had announced their unapproved gene therapy trial a failure, researchers at the NIH were conducting the first FDA approved gene therapy procedure, using retroviruses for *ex vivo* gene transfer to successfully cure a four-year old child with adenosine deaminase-severe combined immunodeficiency (ADA-SCID)[9].

Today, there are thousands of gene therapy clinical trials ongoing around the world, over half of which utilize viral vectors as gene delivery carriers[10]. The recent clinical successes of Zolgensma to treat spinal muscular atrophy[11] and Luxturna for inherited blindness[12] highlight the opportunity for *in vivo* gene therapy to treat debilitating developmental disorders at their genetic source. However, the successes of the gene therapy field did not come without its fair share of setbacks, including multiple high-profile deaths in the clinic over the past two decades, with recent concerns focused on hepatoxicity associated with high-dose AAV[13–15]. Given these concerns, there is intense interest in developing safer and more efficacious viral vectors. Outside of the clinic, viral vectors are powerful research tools for gene delivery and manipulation to further our fundamental

understanding of basic biology, especially for *in vivo* gene transfer to the brain. As such viral vector engineering serves the dual purpose of unlocking newer therapies in the clinic and building better tools that can inform our understanding of complex biological systems, such as the mammalian brain.

1.2 Adeno-associated viral (AAV) vectors for neuroscience research

In parallel with their importance in clinical gene therapy, viral vectors have emerged as a powerful tool in neuroscience for enabling labeling studies to define neural circuitry[16–19]. In particular, adeno-associated viruses (AAVs)—first identified as adenoviral contaminants in the 1960s[20–22]—are known to be relatively nonpathogenic, can transduce dividing and post-mitotic cells, and have low frequencies of viral genome integration relative to other viral platforms. This unique combination of properties have helped to make AAVs a popular vector of choice for basic researchers[23–26] and clinicians[27,28] alike.

AAVs are small, single stranded viruses (~25 nanometers in diameter) part of the Parvovirus family (for comprehensive reviews, see refs. 26 and 29). As the name implies, wild-type AAV requires co-infection with a helper virus, most commonly adenovirus, for viral replication. In the absence of the helper virus co-infection, AAVs enter a lysogenic cycle and the viral genome lies dormant in the cell until co-infection of helper virus catalyzes viral replication, and subsequent transition to the lytic cycle. AAV's innate

replication deficiency are a feature for *in vivo* use, as the lack of a lytic phase in the AAV life cycle contributes to the lack of AAV pathogenicity.

AAV entry is mediated by cell-surface glycoproteins and proteoglycans, and many of these "attachment factors" for the natural AAV serotypes have been identified[30]. In addition to the glycan attachment factors, AAVs are also thought to leverage various co-receptors to mediate cell entry and infection, with the membrane-associated AAV receptor (AAVR) piquing the most interest from the field, as it has been known to be necessary for AAV infection of a majority of the natural AAV serotypes[31,32]. Once cell entry has been completed, AAVs are thought to escape into the cytosol using a catalytic phospholipase motif that becomes unmasked in the low pH environment of the endosome, allowing the packaged transgene to translocate to the nucleus to be expressed using the host cell machinery.

The abundance of structural data of the AAV capsid has enabled much of our understanding of the AAV infectious pathway and has also unraveled avenues of potential biochemical intervention to engineer variant tropism[33–35]. There are 9 variable regions (VRs) on the AAV capsid which are surface exposed loops that show the greatest variation amongst the natural AAV serotypes. These surface exposed loops have been thought to help determine serotype tropism, especially the most surface exposed loops that exist on

the three-fold protrusions of the capsid surface. Multiple groups have shown that mutating the residues on surface exposed variable regions can be used to alter AAV tropism[26,35–37].

In totality, AAVs have been shown to be safe when used *in vivo*, while remaining efficient gene-delivery carriers and tolerant to changes on the capsid surface. These unique features have made AAVs a useful tool for neuroscientists, and AAVs now regularly enable *in vivo* delivery of molecular actuators to stimulate neural activity (e.g., optogenetics and chemogenetics) and sensors to record of neural activity (e.g., calcium sensing) in various animal models and experimental contexts. Given the diverse applications of AAVs to study the brain, capsid engineering efforts have focused on trying to improve on tropisms of current AAVs. Importantly, AAV9 has been shown to weakly cross the blood-brain-barrier, and there has been renewed interest in developing and understanding the biochemical underpinnings of AAV9's neurotropic properties[26,38]. As such, there is intense shared interest across both academia and industry to engineer novel AAVs, especially as it pertains to enabling new research avenues and unlocking new opportunities for therapeutic intervention, such as accessing the brain from the bloodstream.

1.3 Engineering novel, designer AAV capsids for the brain

Over the past decade, the convergence of knowledge from AAV structural data with advances in next-generation sequencing (NGS) and protein engineering technologies has catalyzed a renaissance in developing new AAV variants for *in vivo* gene transfer to the

brain. Our lab has developed a method for efficient *in vivo* selections in Cre-transgenic mouse lines, which utilizes a Cre-dependent molecular switch to confer additional selective pressure during AAV engineering[39,40]. This Cre-recombination-based AAV targeted evolution (CREATE) method has led to the development of the neurotropic capsids such as AAV-PHP.B, AAV-PHP.eB, and AAV-PHP.S. More recently, Kumar et al. improved on the CREATE method, employing NGS to multiplex selection in several different Cre-lines for simultaneous positive and negative selections[41]. This multiplex-CREATE (M-CREATE) method, has led to numerous cell-type specific variants, including AAV.CAP-B10/22[42] (neuron specific and liver detargeted) and AAV-X1 (endothelial specific)[43].

The overwhelming majority of previous engineering efforts for the brain have focused exclusively on engineering variable region VIII (VR-VIII) of the AAV9 capsid. While VR-VIII engineering has been productive at producing new variants, there has been some interest in engineering other locations of the AAV capsid. More recently, we have explored engineering at both VR-I and VR-IV of the AAV9 capsid. VR-I is uniquely positioned near the glycan binding site of AAV9[44] and has also been implicated in AAVR binding[45,46], making it a potential area of further evolution. The details of the extent of VR-I engineering completed in our lab to date are the subject of section 4.2. Engineering at VR-IV produced the variants AAV.CAP-B10 and AAV.CAP-B22, which were selected in mice but show conserved trans-blood-brain-barrier tropism in the common marmoset, a popular non-human primate (NHP) model in the neuroscience community[42]. Inspired by

the efficacy of these variants in the marmoset, AAV capsid engineering efforts have now turned their focus towards evolving capsids that are directly selected for and efficacious in NHPs.

1.4 Current state of AAV gene delivery to the non-human primate brain

Despite PHP.B's impact on enabling rodent research, its inability to cross the blood-brain-barrier in NHPs is well-documented[47,48]. PHP.B and many of the variants discovered up until this point were primarily selected and characterized in rodents. While mice last shared a common ancestor with humans approximately 80-90 million years ago (mya), marmosets and macaques are believed to have shared their last ancestors with humans 35-40 mya and 25-30 mya, respectively (Fig. 1.1)[24,49]. As such, it is not surprising that engineering efforts in rodents have failed to translate to higher species. Additionally, that NHPs have a more recent common ancestor with humans compared to rodents highlights their value as animal model for neuroscientists. While marmosets, a New World primate, still offer an advantage over rodents as an animal model, Old World primates, like the rhesus macaque, remain the predominant NHP model of choice. Compared to the New World primates, Old World monkeys are more similar to humans developmentally, have more similar brain sizes and structural organization as humans, and have a larger immune cell repertoire compared to marmosets[50–52]. Given the lack of AAV capsids that translate from rodents to Old World primates, and the importance of Old World primates to

deepening our understanding of human brain function, there is a need for better tools that can access the macaque brain.

In lieu of a vector that efficiently crosses the blood-brain-barrier in Old World primates, direct intraparenchymal injections can be used to circumvent the blood-brain-barrier. However, due to poor spatial distribution, they must typically administer AAV in multiple locations, invasively penetrating the brain parenchyma each time,[53–60] with each surgery requiring resource-intensive pre-planning and real-time monitoring of infusions[57–66]. More recently, several groups have utilized intrathecal routes of administration via lumbar puncture[67] or intra-cisterna magna (ICM)[68] injection to overcome the poor spatial distribution of direct injections. However, these intrathecal routes of administration have limited efficacy in the brain[68–72], with reports of adverse transduction in peripheral tissue, especially in the dorsal root ganglia[72–75].

In response to the lack of tools available to NHP researchers to date, this dissertation outlines some of the tools that are just becoming available for researchers to use study the NHP brain. It is my hope that the vectors and experiments outlined here will be the first of many that enable a new age of understanding brain function, and a second renaissance of AAV capsid development that extends the limits of the current AAV toolbox outside of rodent-specific vectors, to include capsids that are enable deeper study of the non-human primate brain.

Figure 1.1: Evolutionary tree depicting the phylogenetic relationship of common research species.

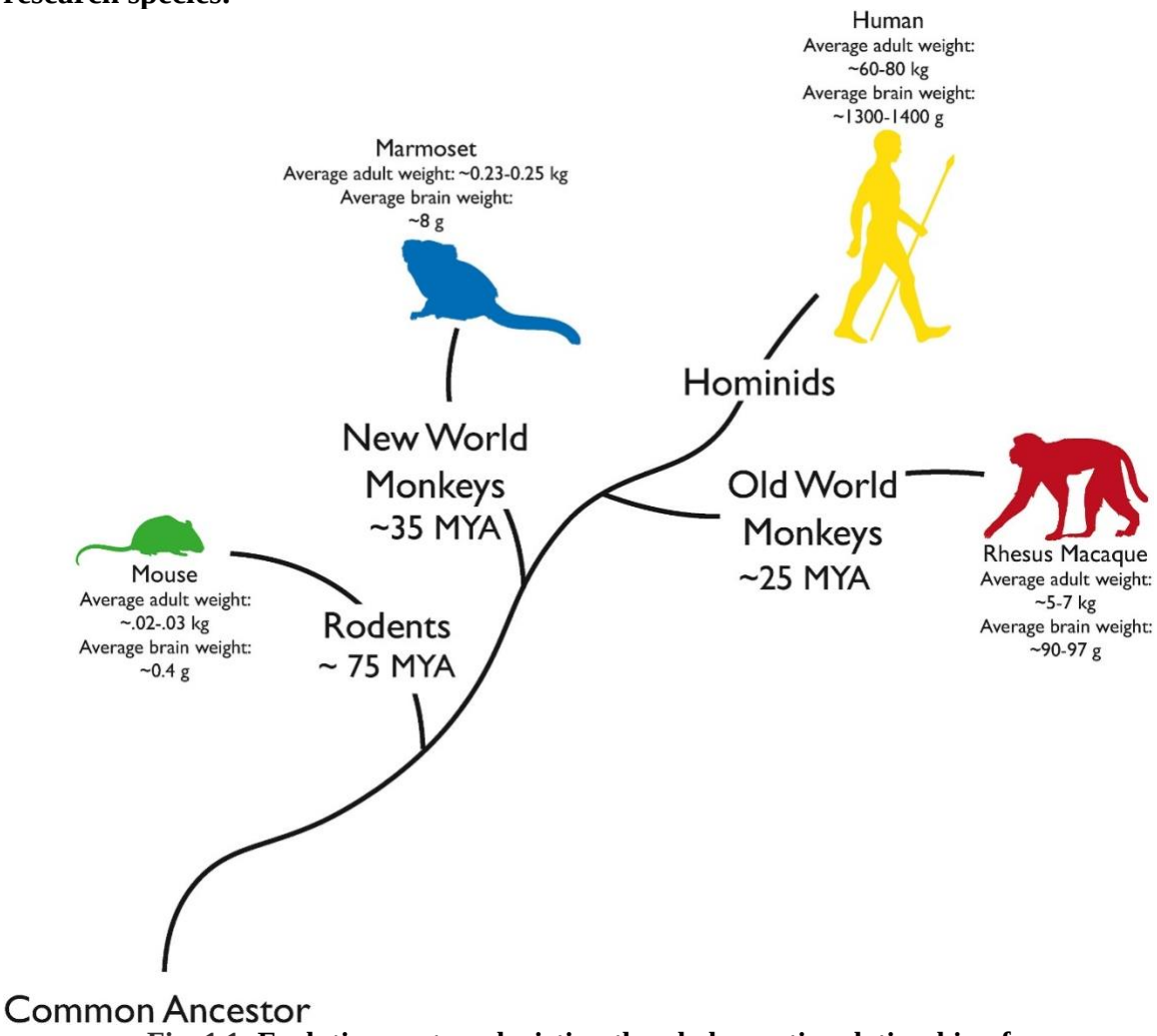

Fig. 1.1: Evolutionary tree depicting the phylogenetic relationship of common research species. Among these species, Old World Monkeys, like the rhesus macaque, are approximately more similar to humans than New World Monkeys and rodents. Figure from ref. [24].

Chapter 2

SELECTING BRAIN-PENETRATING CAPSIDS IN MULTIPLE NON-HUMAN PRIMATE SPECIES

Chuapoco MR*, Flytzanis NC*, Goeden N, Octeau J, Roxas K, Chan K, Scherrer J, Winchester J, Blackburn R, Campos L, Man KN, Sun J, Chen X, Lefevre A, Singh V, Arokiaraj C, Miles T, Vendemiatti J, Jang M, Mich J, Bishaw Y, Gore B, Omstead V, Taskin N, Weed N, Levi BP, Ting J, Miller C, Deverman B, Pickel J, Tian L, Fox A, Gradinaru V. Intravenous functional gene transfer throughout the brain of non-human primates using AAV. Nature Nanotechnology. PMID: 36789432. *Authors contributed equally

2.1 Summary

AAVs have failed to translate from mice to primates in part due to the lack of capsid discovery efforts that use primates, as many capsid library selections have been conducted in mice up until this point. To address this challenge, we used multiple non-human primate species for capsid selections, beginning with a library selection in the adult marmoset and choosing 2 candidate capsids to be tested in newborn rhesus macaques. In choosing our 2 capsids for characterization in the newborn macaque, we clustered high performing

variants with sequence homology to visualize key variants of interest, similar to the clustering analysis from Kumar et al[41]. We included these 2 capsids to a pool of 8 total capsids, including controls and other engineered capsids from rodent selections. By combining the capsid pool strategy with the clustering visualizations, we show that the variants selected in adult marmoset are more enriched in the brain compared to the variants selected in mice. In conclusion, we find that one of the variants selected in the marmoset, AAV.CAP-Mac, is a key candidate capsid that can potentially be used for further enabling studies in Old World primates such as the rhesus macaque (Fig 2.1a). The results from this chapter reveal the importance of conducting selections in non-human primates when attempting to identify a capsid for the primate brain.

Work from this chapter was completed by and in collaboration with Dr. Ben Deverman, Dr. Ken Chan, Dr. Nick Flytzanis, Dr. Nick Goeden, and Dr. Tim Shay.

2.2 Motivation and introduction

Discovery of neurotropic AAV variants in rodents was catalyzed by advances in protein engineering, sequencing technologies, and understanding of AAV structure and function. For example, some of the first variants to efficiently traverse the BBB after intravenous (IV) administration in mice (AAV-PHP.B/eB) were engineered using Cre recombinase-based AAV targeted evolution (CREATE), which leverages Cre-transgenic mouse lines to impose additional selective pressure during library selections[39,40].

Implementing next-generation sequencing (NGS) and mutagenesis at different locations on the capsid surface has since led to variants with enhanced neurotropic properties, such as the ability to cross the BBB across different mouse strains, decreased transduction in non-CNS tissue, and biased tropism towards cell types in the brain[40–42,76–78].

Figure 2.1: Selecting and characterizing AAV variants in non-human primates.

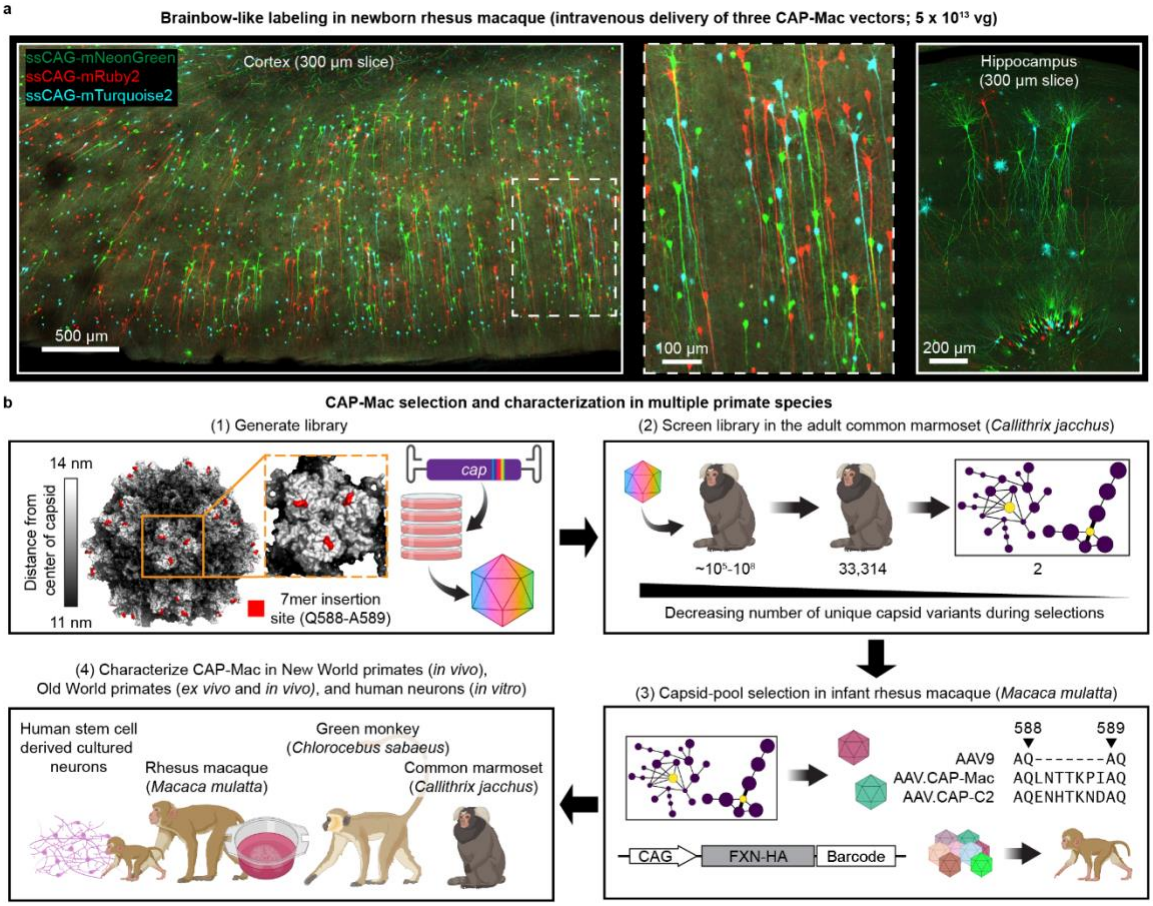

Fig. 2.1: Selecting and characterizing AAV variants in non-human primates. a, AAV.CAP-Mac is a novel vector that enables brain-wide, systemic gene transfer in non-human primates. Representative images are shown from a newborn rhesus macaque brain expressing 3 fluorescent

reporters delivered intravenously using AAV.CAP-Mac (5×10^{13} vector genomes total dose, 4 weeks post-injection). **b,** Schematic of the CAP-Mac selection strategy. (1) CAP-Mac is an AAV9 variant that we selected from a library screened in the adult common marmoset. We generated diversity by introducing 21 NNK degenerate codons after Q588 in the AAV9 *cap* genome and produced the capsid library for *in vivo* selections in adult male marmosets. (2) In two rounds of selections, we intravenously administered 2×10^{12} vector genomes (vg) per marmoset (2 marmosets per round), narrowing our variant pool with each round of selection. After the first round of selection, we recovered 33,314 unique amino acid sequences in the brain. For the second round of selection, we generated a synthetic oligo pool containing each unique variant plus a codon modified replicate (66,628 total sequences). After the second round of selection, we constructed network graphs of high-performing variants, and selected two capsids—AAV.CAP-Mac and AAV.CAP-C2—to be included in pool selections in newborn rhesus macaques. (3) For pool selections, we produced 8 capsids packaging ssCAG-hFXN-HA, each with a unique molecular barcode in the 3' UTR. This construct design enabled us to assess protein expression of the pool by staining for the hemagglutinin (HA) epitope and quantify barcodes in viral DNA and whole RNA extracts. We injected 1×10^{14} vg/kg of the virus pool into 2 newborn rhesus macaques via the saphenous vein and recovered tissue 4 weeks post-injection. (4) We moved forward with individual characterization of AAV.CAP-Mac in various contexts (*ex vivo, in vitro, in vivo*) in multiple primate species.

While AAV capsid engineering has enabled intravenous gene transfer to the rodent central nervous system (CNS), tools for non-human primates (NHPs) are sparse. Some capsids selected in rodents translate to the common marmoset[42] (*Callithrix jacchus*), a New

World primate species, but few translate to Old World primates, which are more closely evolutionarily related to humans and are well-established animal models of human cognition, neurodevelopment, neuroanatomy, and physiology[50,79,80]. Notably, despite its success in mice, the BBB-crossing tropism of AAV-PHP.B does not translate to the rhesus macaque (*Macaca mulatta*)[47,48].

2.3 Library selections in the common marmoset

Our overarching goal was to develop an AAV variant efficacious in NHPs after systemic administration. To do that, we used a multi-species screening and characterization strategy to select for variants with enhanced BBB-crossing tropism in NHPs (Fig. 2.1b). Briefly, we constructed a library as previously described by inserting 7mer sequences after Q588 in the structural *cap* gene of AAV9[39–41] (Supplementary Fig. 2.1a-c). We initially screened this library in 2 rounds of selection in the adult marmoset (2 marmosets per round; 2 x 10^{12} vector genomes [vg] of viral library per marmoset via IV administration), where we identified 33,314 unique variants present in the brain.

2.4 Overcoming the challenges of selections in non-human primates

In the past, we used our CREATE methodology to increase stringency during selections by only recovering variants that underwent cis-Cre-Lox mediated inversion[39,41]. However, since Cre-transgenic marmosets are not yet available, we pursued other strategies to compensate for the loss of this additional selective pressure. We previously

demonstrated the utility of clustering capsid variants based on sequence similarity to generate network graphs as an aid in choosing variants for further characterization[41]. Briefly, we filtered variants based on user-defined performance criteria and clustered high-performing variants into network graphs (Supplementary Fig. 2.1d-g), wherein each node is a capsid variant, and each edge represents shared sequence identity between related variants (i.e., the pairwise reverse Hamming distance). We reasoned that this clustering analysis would let us efficiently sample variants from our selections while (1) limiting the number of animals used for individual characterization and (2) partially overcoming the absence of the CREATE selective pressure. Based on these network graphs, we chose two variants out of the 33,314 recovered from the marmoset for further characterization: AAV.CAP-Mac (CAP-Mac) and AAV.CAP-C2 (CAP-C2).

Figure 2.2: CAP-Mac outperforms other engineered variants in newborn rhesus macaque in pool testing.

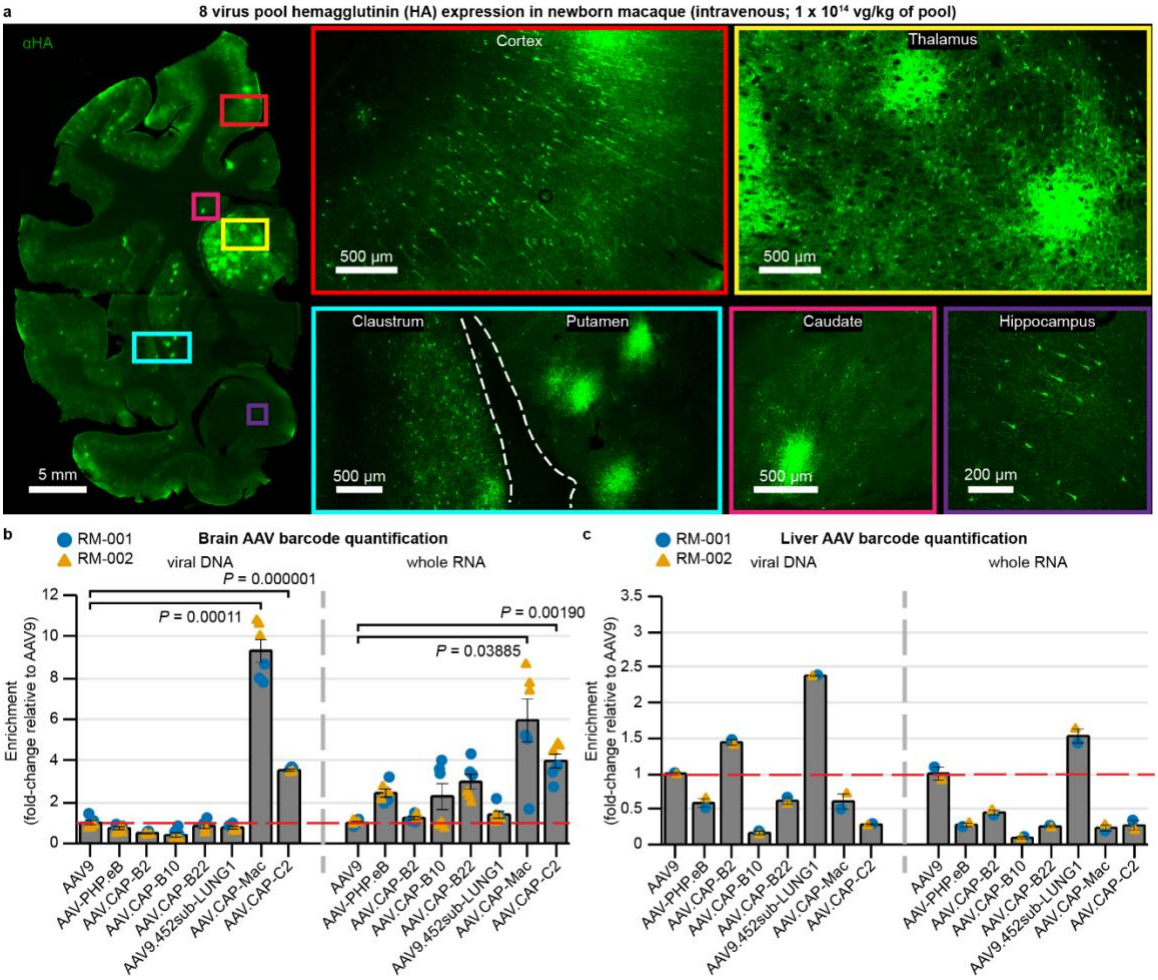

Fig. 2.2: CAP-Mac outperforms other engineered variants in newborn rhesus macaque in pool testing. a, Representative images of expression in cortex, thalamus, caudate nucleus, putamen, hippocampus and claustrum after intravenous administration of 1 x 10^{14} vg/kg of an 8-capsid pool (1.25 x 10^{13} vg/kg of each variant) packaging hemagglutinin (HA) tagged human frataxin with a unique barcode in each capsid. HA epitope expression in the cortex and hippocampus is observable in single cells with clear projections that resemble the apical dendrites of pyramidal cells. Furthermore, the thalamus and dorsal striatum contain dense areas of HA

expression relative to other brain regions. **b**, **c**, Unique barcode enrichments in viral DNA (left) and whole RNA (right) extracts from the brain (**b**; n=6 brain samples from 2 newborn macaques) and the liver (**c**; n=2 liver tissue samples from 2 newborn macaques). Each data point represents the fold-change relative to AAV9 within each tissue sample. Mean ± s.e.m. shown. The red dashed line denotes AAV9 performance in pool. One-way ANOVA using Tamhane's T2 correction tested against AAV9 enrichment.

Following library selection in the adult marmoset, we used capsid-pool studies in newborn rhesus macaques to assess the translatability of several engineered AAVs to Old World primates. We pooled 8 capsid variants: AAV9, CAP-Mac, CAP-C2, and five other previously-engineered AAVs[40,42,81]. Each variant packaged a single-stranded human frataxin transgene fused to a hemagglutinin (HA) epitope tag under control of the ubiquitous CAG promoter (ssCAG-hFXN-HA) with a unique molecular barcode in the 3' UTR. This construct design allowed us to assess protein expression of the virus pool via immunostaining of the HA epitope tag while also quantifying the relative enrichment of each unique barcode in DNA and RNA recovered from tissue. We administered 1 x 10^{14} vg/kg of the virus pool to 2 newborn rhesus macaques via the saphenous vein and, at 4 weeks post-injection, observed robust expression of the HA epitope throughout the brain (Fig. 2.2a). In the cortex and hippocampus, we observed single cells with clear projections that resemble the apical dendrites of pyramidal cells. Furthermore, we saw increased HA epitope expression in the thalamus and dorsal striatum (Fig. 2.2a, insets).

2.5 AAV.CAP-Mac: an engineered AAV variant with enhanced neurotropic properties

When we quantified the relative enrichment of each barcode in the brain, we found that the CAP-Mac-delivered barcode was 9 and 6 times more abundant than the AAV9-delivered barcode in the viral DNA and total RNA, respectively (Fig. 2.2b). The CAP-C2-delivered barcode was approximately 4-fold enriched relative to the AAV9 barcode in both DNA and RNA extracts. Interestingly, the viral DNA levels of all other variants, which were originally selected in mice, were on par with AAV9. In the liver, CAP-Mac and CAP-C2 were negatively enriched, as were some of the previously-engineered controls known to be de-targeted from the liver in rodents[42] (Fig. 2.2c).

2.6 Discussion

In vivo AAV capsid selections have been primarily conducted in mice, in part due to the utility of Cre-transgenic mouse lines to increase selective pressure, which can yield neurotropic capsids in as few as two rounds of selection[39,41,42]. However, these engineered variants have largely failed to translate to NHPs[47,48]. The notable exceptions are AAV.CAP-B10 and AAV.CAP-B22, which were identified using multiplexed-CREATE (M-CREATE)[41] selections in mice and retain their BBB crossing and reduced liver tropism in the common marmoset[42], a New World primate. However, our pool testing here showed that these variants perform only on par with AAV9 in delivering DNA to the brains of infant macaques, an Old World primate. While mice last shared a common ancestor with

humans approximately 80-90 million years ago (mya), marmosets and macaques are believed to have shared their last ancestors with humans 35-40 mya and 25-30 mya, respectively[49]. Given this evolutionary distance, it is not surprising that most variants selected in mice have failed to translate to Old World primates, and vice versa. Interestingly, our pool studies in macaques showed that variants identified via Cre-independent selections in marmosets and chosen using network graphs (CAP-Mac and CAP-C2) generally outperformed variants identified via Cre-dependent selections in mice (Fig. 2.2b). This suggests that while enhancing selective pressure is important when evolving engineered AAVs *in vivo*, it is also vital to consider the evolutionary relatedness between the selection and target species. Notably, several transgenic marmoset lines are currently available[82,83], and the generation of Cre-transgenic marmosets is underway[84], offering the potential to perform M-CREATE in NHPs. Given that the evolutionary distance between mice and marmosets (40-55 mya) is slightly larger than that between marmosets and humans (35-40 mya), the observation that AAV.CAP-B10 and AAV.CAP-B22 retain their BBB-crossing tropisms in marmosets offers hope that NHP selections can identify capsid variants efficacious in humans.

2.7 Methods

AAV capsid library selection in marmosets

AAV DNA library generation

The details of this procedure can be found on protocols.io (DOI: 10.17504/protocols.io.5jyl8jy89g2w/v1). We initially generated diversity at the DNA level, which we then used to produce transfection material to produce the AAV capsid library, as described previously in detail[41]. For the round 1 library, we introduced this genetic diversity using primers containing degenerate nucleotides inserted between amino acids (AA) 588 and 589[39–41] (VP1 numbering; Supplementary Fig. 2.1a). We used a reverse primer containing 21 degenerate nucleotides ([NNK] x 7) to randomly generate PCR fragments containing unique 7mer sequences inserted into the *cap* gene. For the round 2 DNA library, we used a synthetic oligo pool (Twist Bioscience) as a reverse primer, encoding only variants selected for further screening (66,628 DNA oligos total: 33,314 variants recovered after round 1 selections plus a codon-modified replicate of each). All reverse primers contained a 20 bp 5' overhang complementary to the *cap* sequence near the AgeI restriction enzyme sequence and were paired with a forward primer containing a 20 bp 5' overhang near the XbaI restriction enzyme sequence. We then inserted the PCR fragments containing the diversified region into the rAAV-ΔCAP-in-cis-Lox plasmid via Gibson assembly to generate the resulting AAV DNA library, rAAV-CAP-in-cis-Lox, using NEBuilder HiFi DNA Assembly Master Mix (New England Biolabs, E2621).

AAV capsid library production

The details of this procedure can be found on protocols.io (DOI: 10.17504/protocols.io.5jyl8jyz9g2w/v1). We generated AAV capsid libraries according to previously published protocols[41,85]. Briefly, we transfected HEK293T cells (ATCC, cat # CRL-3216; RRID: CVCL_0063) in 150 mm tissue culture plates using transfection grade, linear polyethylenimine (PEI; Polysciences, Inc). In each plate, we transfected 4 plasmids: (1) the assembled rAAV-Cap-in-cis-Lox AAV DNA library, which is flanked by inverted terminal repeats (ITR) required for AAV encapsidation; (2) AAV2/9 REP-AAP-ΔCAP, which encodes the REP and AAP supplemental proteins required for AAV production with the C-terminus of the *cap* gene excised to prevent recombination with the AAV DNA library and subsequent production of replication-competent AAV; (3) pHelper, which encodes the necessary adenoviral proteins required for AAV production; and (4) pUC18 (Addgene: 50004), which contains no mammalian expression vector but is used as filler DNA to achieve the appropriate nitrogen-to-phosphate ratio for optimal PEI transfection. During preparation of the PEI-DNA mixture, we added 10 ng of our AAV DNA library (rAAV-Cap-in-cis-Lox) for every 150 mm dish and combined AAV2/9 REP-AAP-ΔCAP, pUC18, and pHelper in a 1:1:2 ratio, respectively (40 µg of total DNA per 150 mm dish). At 60 hours post-transfection, we purified AAV capsid library from both the cell pellet and media using polyethylene glycol precipitation and iodixanol gradient ultracentrifugation. Using quantitative PCR, we then determined the titer of the AAV capsid libraries by

amplifying DNaseI-resistant viral genomes relative to a linearized genome standard according to established protocols[85].

Marmoset procedures and tissue handling

The details of this procedure can be found on protocols.io (DOI: 10.17504/protocols.io.bp2l695zklqe/v2). All marmoset (*Callithrix jacchus*) procedures for library selections were performed at the National Institutes of Mental Health (NIMH) and approved by the local Institutional Animal Care and Use Committee (IACUC) under protocol TGC-03. Marmosets were born and raised in NIMH colonies and housed in family groups under standard conditions of 27 °C and 50% humidity. They were fed ad libitum and received enrichment as part of the primate enrichment program for NHPs at the National Institutes of Health. For all marmosets used in this study, there were no detectible neutralizing antibodies at a 1:5 serum dilution prior to IV infusions (assayed by The Penn Vector Core, University of Pennsylvania). They were then housed individually for several days and acclimated to a new room before injections. Four adult males were used for the library screening, 2 each for first- and second-round libraries. The day before infusion, the animals' food was removed. Animals were anesthetized with isoflurane in oxygen, the skin over the femoral vein was shaved and sanitized with an isopropanol scrub, and 2×10^{12} vg of the AAV capsid library was infused over several minutes. Anesthesia was withdrawn and the animals were monitored until they became active, upon which they were returned

to their cages. Activity and behavior were closely monitored over the next 3 days, with daily observations thereafter.

At 4 weeks post-injection, marmosets were euthanized (Euthanasia, VetOne) and perfused with 1X phosphate-buffered saline (PBS). After the round 1 library, the brain was cut into 4 coronal blocks, flash frozen in 2-methylbutane (Sigma Aldrich, M32631), chilled with dry ice, and stored at −80 °C for long term storage. After the round 2 library, the brain was cut into 6 coronal blocks and, along with sections of the spinal cord and liver, was flash frozen and stored at −80 °C for long term storage.

Viral library DNA extraction and NGS sample preparation

The details of this procedure can be found on protocols.io (DOI: 10.17504/protocols.io.bp2l695zklqe/v2). We previously reported that viral library DNA and endogenous host RNA can be isolated using TRIzol by precipitating nucleic acid from the aqueous phase[39,41]. Therefore, to extract viral library DNA from marmoset tissue, we homogenized 100 mg of spinal cord, liver, and each coronal block of brain in TRIzol (Life Technologies, 15596) using a BeadBug (Benchmark Scientific, D1036) and isolated nucleic acids from the aqueous phase according to the manufacturer's recommended protocol. We treated the reconstituted precipitate with RNase (Invitrogen, AM2288) and digested with SmaI to improve downstream viral DNA recovery via PCR. After digestion,

we purified with a Zymo DNA Clean and Concentrator kit (D4033) according to the manufacturer's recommended protocol and stored the purified viral DNA at −20 °C.

To append Illumina adapters flanking the diversified region, we first PCR-amplified the region containing our 7mer insertion using 50% of the total extracted viral DNA as a template (25 cycles). After Zymo DNA purification, we diluted samples 1:100 and further amplified around the variable region with 10 cycles of PCR, appending binding regions for the next PCR reaction. Finally, we appended Illumina flow cell adapters and unique indices using NEBNext Dual Index Primers (New England Biolabs, E7600) via 10 more cycles of PCR. We then gel-purified the final PCR products using a 2% low-melting point agarose gel (ThermoFisher Scientific, 16520050) and recovered the 210 bp band.

For the second-round library only, we also isolated the encapsidated AAV library ssDNA for NGS to calculate library enrichment scores, a quantitative metric that we used to normalize for differences in titer of the various variants in our library (see ref. [41] and the next section). To isolate the encapsidated viral genomes, we treated the AAV capsid library with DNaseI and digested capsids using proteinase K. We then purified the ssDNA using phenol-chloroform, amplified viral transgenes by 2 PCR amplification steps to add adapters and indices for Illumina NGS, and purified using gel electrophoresis. This viral library DNA, along with the viral DNA extracted from tissue, was sent for deep sequencing

using an Illumina HiSeq 2500 system (Millard and Muriel Jacobs Genetics and Genomics Laboratory, Caltech).

NGS read alignment, analysis, and generation of network graphs

Raw fastq files from NGS runs were processed with custom-built scripts (see https://github.com/GradinaruLab/protfarm for sequence alignment scripts and https://github.com/GradinaruLab/mCREATE for clustering scripts)[41]. For the first-round library, the pipeline to process these datasets involved filtering to remove low-quality reads, utilizing a quality score for each sequence, and eliminating bias from PCR-induced mutations or high GC-content. The filtered dataset was then aligned by a perfect string match algorithm and trimmed to improve the alignment quality. We then displayed absolute read counts for each variant during the sequencing run within each tissue, and all 33,314 variants that were found in the brain were chosen for round 2 selections.

After round two selections, we performed the same analysis to display variant absolute read count of the injected virus library and of each variant within each tissue. Additionally, we calculated the library enrichment[41] for each variant within each tissue:

$$\widehat{RC}_{x,injected\ library} = \frac{RC_{x,injected\ library}}{\sum_{i=1}^{N_{injected\ library}} RC_{i,injected\ library}}$$

$$\widehat{RC}_{x,tissue} = \frac{RC_{x,virus}}{\sum_{i=1}^{N_{tissue}} RC_{i,tissue}}$$

$$library\ enrichment = log_{10}(\frac{\widehat{RC}_{x,injected\ library}}{\widehat{RC}_{x,tissue}})$$

such that for a given sample y (e.g., the injected virus library or a tissue sample), $RC_{x,y}$ is the absolute read count of variant x, N_y is the total number of variants recovered, and $\widehat{RC}_{x,y}$ is the normalized read count.

To construct the CAP-Mac sequence clustering graph, we filtered the round 2 NGS data based on the following criteria: (1) ≥ 100 read count in the injected library sample (24,186/33,314 variants), (2) ≥ 0.7 library enrichment score in more than 2 brain samples (415 variants), and (3) at least 2 more brain samples with ≥ 0.7 library enrichment than brain samples with < −0.7 library enrichment (323 variants). To construct the CAP-C2 sequence graph, we filtered the round 2 NGS data based on the following criteria: (1) ≥ 100 read count in the injected library sample and (2) both codon replicates present in at least 2 brain samples with ≥ 0.7 library enrichment (95 variants). These variants were then independently processed to determine pair-wise reverse Hamming distances (https://github.com/GradinaruLab/mCREATE) and clustered using Cytoscape (ver. 3.9.0) as described previously[41]. Networks presented show capsid variants (nodes) connected by edges if the pair-wise reverse Hamming distance is ≥ 3.

Cloning individual AAV capsid variants

The details of this procedure can be found on protocols.io (DOI: 10.17504/protocols.io.n2bvj87ebgk5/v1). For single variant characterization, we cloned new variant plasmids by digesting a modified version of the pUCmini-iCAP-PHP.eB (Addgene ID: 103005) backbone using MscI and AgeI. We designed a 100 bp primer that contained the desired 21 bp insertion for each capsid variant and the regions complementary to the AAV9 template with ~20 bp overlapping the digested backbone. We then assembled the variant plasmid using NEBuilder HiFi DNA Assembly Master Mix, combining 5 μL of 200 nM primer with 30 ng of digested backbone in the reaction mixture. The capsid plasmid used to produce AAV.CAP-Mac is available on Addgene (200658).

Individual AAV production and purification

The details of this procedure can be found on protocols.io (DOI: 10.17504/protocols.io.14egn2dqzg5d/v1). To produce variants for pool testing, we followed our previously published protocol[85] using 150 mm tissue culture dishes. For individual AAV.CAP-Mac and AAV9 characterization *in vivo* and *in vitro*, we adopted our published protocol to utilize ten-layer CellSTACKs (Corning, 3320) to efficiently produce viruses at high titer to dose rhesus macaques and green monkeys. Specifically, we passaged 20 150-mm dishes at approximately 70% confluency into a 10-layer CellSTACK 24 h before transfection. On the day of transfection, we prepared the DNA-PEI transfection mixture for 40 150-mm dishes and combined the transfection mixture with media and

performed a complete media change for the CellSTACK. We collected and changed media at 72 h post-transfection similarly to production in 150 mm dishes. At 120 h post-transfection, we added ethylenediaminetetraacetic acid (EDTA, Invitrogen, 15575020) to a final concentration of 10 mM and incubated at 37 °C for 20 min, occasionally swirling and tapping the sides of the CellSTACK to detach the cells. We then removed the media and cell mixture and proceeded with the AAV purification protocol[85]. Of note, during the buffer exchange step after ultracentifugation, we used centrifugal protein concentrators with polyethersulfone membranes (Thermo Scientific, 88533) instead of Amicon filtration devices and used Dulbecco's PBS supplemented with 0.001% Pluronic® F-68 (Gibco, 24040032).

Rhesus macaque AAV characterization

The details of the procedures in this section can be found on protocols.io (DOI: 10.17504/protocols.io.5qpvormddv4o/v1). Neonate rhesus macaques (*Macaca mulatta*; 0.45-1.4 kg) were weaned at birth, and within the first month were infused with AAV vectors either intravenously (IV) or intrathecally (ICM). All adult macaques (8-17 years old; 4.65-11 kg) included in this study were infused with AAV via IV administration only. For IV injections, animals were anesthetized with ketamine (0.1 mL) and the skin over the saphenous vein was shaved and sanitized. AAV (between 2×10^{13} and 1×10^{14} vg/kg) was slowly infused into the saphenous vein over ~1 min in < 0.75 mL of phosphate buffered saline. For ICM injections, animals were administered a sedative intramuscularly and the

area of skin at the neck was shaved and aseptically prepared. A needle was advanced into the cisterna magna to remove a small amount of CSF proportional to the amount of fluid injected. Then, a sterile syringe containing the sterile preparation of the AAV (1.5 x 10^{12} or 2.5 x 10^{13} vg/kg) proportional to the amount of fluid collected was aseptically attached and slowly injected. All animals were monitored during recovery from sedation, throughout the day, and then daily for any adverse findings. All monkeys were individually housed within sight and sound of conspecifics. Tissue was collected 4-11 weeks after injection. Animals were deeply anesthetized and received sodium pentobarbital in accordance with guidelines for humane euthanasia of animals at the CNPRC. All material injected into rhesus macaques was free of endotoxins (<0.1 EU/mL), and protein purity was confirmed by sodium dodecyl sulphate–polyacrylamide gel electrophoresis (SDS-PAGE). See Supplementary Tables 2.1 and 2.2 for route of administration, AAV variants, viral dose, genetic cargo, and duration of expression for each experiment.

Pool testing in newborn rhesus macaques

The details of the procedures in this section can be found on protocols.io (DOI: 10.17504/protocols.io.5qpvormddv4o/v1, 10.17504/protocols.io.3byl4jo68lo5/v1 and 10.17504/protocols.io.j8nlkwxxwl5r/v1). Neonate macaque pool experiments (RM-001 to RM-004) were performed at the CNPRC at UC Davis and approved by the local IACUC (protocol 22525). Adult macaque pool experiments (RMN-001 and RMN-002) were performed at the NIMH and approved by their local IACUC (protocol LN-14). Macaques

were perfused with ice-cold RNase-free PBS. At the time of perfusion, one hemisphere of the brain was flash-frozen and the other hemisphere was sectioned into 4 mm coronal blocks and post-fixed in 4% PFA for 48 hours and transferred to Caltech for further processing. For HA staining, we incubated slices with rabbit anti-HA (1:200; Cell Signaling Technology, cat # 3724; RRID: AB_1549585), performed 3-5 washes with PBS, incubated with donkey anti-rabbit IgG (1:200; Jackson ImmunoResearch Labs, cat # 711-605-152; RRID: AB_2492288), and washed 3-5 times before mounting. We diluted all antibodies and performed all incubations using PBS supplemented with 0.1% Triton X-100 (Sigma-Aldrich, T8787) and 10% normal donkey serum (Jackson ImmunoResearch Labs, cat # 017-000-121; RRID: AB_2337258) overnight at room temperature with shaking.

To isolate viral DNA and whole RNA, 100mg slices from brain and liver were homogenized in TRIzol (Life Technologies, 15596) using a BeadBug (Benchmark Scientific, D1036) and total DNA and RNA were recovered according to the manufacturer's recommended protocol. Recovered DNA was treated with RNase, restriction digested with SmaI, and purified with a Zymo DNA Clean and Concentrator Kit (D4033). Recovered RNA was treated with DNase, and cDNA was generated from the mRNA using Superscript III (Thermo Fisher Scientific, 18080093) and oligo(dT) primers according to the manufacturer's recommended protocol. We used PCR to amplify the barcode region using 50 ng of viral DNA or cDNA as template. After Zymo DNA purification, we diluted samples 1:100 and further amplified the barcode region using

primers to append adapters for Illumina next-generation sequencing. After cleanup, these products were further amplified using NEBNext Dual Index Primers for Illumina sequencing (New England Biolabs, E7600) for ten cycles. We then gel-purified the final PCR products using a 2% low-melting point agarose gel (ThermoFisher Scientific, 16520050). Pool testing enrichment was calculated identically to library enrichment but is represented in Fig. 2.2b and c on a linear scale.

2.8 Supplementary data

Supplementary Figure 2.1: Generating AAV libraries and choosing variants for further characterization.

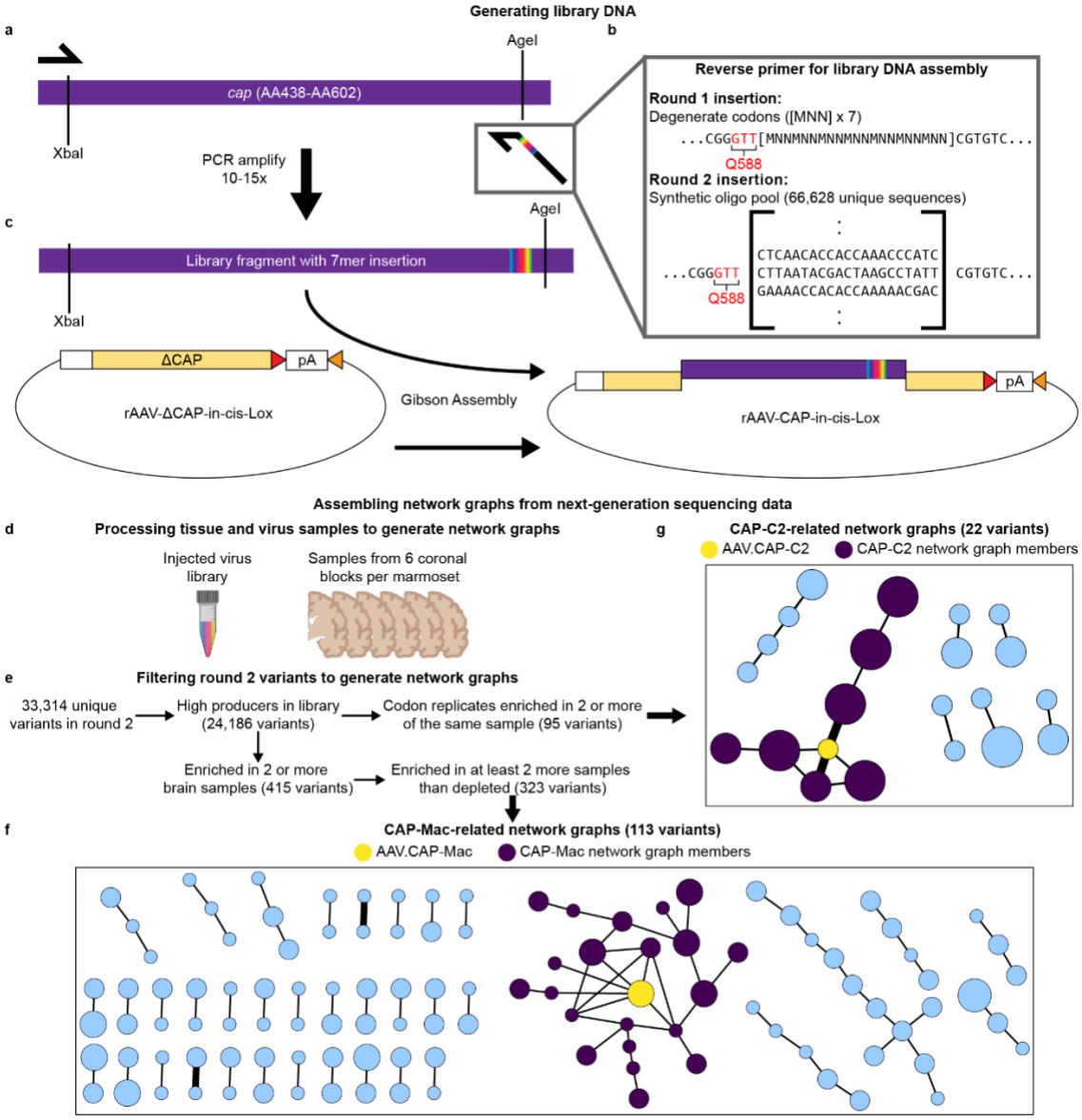

Supplementary Fig. 2.1: Generating AAV libraries and choosing variants for further characterization. a, We introduced diversity into the AAV9 *cap* genome using a reverse primer with a 21-nucleotide

insertion after Q588. The reverse primer was used to generate a PCR fragment approximately spanning the XbaI to AgeI sites of the modified *cap* gene (approximately AA438 to AA602). **b**, For DNA assembly for round 1 selections, the reverse primer contained 21 degenerate codons ([MNN] x 7]). For round 2 selections, we used a synthetic oligo pool to specify each 21 bp sequence that we inserted into *cap*. **c**, The PCR-amplified fragment contained homologous regions that overlap with the rAAV-ΔCAP-in-cis-Lox digested plasmid, and the two fragments were assembled using Gibson assembly to create the final assembled library DNA. **d-g**, Process to assemble network graphs from next-generation sequencing data. While our previous CREATE-based selections have relied on Cre-transgenic mouse lines to increase selection stringency, Cre-transgenic marmosets are currently unavailable, and we were unable to confer this additional selective pressure during selections. We reasoned that through this clustering analysis, we could efficiently and productively sample variants from our selections to (1) limit the number of animals used for individual characterization and (2) partially overcome the absence of the selective pressure provided by Cre-transgenic mice in CREATE. **d**, To generate network graphs, we processed the injected virus library and sampled from each of the 6 brain sections from each animal. **e**, From our next-generation sequencing data, we calculated library enrichment scores and filtered the variants using two separate criteria. **f**, **g**, Network graphs for AAV.CAP-Mac (**f**) and AAV.CAP-C2 (**g**). CAP-Mac and CAP-C2 were both chosen because they were the most interconnected nodes within their respective networks. Each node represents a unique variant recovered from the round 2 selection and each edge represents pairwise reverse Hamming distance ≥ 3.

Supplementary Table 2.1: Rhesus macaque information for variant pool testing.

Macaque ID	Age	Sex	Route of administration	Weight at injection (kg)	Total dose (vg/kg)	Expression length (days)
RM-001	1 day	Male	Intravenous	0.602	1×10^{14}	31
RM-002	1 day	Male	Intravenous	0.454	1×10^{14}	31
RM-003	150 days	Female	Intra-cisterna magna	1.407	1.5×10^{12}	55
RM-004	150 days	Female	Intra-cisterna magna	1.307	1.5×10^{12}	55
RMN-001	7.9 years	Male	Intravenous	5.3	7.5×10^{13}	40
RMN-002	7.8 years	Female	Intravenous	4.65	7.5×10^{13}	41

RMN-001 and RMN-002 experiments were performed at the NIMH. All other experiments were performed at the California National Primate Research Center at UC Davis. All macaques were injected with pool of 8 variants (AAV9, PHP.eB, 452sub-LUNG1, CAP-B2, CAP-B10, CAP-B22, CAP-Mac, CAP-C2) packaging CAG-hFXN-HA-Barcode.

Supplementary Table 2.2: Rhesus macaque information for characterization of CAP-Mac.

Macaque ID	Age	Sex	Route of administration	Capsid*	Cargo*	Weight at injection (kg)	Total dose (vg/kg)	Expression length (days)
RM-008	29 days	Male	Intra-cisterna magna	AAV.CAP-Mac	CAG-GCaMP7s	0.74	2.5×10^{13}	68
RM-009	2 days	Male	Intravenous	AAV.CAP-Mac	CAG-mNeonGreen, CAG-mRuby2, CAG-mTurquoise2 cocktail	0.956	5×10^{13}	29
RM-010	2 days	Male	Intravenous	AAV.CAP-Mac	CAG-mNeonGreen, CAG-mRuby2, CAG-mTurquoise2 cocktail	0.522	5×10^{13}	77
RM-015	3 days	Male	Intravenous	AAV.CAP-Mac	CAG-GCamP8s and hSyn-hM3D(Gq)-mCherry cocktail	0.635	4×10^{13}	34
RM-017	1 days	Female	Intravenous	AAV.CAP-Mac	CAG-GCaMP8s and CAG-ChRmine-TS-mRuby3 cocktail	0.46	4×10^{13}	43
RM-020	17.2 years	Female	Intravenous	(1) AAV.CAP-Mac (2) AAV9	(1) CAG-eGFP (2) CAG-mRuby3	11.04	2×10^{13}	43

*All experiments were performed at the California National Primate Research Center at UC Davis. *Numbers in "Capsid" and "Cargo" column correspond to capsid-cargo pairs for each dual injection.*

Chapter 3

INTRAVENOUS FUNCTIONAL GENE TRANSFER THROUGHOUT THE BRAIN OF OLD WORLD PRIMATES USING CAP-MAC

Chuapoco MR*, Flytzanis NC*, Goeden N, Octeau J, Roxas K, Chan K, Scherrer J, Winchester J, Blackburn R, Campos L, Man KN, Sun J, Chen X, Lefevre A, Singh V, Arokiaraj C, Miles T, Vendemiatti J, Jang M, Mich J, Bishaw Y, Gore B, Omstead V, Taskin N, Weed N, Levi BP, Ting J, Miller C, Deverman B, Pickel J, Tian L, Fox A, Gradinaru V. Intravenous functional gene transfer throughout the brain of non-human primates using AAV. Nature Nanotechnology. PMID: 36789432. *Authors contributed equally

3.1 Summary

AAV.CAP-Mac is an observable improvement over AAV9 and other engineered capsids when administered in capsid pool in newborn rhesus macaques. Given the potential of such a capsid to enabling primate research, we chose to use CAP-Mac in several different experimental contexts to demonstrate the utility of such a neurotropic variant in rhesus macaques. We demonstrate two such experiments here: (1) Brainbow-like labeling of neuronal projections using a cocktail of three fluorescent proteins and (2) *ex vivo* calcium

imaging of GCaMP. In both experimental contexts, the genetic cargos were safely delivered using CAP-Ma after intravenous (IV) administration, and the protein were stably expressed and functional. We show here one of the first demonstrations of a systemically delivered genetically encoded tools that can be used to elucidate neural activity in Old World primates.

Work from this chapter was completed by and in collaboration with Capsida Bioherapeutics (Dr. Nick Flytzanis, Dr. Nick Goeden, Dr. J. Christopher Octeau, Kristina Roxas, Jon Scherrer, Janet Winchester, Roy Blackburn), the Andrew S. Fox lab at UC Davis (Lillian Campos), and the Lin Tian lab at UC Davis (Kwuk Nok Mimi Man and Junqing Sun).

3.2 Motivation and introduction

The BRAIN initiative was commissioned in 2013 with a stated focus on "the development and use of tools for acquiring fundamental insight about how the nervous system functions in health and disease"[86]. Part of that initiative includes "new technologies for germline modification-independent approaches to cell type access across species, including non-human primates." There are major technical and ethical challenges associated with germline engineering of NHPs, and current methods for somatic cell gene delivery in NHPs are insufficient. As alternative solution, recombinant AAVs, such as AAV.CAP-Mac, have a demonstrated ability for brain-wide gene transfer in the Old World

primate brain. As such, while there continues to be a need for better viral capsids that access the NHP brain, there is also a major need to disseminate the existing capsids to neuroscientists by developing and demonstrating the types of cargo that can be paired with CAP-Mac. Because of the poor spatial distribution of direct intraparenchymal injections, some studies have used optimized injection methods, like convection-enhanced delivery, in areas such as the thalamus, which are densely populated with axonal projections from distal areas of the cortex. By injecting in these areas, they hypothesized that AAV enter neurons in the axonal projections and migrate to the cell body to express the packaged transgene, increasing the volume of transduced brain tissue[62–64]. While these methods had provided a new avenue for more widespread transduction using AAV, they are still limited to a small number of cortical and subcortical brain areas. As such, there is an opportunity to for systemically administered viral vectors—which can be administered without the use of invasive surgery and theoretically can access the entire brain—to improve on current methods to help researchers.

3.3 Screening cargo in mice prior to use in NHPs

Given the experimental complexity and limited accessibility of NHPs, when designing our GCaMP experiments, we performed initial cargo screening in mice. We therefore first characterized CAP-Mac in three mouse strains. We found that the neuronal bias of CAP-Mac extended to mice when delivered to the adult brain through ICV (Supplementary Fig. 3.1a) but not IV administration, where it primarily transduced cells

with vasculature morphology (Supplementary Fig. 3.1b), with no apparent differences between the three mouse strains. We also found that in P0 C57BL/6J mice, IV-administered CAP-Mac was expressed in various cell types in the brain, including neurons, astrocytes, and vasculature (Supplementary Fig. 3.1c). Given the strong neuronal tropism of CAP-Mac following ICV administration, we used this method to screen two genetic cargos (either one-component or two-component vectors) in mice prior to applying them to NHPs (Supplementary Fig. 3.1d-g). Given our results from this cargo selection in mice, we moved forward with a one-component system using the CAG promoter.

3.4 Intravenous delivery in two infant Old World primate species

Because CAP-Mac outperformed AAV9 and other engineered variants in our pool study, we moved forward with single characterization in two species of Old World primates. In the newborn rhesus macaque, we intravenously administered a cocktail of CAP-Mac vectors (5×10^{13} vg/kg total dose via the saphenous vein) packaging 3 different fluorescent reporters under control of the CAG promoter. Fluorescent protein (XFP) expression was observed in multiple coronal slices along the anterior-posterior axis (Fig. 3.1a) and was robust in all four lobes of cortex and in subcortical areas like the dorsal striatum and hippocampus. While expression was particularly strong in several nuclei of the thalamus (e.g., lateral and medial nuclei, lateral geniculate nucleus, pulvinar nucleus), we noted that expression was not found in all brain regions (e.g., the amygdala). Even with a ubiquitous promoter, we observed expression primarily in NeuN+ neurons (mean

[XFP+NeuN+]/XFP+ between 47-60% across sampled brain regions) and rarely in S100β+ astrocytes (mean [XFP+S100β+]/XFP+ between 0-3%; Fig. 3.1b and Supplementary Fig. 3.2). We also attempted to deliver CAP-Mac via ICM administration in newborn rhesus macaques, but found that efficiency throughout the brain was noticeably decreased compared to IV administration (Supplementary Fig. 3.3). Expression was especially low in subcortical structures, as reported previously[68–72].

Figure 3.1: CAP-Mac is biased towards neurons throughout infant green monkey and newborn rhesus macaque brains.

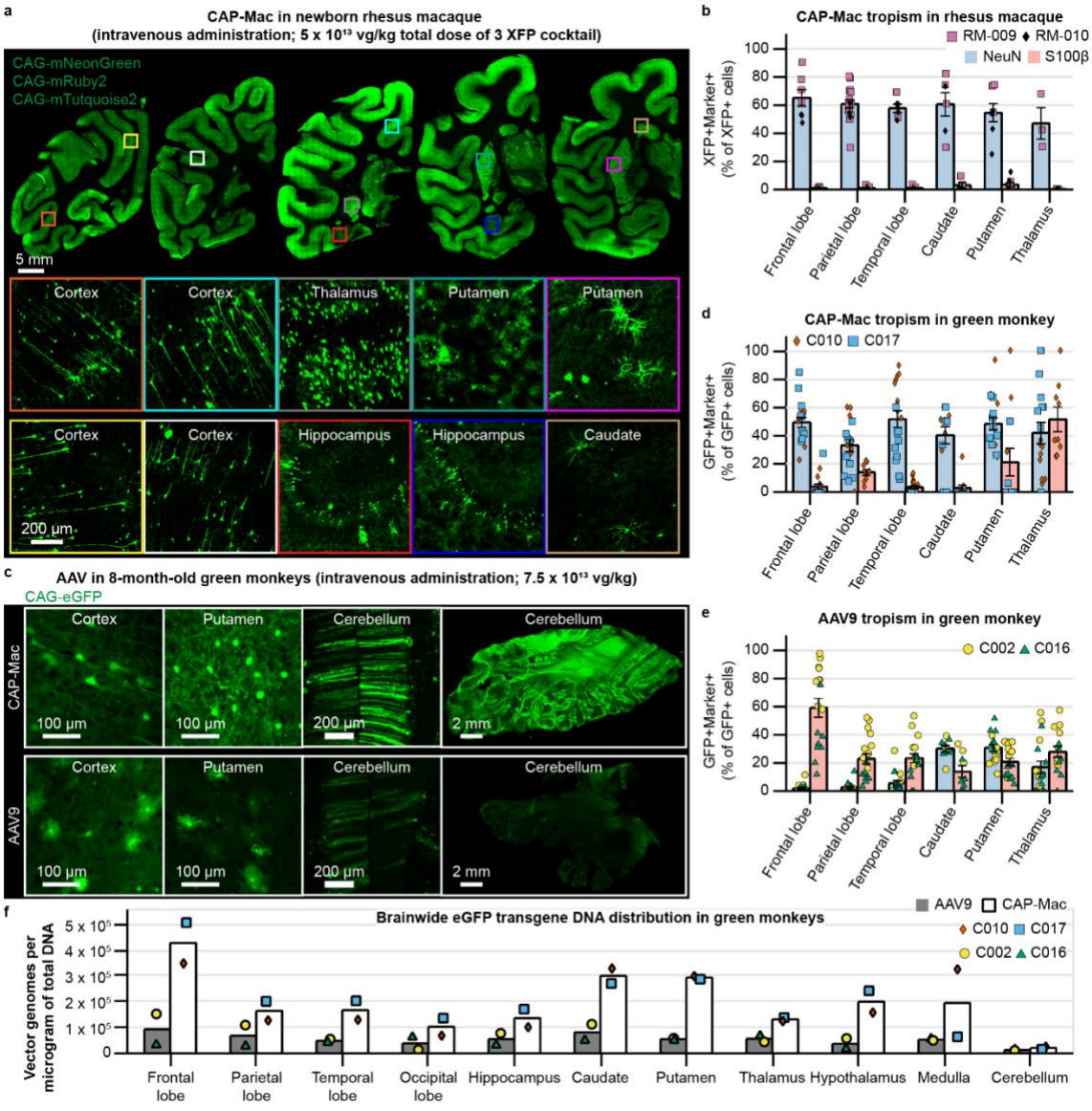

Fig. 3.1: CAP-Mac is biased towards neurons throughout infant green monkey and newborn rhesus macaque brains. a, Distribution of intravenous CAP-Mac expression in 2-day-old rhesus macaques (5 x 10^{13} vg/kg via saphenous vein) across coronal slices showing fluorescent reporter expression (ssCAG-mNeonGreen, ssCAG-mRuby2, ssCAG-

mTurquoise2) in cortical and subcortical brain regions (insets). Imaging channels of reporters are identically pseudo-colored. **b**, Colocalization of fluorescent reporters with NeuN (neurons) or S100β (astrocytes) in 2-day-old rhesus macaques treated with CAP-Mac (n=2 macaques). Values are reported as a percentage of all XFP+ cells. Mean [XFP+NeuN+]/XFP+ range between 47-60% and mean [XFP+S100β+]/XFP+ between 0-3%. Overall, CAP-Mac targeted 1.03% and 0.04% of all NeuN+ and S100β+ cells, respectively **c,** Representative images from 8-month-old green monkeys intravenously dosed with CAP-Mac (top) or AAV9 (bottom) packaging ssCAG-eGFP (7.5×10^{13} vg/kg via saphenous vein). **d**, **e**, Colocalization of fluorescent reporters with NeuN (neurons) or S100β (astrocytes) in infant green monkeys treated with CAP-Mac (**d**; n=2 green monkeys) or AAV9 (**e**; n=2 green monkeys). Values are reported as a percentage of all GFP+ cells. CAP-Mac: mean [GFP+NeuN+]/GFP+ between 33-51% and mean [GFP+ S100β+]/GFP+ between 3-21%. AAV9: mean [GFP+NeuN+]/GFP+ between 2-10% and mean [GFP+S100β+]/GFP+ between 23-59%. Overall, CAP-Mac targeted 1.3% and 0.06% of NeuN+ and S100β+ cells, respectively, in the green monkey brain. In contrasts, AAV9 targeted 0.45% of NeuN+ cells and 1.86% of S100β+ cells. **f**, Distribution of CAP-Mac and AAV9-delivered eGFP transgene in 11 brain regions of green monkeys (n=4 green monkeys). Each data point represents measured vector genomes per microgram of total DNA in a section of tissue from each region and monkey. Mean ± s.e.m. shown.

AAV variants engineered for BBB-crossing in mice are known to have strain-dependent behavior[41,48,87–89]. Therefore, in parallel with the rhesus macaque experiments, we characterized CAP-Mac in green monkeys, another Old World primate species. We

administered either AAV9 or CAP-Mac packaging green fluorescent protein under control of CAG (ssCAG-eGFP) to individual 8-month-old monkeys (7.5×10^{13} vg/kg via the saphenous vein). In the CAP-Mac-dosed green monkeys, we saw broad and strong expression in cortex and various subcortical regions, including the putamen (Fig. 3.1c), consistent with the capsid-pool (Fig. 2.1a) and rhesus macaque (Fig. 3.1a and b) results. We saw particularly strong eGFP expression throughout the cerebellum in the CAP-Mac-dosed green monkey. Except in the thalamus, CAP-Mac eGFP expression was again found primarily in neurons (mean [GFP+NeuN+]/GFP+ between 33-51%) and not astrocytes (mean [GFP+ S100β+]/GFP+ between 3-21%; Fig. 3.1d). In the thalamus, 42% of GFP+ cells were neurons and 51% astrocytes. In AAV9-dosed monkeys, AAV9 eGFP expression was primarily biased towards astrocytes in cortex (mean [GFP+S100β+]/GFP+ between 23-59%) with low neuronal transduction (mean [GFP+NeuN+]/GFP+ between 2-10%; Fig. 3.1e), which is consistent with other reports[68,72,90,91]. Notably, recovered CAP-Mac transgenes were more abundant throughout the brain compared to AAV9, suggesting overall higher brain penetrance of CAP-Mac (Fig. 3.1f and Supplementary Fig. 3.4a). Interestingly, the cerebellum contained the fewest vector genomes per microgram of DNA in both CAP-Mac monkeys despite strong eGFP expression, most likely due to the high density of cells and processes within the cerebellum[92,93]. In most non-brain tissue, eGFP biodistribution and expression was comparable between CAP-Mac- and AAV9-treated animals (Supplementary Fig. 3.4). It should be noted that the cell-type tropism differences

between CAP-Mac and AAV9 in the brain may apply to non-brain tissue as well, with each vector transducing distinct cell types. Even in highly homogenous cell populations, there is significant viral infection variability[94–96], so measuring AAV genomes in bulk may not fully reflect capsid penetrance in tissue across variants and cell types.

3.5 Functional interrogation of the rhesus macaque brain using CAP-Mac

The BRAIN initiative emphasizes the importance of developing novel tools for genetic modulation in NHPs to inform further understanding of the human brain[86,97]. Accordingly, we explored if we could leverage CAP-Mac's neuronal tropism in newborn macaques to deliver genetically-encoded reporters to interrogate the brain. First, we tested whether CAP-Mac can be used as a non-invasive method to define neuronal morphology. Having administered a cocktail of 3 CAP-Mac vectors packaging different fluorescent proteins (Fig. 3.2a), we attempted Brainbow-like labeling[40,98,99] in an Old World primate. We observed widespread expression of all 3 fluorescent proteins in cerebellum, cortex, and the lateral geniculate nucleus of the thalamus (Fig. 3.2b-d). In the cerebellum and thalamus, we observed a high density of transduced cells, and the highest proportion of co-localization of 2 or 3 fluorescent proteins. However, co-localization of multiple fluorescent proteins was rare, suggesting that co-infection was uncommon after systemic administration. With broad and robust expression of fluorescent proteins throughout the brain, we were able to assemble morphological reconstructions of medium spiny neurons (Fig. 3.2e) and cortical pyramidal cells (Fig. 3.2f).

We intravenously delivered ssCAG-GCaMP8s to newborn macaques (3×10^{13} vg/kg via the saphenous vein) and after 4-6 weeks of expression, we removed tissue for *ex vivo* 2P imaging. In the hippocampus, thalamus, and cortex we successfully recorded field potential-evoked calcium gradients in GCaMP-expressing cells (Fig. 3.2h). Cells were responsive to restimulation throughout the experiment and, importantly, the mean peak $\Delta F/F$ of GCaMP signal increased with increases in number of field potential pulses (Supplementary Fig. 3.5a). Cellular calcium dynamics differed across the four sampled brain regions (Supplementary Fig. 3.5b-e). Consistent with our previous profiling, we saw GCaMP expression primarily in cell types with neuronal morphology throughout the brain (Fig. 3.2i).

Figure 3.2: Experimental utility of CAP-Mac for interrogation of the newborn rhesus macaque brain.

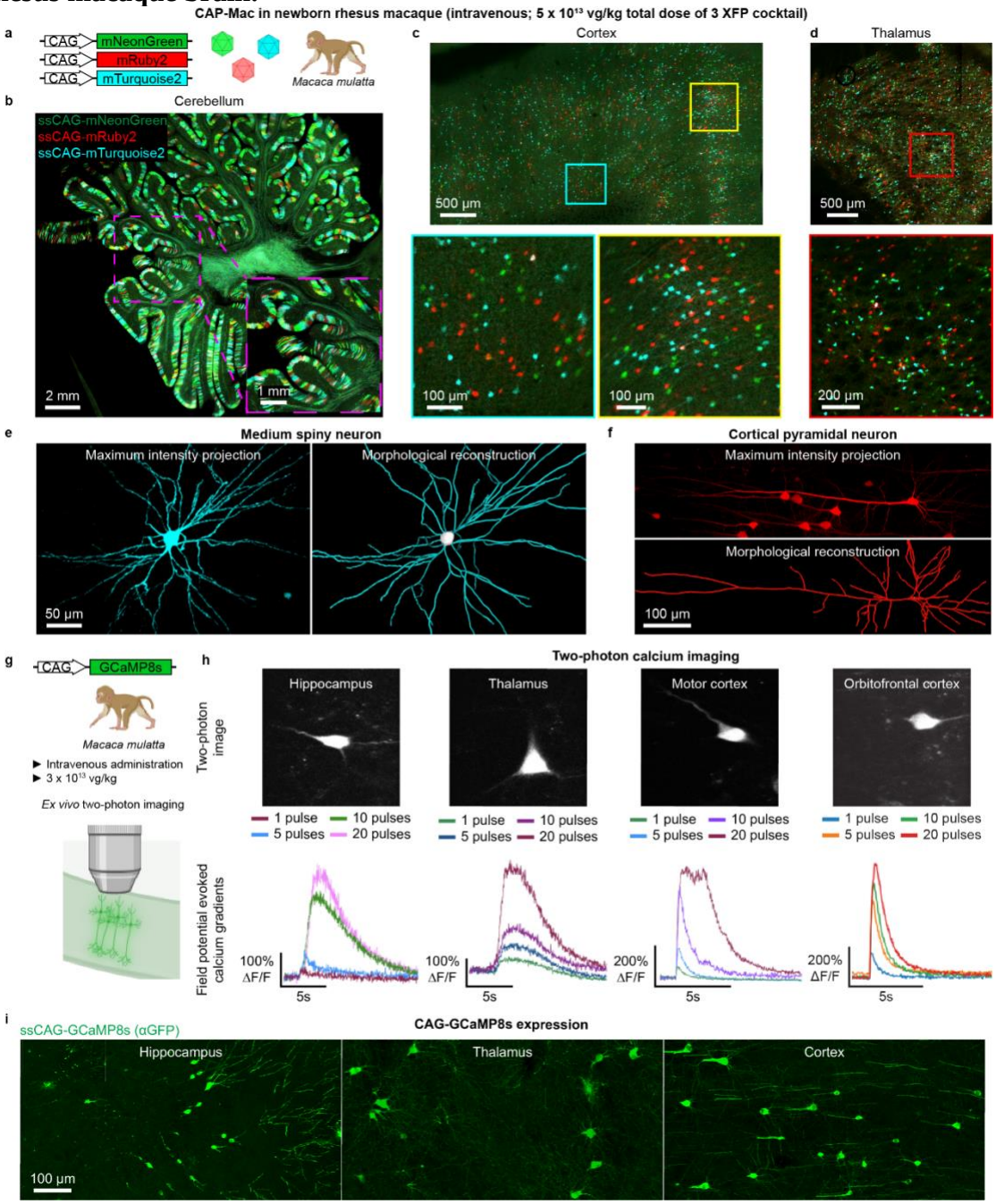

Fig. 3.2: Experimental utility of CAP-Mac for interrogation of the newborn rhesus macaque brain. a-f, CAP-Mac packaging three

fluorescent reporters (**a**) to generate Brainbow-like labeling in rhesus macaque cerebellum (**b**), cortex (**c**), and thalamus (lateral geniculate nucleus) (**d**), enabling morphological reconstruction of neurons (**e** and **f**). **g-i,** Non-invasive delivery of ssCAG-GCaMP8 using CAP-Mac (**g**) for *ex vivo* two-photon imaging (**h**) and brain-wide GCaMP expression (**i**).

3.6 Discussion

The overarching goal of these experiments was to define and disseminate a suite of genetic tools to study the NHP brain, especially in Old World primates. This includes characterizing cargo that can be delivered by CAP-Mac, as both self and non-self proteins (e.g., GFP) are known to be immunogenic in certain contexts[100–103]. To that end, we describe two functional cargos for studying the Old World primate brain: (1) a cocktail of three fluorescent reporters for Brainbow-like[98,99] labeling, and (2) GCaMP8s for optical interrogation of *ex vivo* neuronal activity. Encouragingly, our GCaMP recordings demonstrate that cells expressing CAP-Mac-delivered molecular sensors are physiologically active and healthy in *ex vivo* rhesus macaque slices. To our knowledge, this is the first description of using a non-invasive, systemic vector to deliver genetically-encoded sensors to the macaque brain, a transformational technique previously limited to rodents. Notably, none of the rhesus macaques dosed in this study experienced adverse events or abnormal liver function and assessment by an independent pathologist confirmed that the vectors were administered safely (Supplementary Fig. 3.6 and Supplementary Table 3.1). Moving forward, we expect CAP-Mac-mediated gene transfer to help

illuminate circuit connectivity and neuronal function in the macaque brain[104,105] and, more generally, assist major efforts such as the BRAIN Initiative[97] to understand the inner workings of the primate CNS.

3.7 Methods

Rodent AAV characterization

All rodent procedures were performed at Caltech under protocol 1738, approved by the Caltech IACUC. We purchased C57BL/6J (strain #: 000664; RRID: IMSR_JAX:000664), BALB/cJ (strain #: 000651; RRID: IMSR_JAX:000651), and DBA/2J (strain #: 000671; RRID: IMSR_JAX:000671) mice (all males, 6–8 weeks old) from The Jackson Laboratory. For IV administration in mice, we delivered 5 x 10^{11} vg of virus through the retro-orbital sinus[85,106] using a 31 G insulin syringe (BD, 328438). See protocols.io for more details on retro-orbital injections of AAV in mice (DOI: 10.17504/protocols.io.3byl4joy8lo5/v1). For intracerebroventricular (ICV) administration in mice, we injected 5 x 10^{10} or 1.5 x 10^{11} vg into the lateral ventricle. Briefly, we anesthetized mice using isoflurane (5% for induction, 1-3% for maintenance) with 95% O_2/5% CO_2 (1 L/min) and mice were head-fixed in a stereotaxic frame. After shaving the head and sterilizing the area with chlorohexidine, we administered 0.05 mL of 2.5 mg/mL bupivacaine subcutaneously, and a midline incision was made and the skull was cleaned of blood and connective tissue. After leveling the head, burr holes were drilled above the lateral ventricles bilaterally (0.6 mm posterior to bregma, 1.15 mm from the midline). Viral

vectors were aspirated into 10 µL NanoFil syringes (World Precision Instruments) using a 33-guage microinjection needle, and the needle was slowly lowered into the lateral ventricle (1.6 mm from the pial surface). The needle was allowed to sit in place for approximately 5 min and 3-5 µL of viral vector was injected using a microsyringe pump (World Precision Instruments, UMP3) and pump controller (World Precision Instruments, Mircro3) at a rate of 300 nL/min. All mice received 1 mg/kg of buprenorphine SR and 5 mg/kg of ketoprofen subcutaneously intraoperatively and 30 mg/kg of ibuprofen and 60 mg/kg of trimethoprim/ sulfamethoxazole (TMPS) for 5 days post-surgery. See protocols.io for more details on ICV injections of AAV in mice (DOI: 10.17504/protocols.io.5qpvorm4dv4o/v1). After 3 weeks of expression, all mice were perfused with PBS and fixed in 4% paraformaldehyde (PFA). All organs were extracted, incubated in 4% PFA overnight, transferred into PBS supplemented with 0.01% sodium azide, and stored at 4˚C for long-term storage. We sliced the brain into 100 µm sections with a vibratome (Leica Biosystems, VT1200S), mounted in Prolong Diamond Antifade (Invitrogen, P36970), and imaged using a confocal microscope (Zeiss, LSM 880) using Zen (Black edition). See protocols.io for more details on tissue handling (DOI: 10.17504/protocols.io.5qpvormddv4o/v1 and 10.17504/protocols.io.j8nlkwxxwl5r/v1).

Individual characterization of CAP-Mac in rhesus macaques

The details of the procedures in this section can be found on protocols.io (DOI: 10.17504/protocols.io.5qpvormddv4o/v1 and 10.17504/protocols.io.j8nlkwxxwl5r/v1).

Neonate macaques were perfused with PBS and 4% PFA. The brain was sectioned into 4 mm coronal blocks and all tissue was post-fixed in 4% PFA for 3 days before storage in PBS. The single adult macaque used for *in vivo,* individual characterization (RM-020; 17 years old, 11 kg) was perfused with RNase-free PBS, and one half-hemisphere was flash-frozen and the other sectioned into 4 mm coronal blocks and post-fixed in 4% PFA. All tissue was transferred to Caltech for further processing. Brains and liver were sectioned into 100 μm slices using vibratome. Additionally, sections of brain and spinal cord were incubated in 30% sucrose overnight and embedded in Optimal Cutting Temperature Compound (Scigen, 4586) and sectioned into 50 μm slices using a cryostat (Leica Biosystems, CM1950). All slices were mounted using Prolong Diamond Antifade and imaged using a confocal microscope. For GFP staining of spinal cord and brain slices from the ICM-administered macaque, we incubated slices with chicken anti-GFP (1:500; Aves Labs, cat # GFP-1020; RRID: AB_10000240), performed 3-5 washes with PBS, incubated with donkey anti-chicken IgY (1:200; Jackson ImmunoResearch Lab, cat # 703-605-155; RRID: AB_2340379), and washed 3-5 times before mounting. We diluted all antibodies and performed all incubations using PBS supplemented with 0.1% Triton X-100 (Sigma-Aldrich, T8787) and 10% normal donkey serum (Jackson ImmunoResearch, 017-000-121) overnight at room temperature with shaking.

For morphological reconstruction, we sectioned brains into 300 μm sections and incubated them in refractive index matching solution (RIMS)[107] for 72 hours before

mounting on a slide immersed in RIMS. We imaged using a confocal microscope and 25x objective (LD LCI Plan-Apochromat 25x/0.8 Imm Corr DIC) using 100% glycerol as the immersion fluid. We captured tiled Z-stacks (1024x1024 each frame using suggested capture settings) around cells of interest and cropped appropriate fields of view for tracing. Tracing was done in Imaris (Oxford Instruments) using semi-automated and automated methods.

For neuron (NeuN) and astrocyte (S100β) quantification, slices were stained using anti-NeuN (EPR12763) antibody (1:200; Abcam, cat. # ab177487; RRID: AB_2532109) or anti-S100β antibody (1:200; Abcam, cat. # ab52642; RRID: AB_882426) overnight in PBS supplemented with 0.1% Triton X-100 and 10% normal donkey serum. Slices were washed 3-5 times with PBS and incubated overnight in anti-rabbit IgG antibody conjugated with Alexa Fluor 647 (1:200; Jackson ImmunoResearch Labs, cat. # 711-605-152; RRID: AB_2492288) in PBS + 0.1% Triton X-100 + 10% normal donkey serum. After 3-5 washes and mounting using Prolong Diamond Antifade, we obtained z-stacks using a confocal microscope and a 25x objective. We segmented NeuN and XFP-positive cells using custom scripts in Python and Cellpose (https://www.cellpose.org/)[108].

Ex vivo two-photon imaging

Brain slices of sizes suitable for imaging were prepared with a thickness of 400 µm from larger slices using a vibratome and stored in artificial cerebrospinal fluid bubbled

with carbogen gas before two-photon imaging, as previously described[109,110]. For testing GCaMP8s responses, electrical stimulation (4-5 V, 80 Hz, 0.3 second duration) with the indicated number of pulses was delivered using an extracellular monopolar electrode placed 100-200 μm away from the neuron imaged. The frame rate of imaging was 30 Hz. Traces of segmented ROIs were plotted as $\Delta F/F_0 = (F(t) - F_0)/F_0$, where F_0 is defined as the average of all fluorescence value before the electrical stimulation. The rise time was defined as the time required for the rising phase of the signal to reach from 10% of the peak to 90% of the peak. The decay time constant was obtained by fitting sums of exponentials to the decay phase of the signal. The signal-to-noise ratio (SNR) was obtained by dividing the peak amplitude of the signal by the standard deviation of the fluorescence trace before the electrical stimulation.

Green monkey experiments

All green monkey (*Chlorocebus sabaeus*) procedures were performed at Virscio, Inc. and approved by their IACUC. All monkeys were screened for neutralizing antibodies and confirmed to have < 1:5 titer. At approximately 7-8 months of age (1-1.3 kg), monkeys were dosed intravenously (see Supplementary Table 3.2 for details). Dose formulations were allowed to equilibrate to approximately room temperature for at least 10 minutes, but no more than 60 minutes prior to dosing. IV dose volumes were based on Day 0 body weights. Animals were sedated with ketamine (8 mg/kg) and xylazine (1.6 mg/kg). The injection area was shaved and prepped with chlorohexidine and 70% isopropyl alcohol,

surgically scrubbed prior to insertion of the intravenous catheter. Dosing occurred with a single intravenous infusion of AAV (7.5×10^{13} or 7.6×10^{13} vg/kg) on Day 0 via a saphenous vein administered using a hand-held infusion device at a target rate of 1 mL/minute. General wellbeing was confirmed twice daily by cage-side observation beginning one week prior to dosing. At the scheduled sacrifice time, monkeys were sedated with ketamine (8-10 mg/kg IM) and euthanized with sodium pentobarbital (100 mg/kg IV to effect). Upon loss of corneal reflex, a transcardiac perfusion (left ventricle) was performed with chilled phosphate buffered saline (PBS) using a peristaltic pump set at a rate of approximately 100 mL/min until the escaping fluid ran clear prior to tissue collection. Cubes of tissue were collected from the left brain hemisphere and various other organs and frozen in the vapor phase of liquid nitrogen for further processing for biodistribution. The right brain hemisphere was removed and cut into ~4 mm coronal slices and post-fixed intact with approximately 20 volumes of 10% neutral-buffered formalin (NBF) for approximately 24 hours at room temperature.

Genomic DNA was extracted from CNS and peripheral tissues using the ThermoFisher MagMax DNA Ultra 2.0 extraction kit (Catalog number: A36570). DNA was assessed for yield by fluorometric quantification with the Qubit dsDNA assay. Approximately 20 ng of DNA was loaded into each 20 μL reaction and plates were run on the BioRad CFX Connect Real-Time PCR Detection System (Catalog number: 1855201). The viral copy number assay was validated for specificity by detection of a single amplified

product, sensitivity by assessing the lower limit of detection to be greater than 10 copies per reaction, and linearity by ensuring the standard curve r^2 was > 0.95. Reactions were assembled in FastStart Universal SYBR Green Master (Rox) (catalogue number: 4913850001). The sequences of the primers were: forward "ACGACTTCTTCAAGTCCGCC," reverse "TCTTGTAGTTGCCGTCGTCC." The PCR protocol used an initial denaturation step of 95 ˚C for 180 seconds, followed by 40 cycles of 95 ˚C for 15 seconds, and 60 ˚C for 60 seconds, with an imaging step following each 60 ˚C cycle. A standard curve was generated with linearized plasmid containing the GFP template sequence present in the virus from 1e8-1e0 copies, diluted in naïve untreated macaque DNA samples prepared using an identical kit as the samples in this study to control for matrix effects. Copies of viral DNA were calculated from the standard curve using the equation for the line of the best fit. MOI values were calculated based on the measured total genomic weight of host cell DNA per reaction.

Post fixation, tissues were placed into 10% > 20% > 30% sucrose for 24 hours each at 4 ˚C then embedded in Optimal Cutting Temperature Compound and stored at -80 ˚C until cryosectioning. Tissue blocks were brought up to -20 ˚C in a cryostat before sectioning into 30 μm slices and dry-mounted onto slides after cryosectioning. After sectioning, the slides were left at room temperature overnight to dry. To assist in neuron quantification, we stained sections with the following antibodies and concentrations: rabbit anti-GFP (1:100; Millipore-Sigma, cat. # AB3080; RRID:AB_91337) and mouse anti-

NeuN (A60) (1:500; Millipore-Sigma, cat. # MAB377; RRID:AB_2298772). For secondary antibody staining, the following secondary antibodies and concentrations were used: donkey anti-rabbit Alexa Fluor 488 (1:500; Thermo Fisher Scientific, cat. # A-21206; RRID:AB_2535792) and donkey anti-mouse Alexa Fluor 647 (1:500; Thermo Fisher Scientific, cat. # A-31571; RRID:AB_162542). All antibodies were diluted with 1X PBS supplemented with 0.25% Triton X-100 (PBST) and 5% normal donkey serum. Primary antibody incubations were left overnight at room temperature. Sections were then washed with PBST. Secondary antibody incubations were 2 hours at room temperature. The sections were washed 3x in PBST. Sections were incubated in DAPI solution (1:10,000; Invitrogen, D1306) at room temperature for 5 minutes, then washed. Sections were coverslipped using Prolong Diamond Antifade.

3 sections per animal were stained and imaged. Each section was imaged in triplicate with each ROI having a total of 9 images. Tissue ROIs were imaged with a Keyence BZ-X800 with the following acquisition parameters: GFP (1/500 s), Cy5 (1 s), DAPI (1/12 s), High Resolution, Z-stack at 1.2 um pitch. The following brain subregions were imaged frontal, parietal, temporal, occipital cortices, cerebellum, caudate, putamen, and thalamus (medial, ventral lateral, and ventral posterior nuclei). A semi-automated cell counting method was performed using ImageJ for quantification. Using thresholds and particle analysis, we quantified NeuN positive and DAPI positive cells. Using ImageJ's cell counter, we manually counted GFP-positive and GFP & NeuN double-positive cells.

3.8 Supplementary data

Supplementary Figure 3.1: Tropism in rodents and utilizing mice as a model organism for cargo validation

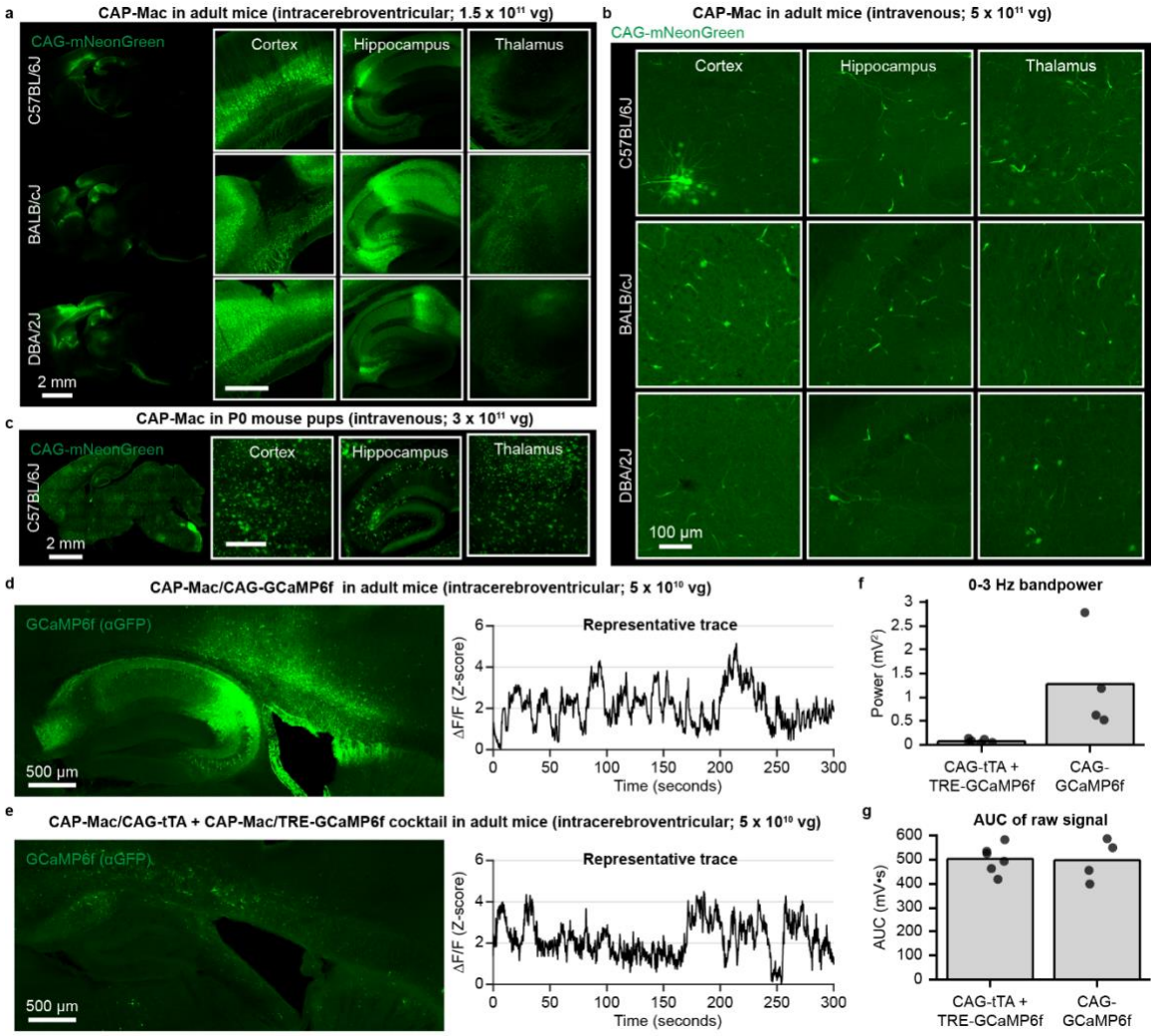

Supplementary Fig. 3.1: Tropism in rodents and utilizing mice as a model organism for cargo validation. a, CAP-Mac after intracerebroventricular (ICV) administration in adult mice primarily transduces neurons, mimicking the CAP-Mac tropism in infant Old World primates after intravenous (IV) administration. **b**, CAP-Mac after IV administration in C57BL/6J, BALB/cJ, and DBA/2J adult mice primarily

transduces vasculature, with no apparent differences between the three mouse strains. **c**, CAP-Mac in P0 C57BL/6J pups after intravenous administration transduces various cell-types, including neurons, astrocytes, and vasculature. **d-g,** Given the neuronal tropism of CAP-Mac via ICV administration, we validated GCaMP cargo in mice prior to non-human primate experiments, testing either one-component or two-component systems. **d**, **e**, GCaMP protein expression and representative ΔF/F traces in mice after delivering CAG-GCaMP6f (n=2 mice) (**d**) or a CAG-tTA/TRE-GCaMP6f cocktail (n=3 mice) using CAP-Mac. **f**, **g**, To determine cargo to move forward with, we found that 0-3 Hz bandpower (two-tailed Welch's t-test, P=0.105) (**f**), but not area under the curve (AUC; **g;** two-tailed Welch's t-test, P=0.626) was indicative of cargo performance.

Supplementary Figure 3.2: CAG-XFP co-localization with cell-type specific histological markers.

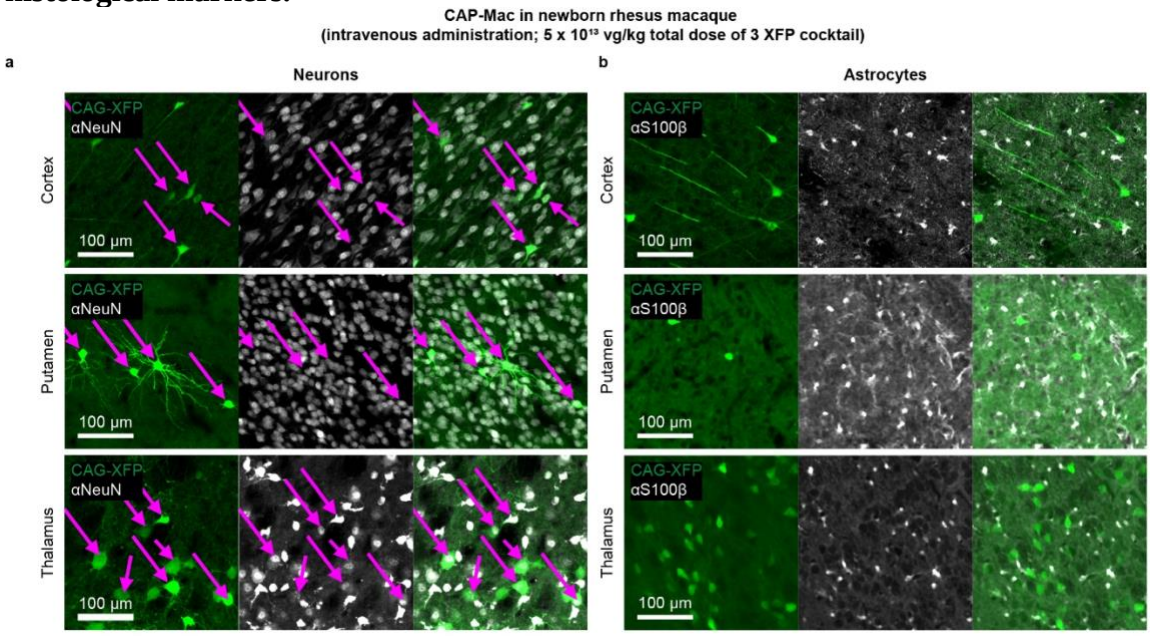

Supplementary Fig. 3.2: CAG-XFP co-localization with cell-type specific histological markers. a, **b**, Representative images of a cocktail

of 3 fluorescent proteins under control of CAG in newborn rhesus macaque tissue with histological markers for neurons (NeuN, **a**) and astrocytes (s100β, **b**). Cells that are positive for both fluorescent protein and histological marker are shown with a purple arrow. Fluorescent proteins are identically pseudo-colored.

Supplementary Figure 3.3: Administering AAV via intra-cisterna magna administration.

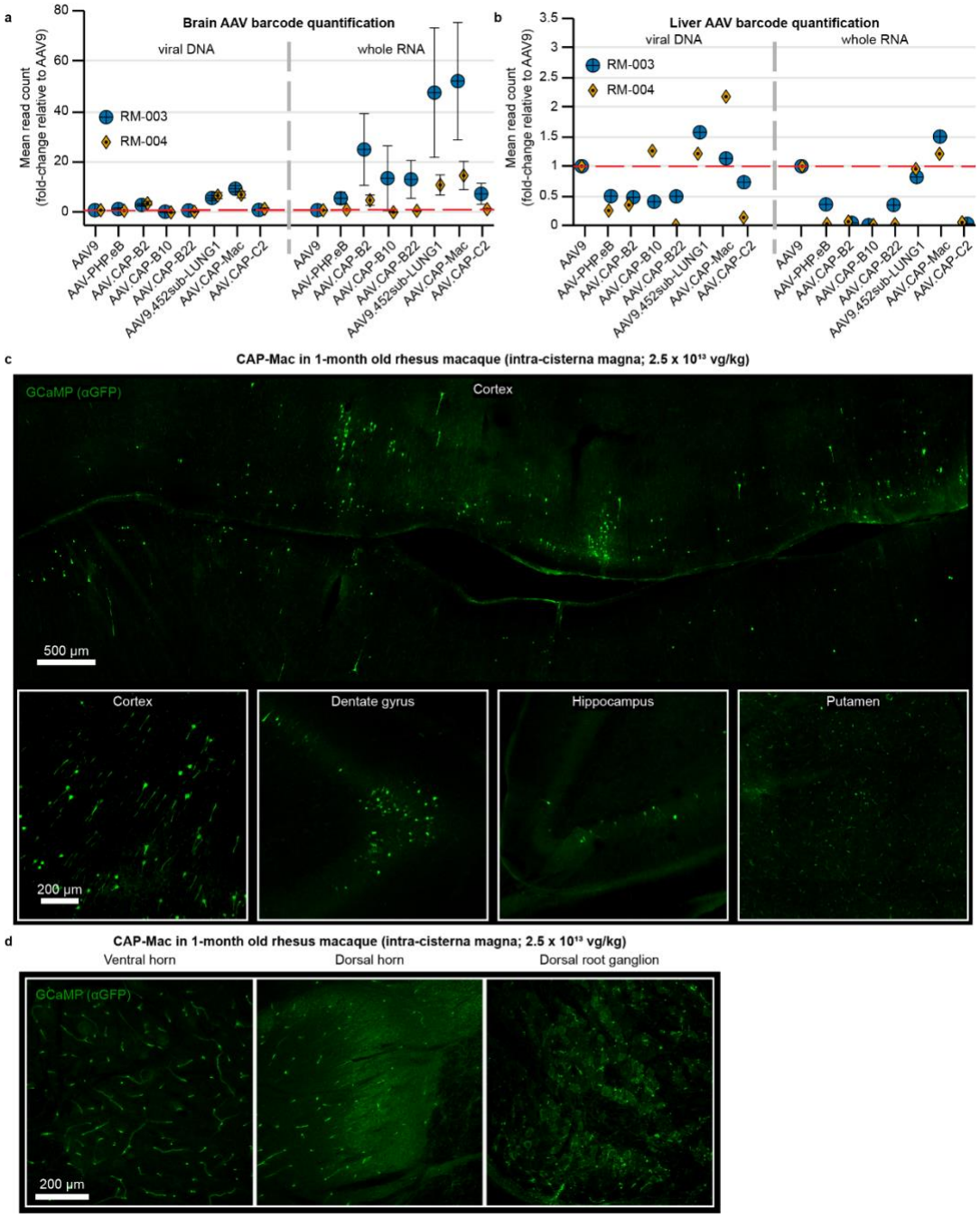

Supplementary Fig. 3.3: Administering AAV via intra-cisterna magna administration. a, **b**, Barcode quantification in viral DNA and whole

RNA from brain (**a**) and liver (**b**) of neonate rhesus macaques (n=2 macaques) treated with a capsid pool via intra-cisterna magna administration. Mean ± s.e.m. shown. **c**, **d**, CAG-GCaMP7s expression in brain (**c**) and spinal cord (**d**) after intra-cisterna magna administration puncture administration using AAV.CAP-Mac.

Supplementary Figure 3.4: CAG-XFP expression in non-brain tissue of Old World primates treated with AAV.

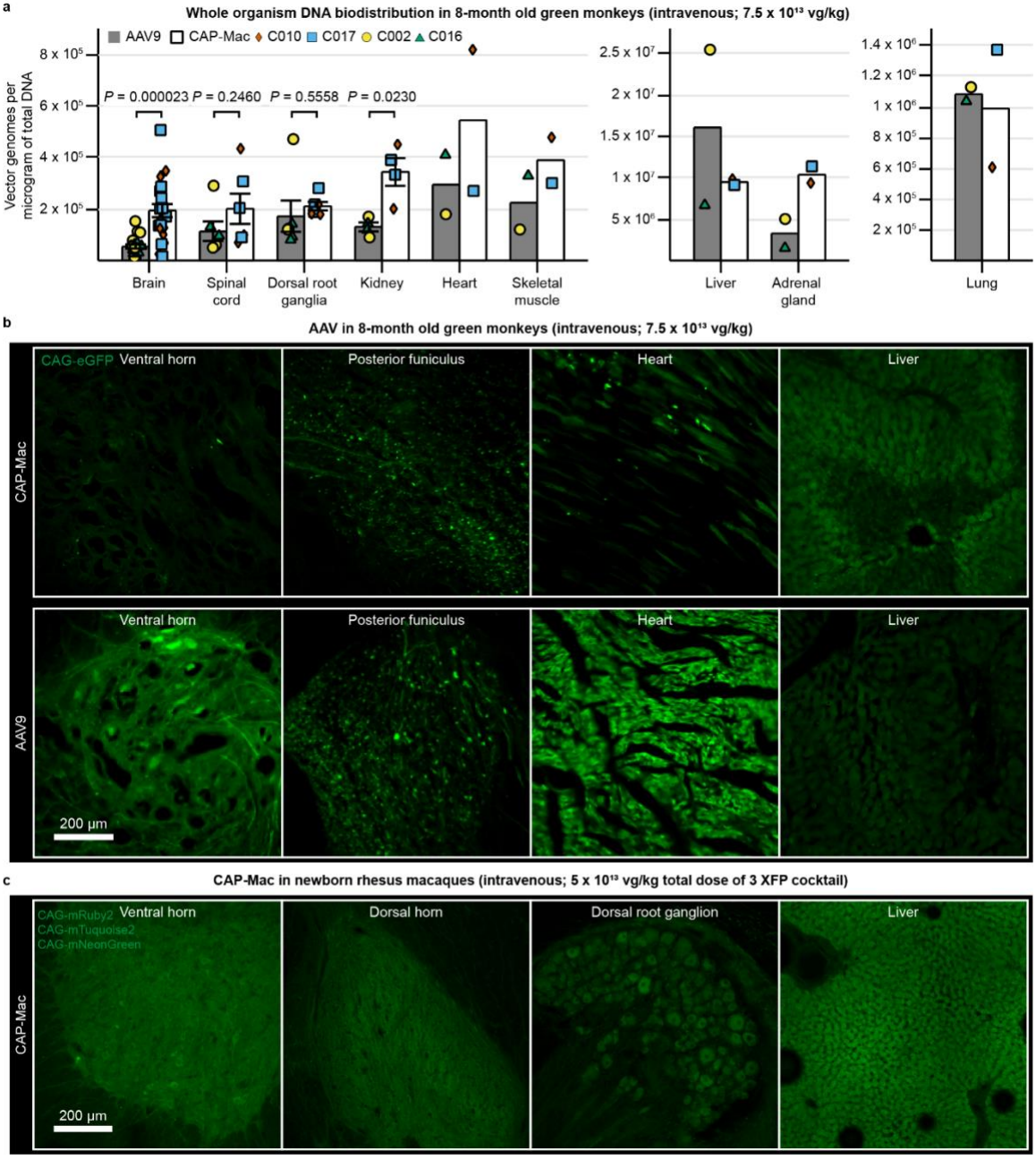

Supplementary Fig 3.4: CAG-XFP expression in non-brain tissue of Old World primates treated with AAV. a, Vector genomes per microgram of total DNA in green monkeys treated with AAV9 (n=2_green

monkeys) or CAP-Mac (n=2 green monkeys), expressed as fold-change relative to mean AAV9. Each data point represents measured vector genomes per microgram of total DNA in a section of tissue from each region and monkey. Mean ± s.e.m. shown. Two-tailed Welch's t-test. **b**, CAG-eGFP expression in the spinal cord, heart, and liver of green monkeys after intravenous expression of either CAP-Mac (top) or AAV9 (bottom). **c**, CAG-XFP expression in the spinal cord, dorsal root ganglia, and liver of newborn rhesus macaque after intravenous administration of CAP-Mac packaging a cocktail of 3 CAG-XFPs. XFPs are pseudocolored identically.

Supplementary Figure 3.5: Group-level analyses of two-photon calcium imaging in rhesus macaque slice.

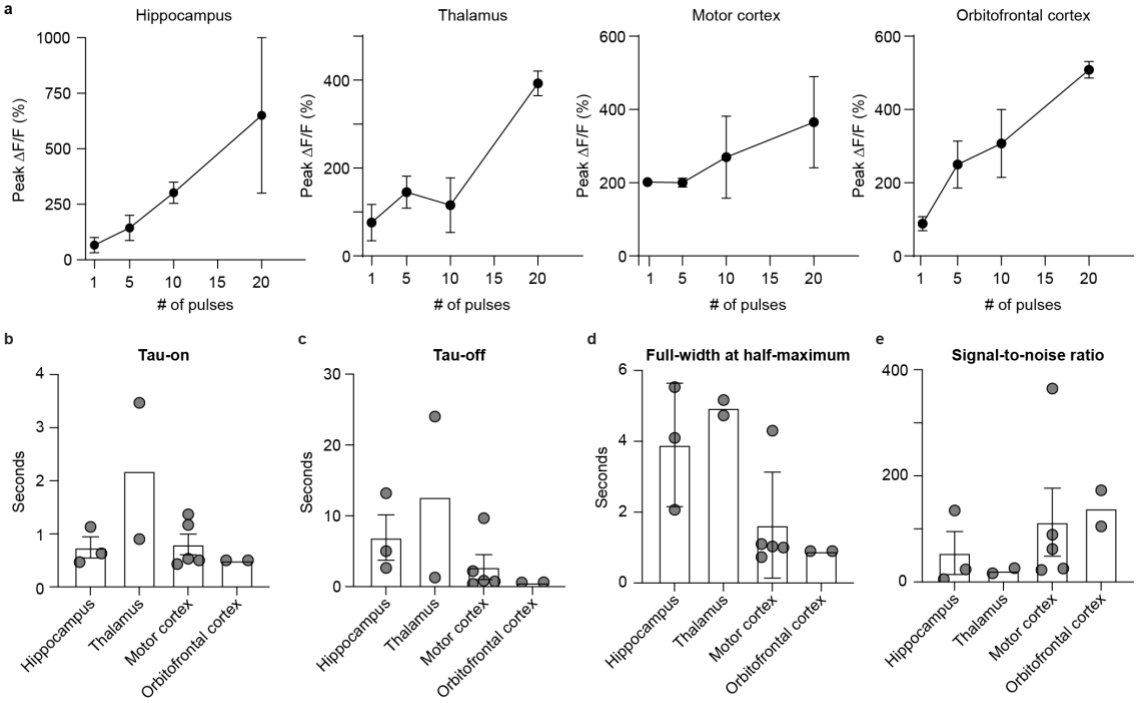

Supplementary Fig. 3.5: Group-level analyses of two-photon calcium imaging in rhesus macaque slice. a, Mean Peak $\Delta F/F_0$ evoked by cells from hippocampus, thalamus, motor cortex, and orbitofrontal cortex, after

applying different number of pulses. **b**, Mean rise time of GCaMP8s responses in the four brain regions. Rise time is defined as time taken for the response to rise from 10% to 90% of the peak of the amplitude. **c**, Mean decay time constant of GCaMP8s responses in the four brain regions. Decay time constant was obtained by fitting sums of exponentials to the decay phase of the traces. **d**, Mean full width at half maximum (FWHM) of GCaMP8s responses in the four brain regions. **e**, Mean signal-to-noise ratio (SNR) of GCaMP8s responses in the four brain regions. SNR is defined as the peak amplitude divided by the standard deviation of the fluorescence signal before the electrical stimulation. Hippocampus: n=3 cells. Thalamus: n=2. Motor cortex: n=5 cells. Orbitofrontal cortex: n=2 cells. Data is plotted as mean ± s.e.m.

Supplementary Figure 3.6: Liver function tests in newborn rhesus macaques treated with AAV.

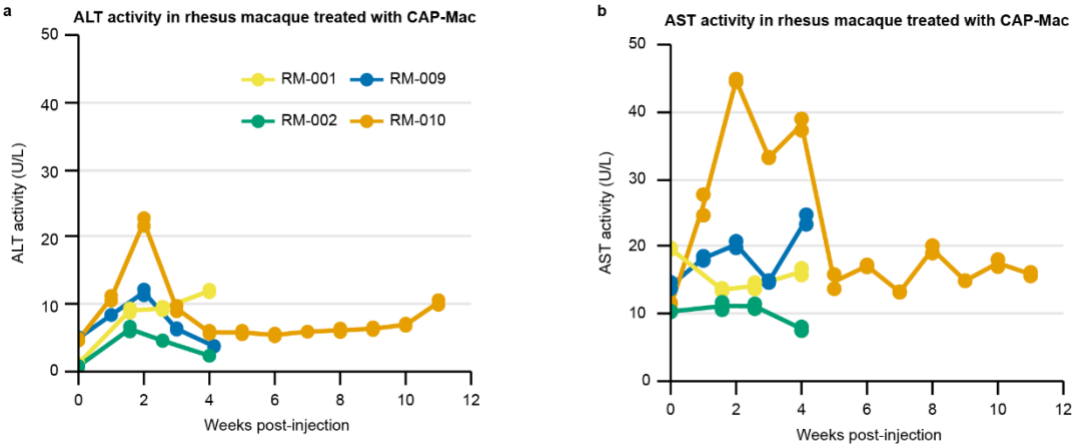

Supplementary Fig. 3.6: Liver function tests in newborn rhesus macaques treated with AAV. a, **b**, Liver function tests show no abnormal signs of adverse liver functionality, as measured by alanine transaminase (ALT; **a**) and aspartate transaminase (AST; **b**) activity.

Supplementary Table 3.1: Assessment of tissue by an independent pathologist.

Animal ID	Capsid	Cargo	Route of administration	Tissue	Degeneration score	Inflammation score
RM-001	8 capsid pool*	CAG-FXN-HA-Barcode	Intravenous	Brain	1	-
RM-002	8 capsid pool*	CAG-FXN-HA-Barcode	Intravenous	Brain	0	1
RM-009	AAV.CAP-Mac	CAG-mNeonGreen, CAG-mRuby2, CAG-mTurquoise2 cocktail	Intravenous	Brain	0	0
				Liver	0	1
				Kidney	0	0
				Spinal cord & dorsal root ganglia	0	0
RM-010	AAV.CAP-Mac	CAG-mNeonGreen, CAG-mRuby2, CAG-mTurquoise2 cocktail	Intravenous	Brain	1	1
RM-010				Liver	0	1
RM-010				Kidney	0	0
RM-010				Spinal cord & dorsal root ganglia	1	1

**8 capsid pool consisted of AAV9, PHP.eB, 452sub-LUNG1, CAP-B2, CAP-B10, CAP-B22, CAP-Mac, CAP-C2.*

Degeneration and inflammation were scored on a scale from 0 (no observed pathology) to 5.

Supplementary Table 3.2: Green monkey information for individual characterization of CAP-Mac.

Green monkey ID	Age (days)	Sex	Route of administration	Capsid	Cargo	Weight at injection (kg)	Total dose (vg/kg)	Expression length (days)
C010	200	Male	Intravenous	AAV.CAP-MAC	CAG-EGFP	1.18	7.5×10^{13}	36
C017	172	Male	Intravenous	AAV.CAP-MAC	CAG-EGFP	1.32	7.6×10^{13}	36
C002	215	Male	Intravenous	AAV9	CAG-EGFP	1.31	7.5×10^{13}	36
C016	178	Male	Intravenous	AAV9	CAG-EGFP	1.02	7.6×10^{13}	37

All experiments were performed at Virscio, Inc.

Chapter 4

OPPORTUNITIES FOR FURTHER CAPSID ENGINEERING

Chuapoco MR*, Flytzanis NC*, Goeden N, Octeau J, Roxas K, Chan K, Scherrer J, Winchester J, Blackburn R, Campos L, Man KN, Sun J, Chen X, Lefevre A, Singh V, Arokiaraj C, Miles T, Vendemiatti J, Jang M, Mich J, Bishaw Y, Gore B, Omstead V, Taskin N, Weed N, Levi BP, Ting J, Miller C, Deverman B, Pickel J, Tian L, Fox A, Gradinaru V. Intravenous functional gene transfer throughout the brain of non-human primates using AAV. Nature Nanotechnology. PMID: 36789432. *Authors contributed equally

4.1 Insights from AAV.CAP-Mac across species

Infant NHPs offer several logistical advantages for AAV characterization. For instance, they are more likely to be seronegative for neutralizing AAV antibodies, and their smaller body weight requires less vector to be produced for a given dose. While the mammalian BBB is fully formed by birth—including intact tight junctions which give rise to the BBB's unique functionality to limit passive molecular transport into the brain—dynamic molecular and cellular processes occurring during development may make the BBB more permissive[111–114]. We therefore wanted to characterize CAP-Mac's tropism in adult macaque to determine tropism differences across developmental stages. To further

de-risk our characterization, we first chose to test CAP-Mac in adult rhesus macaque slices *ex vivo* (Fig. 4.1a). In the gray matter of cultured cortical slices, cargo delivered by CAP-Mac, but not AAV9, co-localized with NeuN+ cells, consistent with our previous results (Fig. 4.1b). Unexpectedly, only 9% as many CAP-Mac viral genomes were recovered as AAV9 genomes, but 3.6-fold more viral transcripts were recovered from CAP-Mac-treated slices than from AAV9-treated slices (Fig. 4.1c).

Figure 4.1: Characterization in adult rhesus macaque.

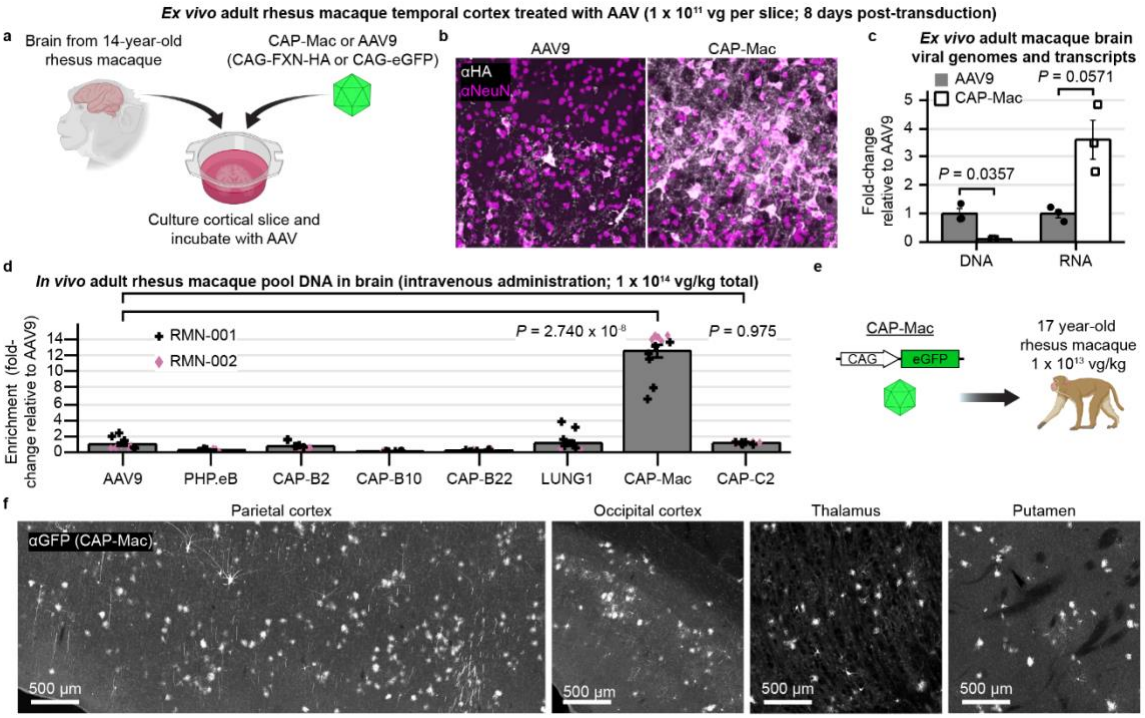

Fig. 4.1: Characterization in adult rhesus macaque. a, AAV in *ex vivo* cortical slice taken from a 14-year-old rhesus macaque. **b**, CAP-Mac is more efficient at transducing neurons in gray matter of cortex. **c**, Quantification demonstrates that CAP-Mac-delivered transgene produces more RNA but not DNA compared to AAV9-delivered transgene. n=3

brain slices. Two-tailed Welch's t-test. **d-f**, AAV in adult rhesus macaques *in vivo*. **d**, Recovered DNA from adult macaque administered with an 8-capsid pool (7.5×10^{13} vg/kg). n=12 brain samples from 2 adult macaques. One-way ANOVA using Tamhane's T2 correction tested against AAV9 enrichment. **e**, We intravenously injected 1×10^{13} vg of CAP-Mac packaging a CAG-eGFP into a 17-year-old rhesus macaque via the saphenous vein to assess CAP-Mac protein expression in the adult macaque. **g**, CAP-Mac-mediated eGFP expression visualized after amplification with GFP antibody. Mean ± s.e.m. shown.

While informative, *ex vivo* characterization does not assess BBB penetration, so we next tested CAP-Mac in adult macaques *in vivo*. We injected two adult rhesus macaques with the same AAV pool that we used in infants and found that CAP-Mac-delivered genomes were 13-fold more abundant in the brain than AAV9 (Fig. 4.1d). Again, the variants originally selected in mice were all less efficient than AAV9, but CAP-C2 was 1.2-fold more efficient than AAV9. To further assess protein expression, we injected CAP-Mac packaging CAG-eGFP (1×10^{13} vg/kg total dose via the saphenous vein) into a 17-year-old adult rhesus macaque (Fig. 4.1e). At the protein level, we observed CAP-Mac-delivered eGFP expression (visualized via eGFP antibody amplification) in parts of the cortex and thalamus, while eGFP expression was absent in other regions of the brain.

Finally, since CAP-Mac was originally identified using *in vivo* selections in the adult common marmoset, we also wanted to characterize the vector in the selection species. As in the adult macaque experiment, we injected CAP-Mac and AAV9 into adult

marmosets (3.8 and 5.8 years old). To our surprise, we found that the tropism of CAP-Mac in adult marmoset was biased primarily towards the GLUT1+ vasculature (Fig. 4.2), consistent with our results in adult mice.

Figure 4.2: CAP-Mac tropism in adult common marmoset compared to AAV9.

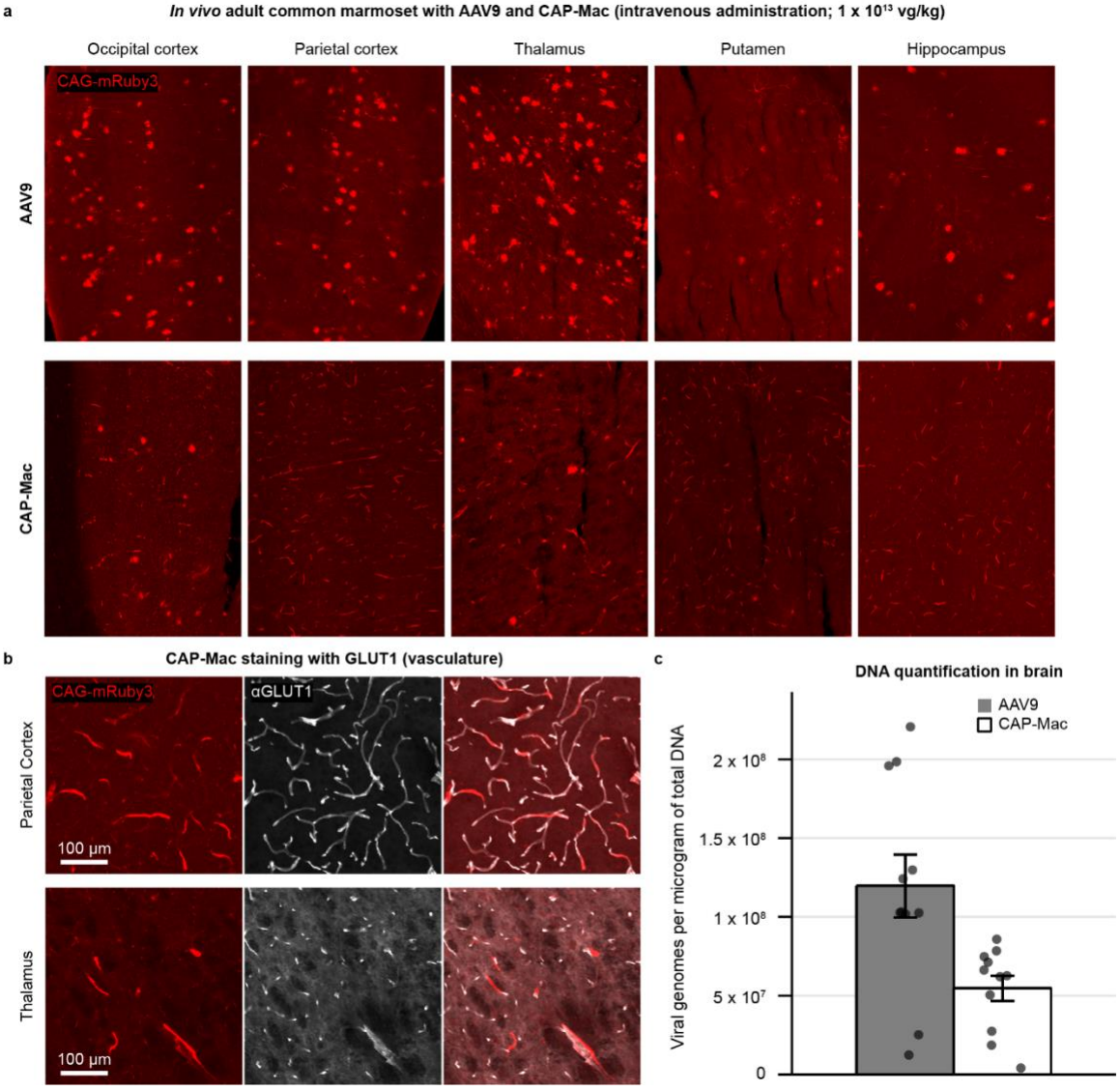

Fig. 4.2: CAP-Mac tropism in adult common marmoset compared to AAV9. a, AAV9 and CAP-Mac tropism in two adult marmosets *in vivo* (3.8- and 5.8-years-old). **b**, CAP-Mac is biased primarily towards GLUT1+ cells (vasculature), consistent with our results in adult mice. **c**, Recovered viral genomes in adult marmoset brain (n=2 marmosets). Mean ± s.e.m. shown. Two-tailed Welch's t-test, P=0.00981.

By comprehensively characterizing CAP-Mac in multiple rodent strains and NHP species, across ages and administration routes, we found that CAP-Mac tropism varies depending on species, developmental state, and route of administration (Table 4.1). This is not surprising given the heterogeneity of the BBB across species and populations[115–117]. Performing such a comprehensive characterization of CAP-Mac in multiple contexts was beneficial for two reasons. First, we discovered that CAP-Mac was primarily biased towards the brain endothelium in the adult marmoset, to our knowledge the first description of a systemic vector that targets the vasculature in adult marmosets. Second, by testing alternative routes of administration in mice, we found that CAP-Mac tropism is shifted towards neurons after ICV administration, mirroring the tropism in newborn macaques and giving us a method to assess expression and functional activity of GCaMP configurations before applying them to NHPs (Supplementary Fig. 3.1). In lieu of a cross-species capsid with conserved tropism and efficiency in rodents and NHPs, this approach can be a valuable tool for users to validate capsid-cargo combinations in mice prior to use in NHPs. Nonetheless, the varied tropism of AAV.CAP-Mac across different species and developmental states highlights the challenge of finding a truly translational AAV capsid, an observation that has been noted in other studies that have used both NHPs and rodents for selection[118–120].

Table 4.1: Summary of CAP-Mac neuro-tropism in multiple species.

Species	Strain or colony of origin	Developmental stage	Route of administration	Cellular tropism
Mus musculus	C57BL/6J (The Jackson Laboratory)	P0	Intravenous (temporal vein)	Non-specific (astrocytes, neurons, vasculature)
Mus musculus	C57BL/6, BALB/cJ, DBA/2J (The Jackson Laboratory)	Adult (6-8 weeks)	Intravenous (retro-orbital sinus)	Vasculature
Mus musculus	C57BL/6, BALB/cJ, DBA/2J (The Jackson Laboratory)	Adult (6-8 weeks)	Intracerebroventricular (lateral ventricle)	Neuronal
Callithrix jacchus	UC San Diego (La Jolla, CA)	Adult	Intravenous (saphenous vein)	Vasculature
Macaca mulatta	California National Primate Research Center (Davis, CA)	Infant	Intravenous (saphenous vein)	Neuronal
Macaca mulatta	California National Primate Research Center (Davis, CA)	Infant	Intra-cisterna magna	Neuronal
Chlorocebus sabaeus	Virscio (St. Kitts)	Infant	Intravenous (saphenous vein)	Neuronal
Macaca mulatta	California National Primate Research Center (Davis, CA)	Adult	Intravenous (saphenous vein)	Astrocyte-biased

Given the efficacy of CAP-Mac in penetrating the brain of infant Old World primates and motivated by our observation that CAP-Mac primarily transduces neurons, we wanted to test whether CAP-Mac offered any improvement over its parent capsid, AAV9, in transducing human neurons. We differentiated cultured human-derived induced

pluripotent stem cells (iPSCs) into mature neurons (Fig. 4.3a) and incubated them with CAP-Mac or AAV9 packaging ssCAG-eGFP at doses ranging from 0 vg/cell to 10^6 vg/cell. We found that eGFP expression was noticeably increased in CAP-Mac-administered cultures compared to AAV9-administered cultures (Fig. 4.3b). AAV9 transduction achieved an efficiency of $EC_{50}=10^{4.68}$ vg/cell, while CAP-Mac achieved $EC_{50}=10^{3.03}$ vg/cell (Fig. 4.3c), a 45-fold increase in potency (P=0.0023 using two-tailed Welch's t-test). Average per-cell eGFP expression measured across transduced cells fit a biphasic step function, with CAP-Mac reaching the first plateau at a dose roughly two orders of magnitude lower than AAV9 (Fig. 4.3d). Overall, the increased potency of CAP-Mac in transducing mature human neurons *in vitro* is consistent with the neuronal tropism we observed in infant Old World primates, suggesting a similar mechanism of neuronal transduction across species.

In addition to CAP-Mac's utility as a tool to study the primate brain, it is also a compelling potential delivery vehicle for genetic medicine in humans. It provides an unprecedented opportunity to deepen our understanding of pharmacodynamics in Old World primate models[59,121,122] and its broad and uniform distribution throughout the CNS opens access to subcortical and midbrain regions for neuroscience researchers, currently difficult in NHPs[68–72]. Additionally, CAP-Mac's enhanced transduction of cultured human neurons supports the potential of using engineered AAVs as a gene-delivery vehicle in humans. Overall, the success of the capsid engineering approach we describe here offers a

roadmap for developing the next class of translational gene therapies with improved safety and efficacy profiles.

Figure 4.3: CAP-Mac is more potent in human cultured neurons compared to AAV9.

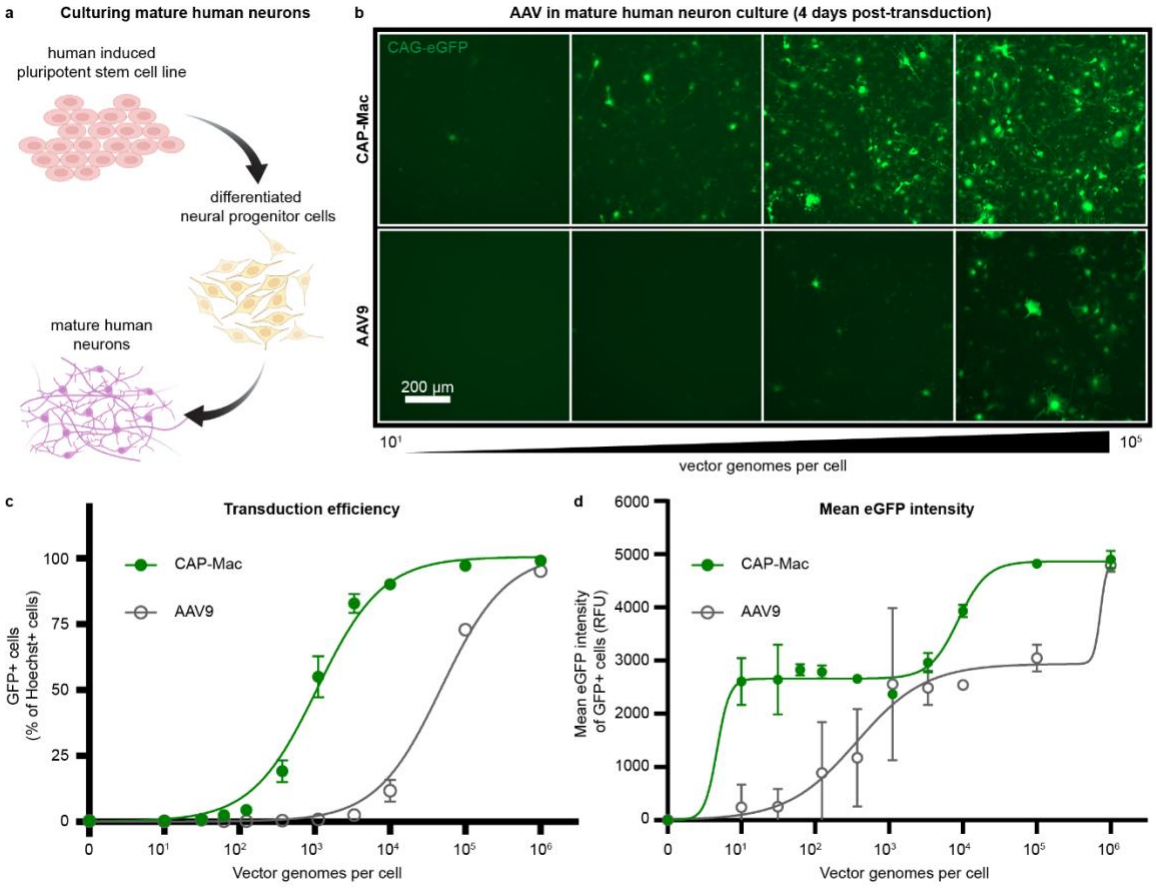

Fig. 4.3: CAP-Mac is more potent in human cultured neurons compared to AAV9. a, Differentiation process starting with a human induced pluripotent stem cell line that was differentiated into neural progenitor cells, which were further differentiated into mature neurons. **b**, Representative images of cultured human neurons after 4 days of incubation with either CAP-Mac (top) or AAV9 (bottom) packaging ssCAG-eGFP across 4 doses of AAV, ranging from 10^2-10^4 vector

genomes per cell. **c**, **d**, Dose response curves of AAV9 (n=3 biologically independent replicates) and CAP-Mac (n=3 biologically independent replicates) in mature human neuron cultures measuring transduction efficiency (**c**) and mean eGFP intensity (**d**). Mean ± s.e.m. shown.

4.2 Receptor-orphan AAV capsids as parent capsids for further evolution

There is concern about the safety of high dose systemic AAV following reports of adverse hepatotoxicity[75,123] and several patient deaths in the clinic[14,124]. Natural AAV serotypes are characterized by a low therapeutic index and high effective dose, and as a result there is urgent need for more efficient—and thus safer—AAVs, particularly for the brain. In recent years, the field has focused on engineering novel capsids to address this problem, including mutagenesis at VRs outside of VR-VIII. The vectors AAV.CAP-B10/B22 contain mutations at both VR-VIII and VR-IV, and have de-targeted from the liver in mice[42]. However, many of these vectors still target other tissue that are of concern for toxicity, such as the dorsal root ganglia[125].

VR-I of the AAV9 capsid plays an integral role in cell-recognition and initiation of cell transduction, as it is situated near the galactose binding domain and has also been implicated in AAVR binding for multiple serotypes[44–46]. We propose here the idea of an "orphan capsid," which lacks a natural cognate receptor because of mutations that break interactions with galactose and AAVR binding due to mutations in VR-I of the AAV9 capsid. Because of VR-I and VR-VIII are found on non-interacting regions of the AAV9

capsid, this opens the opportunity for additive, orthogonal engineering at these two VRs (Fig. 4.4a).

Orphan capsids were identified following by engineering a 7mer substation in AA263-AA269 of the AAV9 capsid (VP1 numbering). After generating the capsid library and selecting variants using M-CREATE, we made the observation that there were a number of variants that were high producers but were not found in any tissue during selections. We hypothesized that these high producing variants were deficient in their ability to enter cells but could be re-functionalized by additional engineering at VR-VIII. Several groups have identified the GPI-anchored surface protein Ly6a to be the cognate receptor for PHP.eB and the main effector responsible for giving PHP.eB its brain penetrating tropism in mice[87,88]. We first cloned and produced the top producing orphan capsid from our VR-I selections, N1, as well as the N1+PHP.eB variant. Consistent with our NGS results from our M-CREATE selections, N1 failed to transduce HEK293 cells, but could be re-functionalized, as the N1+PHP.eB variant expressed mNeonGreen in HEK293 cells expressing Ly6a (Fig. 4.4b). This re-functionalization extended to Ai14 mice *in vivo*, a Cre-reporter mouse line that expresses tdTomato after delivery and expression of Cre (Fig. 4.4c-d)[126,127]. The N1+PHP.eB variant primarily transduced the endothelium of the blood-brain-barrier, as Ly6a is known to be expressed on the luminal surface of the vasculature[87]. Interestingly, the vasculature-biased tropism of N1+PHP.eB

is consistent with results using PHP.eB in AAVR knockout mice, suggesting a similar mechanism of the vasculature-biased tropism[88].

Figure 4.4: Re-directing the orphan capsid N1 using the PHP.eB-Ly6a pair.

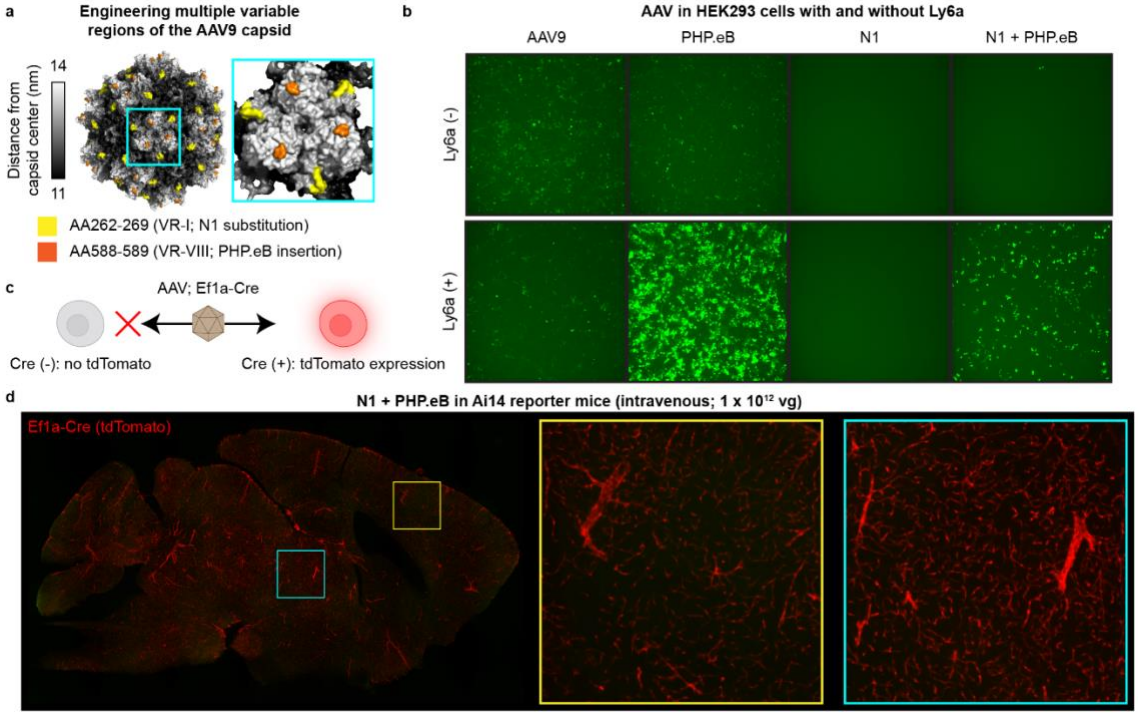

Fig. 4.4: Re-directing the orphan capsid N1 using the PHP.eB-Ly6a pair. **a**, VR-I and VR-VIII on the AAV9 capsid occupy distinct regions of the capsids surface that are non-interacting. **b**, AAV in HEK293 cells with and without Ly6a. Only variants that are expressing the PHP.eB insertion in VR-VIII demonstrate an increase in transduction efficiency in cells that are expressing Ly6a. **c**, Ai14 reporter mice can be used to detect AAV transduction, as the delivery and expression of Cre-recombinase via AAV catalyzes tdTomato expression in Cre-positive cells. **d**, The N1+PHP.eB variant transduces primarily vasculature in Ai14 reporter mice.

4.3 Methods

Marmoset AAV characterization

The details of the procedures in this section can be found on protocols.io (DOI: 10.17504/protocols.io.5qpvormddv4o/v1 and 10.17504/protocols.io.j8nlkwxxwl5r/v1). Two adult common marmosets (*Callithrix jacchus*) were used for this experiment: Conan (male, 2.8 years old, 0.386 kg) and Sandy (female, 5.8 years old, 0.468 kg; see Supplementary Table 4.2 for more details). They were housed under standard conditions of 27 °C and 50% humidity, with ad libitum access to food and water. All animals were group housed, and experiments were performed in the Cortical Systems and Behavior Laboratory at University of California San Diego (UCSD). All experiments were approved by the UCSD IACUC under protocol S09147. The day before infusion, the animals' food was removed. Animals were anesthetized with ketamine (Ketaset, Zoetis 043-304, 20mg/kg), the skin over the saphenous vein was shaved and sanitized with an isopropanol scrub, and 2 x 10^{13} vg/kg of AAV was infused over 5 minutes. The animals were monitored until they became active, upon which they were returned to their cages. Activity and behavior were closely monitored over the next 3 days, with daily observations thereafter. At 31 days post-injection, marmosets were anesthetized with ketamine as described earlier and then euthanized (Euthasol, Virbac 200-071, 1mL/kg) and perfused with 1X PBS. Brains and organs were cut in half, and one half was flash-frozen in 2-methylbutane (Sigma Aldrich, M32631), chilled with dry ice, and stored at −80 °C. The other half was fixed in

4% PFA (Thermo Scientific, J19943-K2) overnight and then stored at 4 °C in PBS-Azide (Sigma Aldrich, S2002-100G, 0.025%). Samples were then shipped to California Institute of Technology (Caltech) for analysis. For GLUT1 staining, we incubated slices with rabbit anti-GLUT1 (1:200; Millipore-Sigma, cat. # 07-1401; RRID: AB_1587074), performed 3-5 washes with PBS, incubated with donkey anti-rabbit IgG (1:200; Jackson ImmunoResearch Labs, cat. # 711-605-152; RRID: AB_2492288), and washed 3-5 times before mounting. We diluted all antibodies and performed all incubations using PBS supplemented with 0.1% Triton X-100 (Sigma-Aldrich, T8787) and 10% normal donkey serum (Jackson ImmunoResearch Labs, cat. # 017-000-121; RRID: AB_2337258) overnight at room temperature with shaking.

Supplementary Table 4.2: Marmoset information for dual-injection characterization of CAP-Mac.

Marmoset ID	Age (years)	Sex	Route of administration	Capsid*	Cargo*	Weight at injection (kg)	Total dose (vg/kg)	Expression length (days)
Sandy	5.8	Female	Intravenous	(1) AAV9 (2) AAV.CAP-Mac	(1) CAG-eGFP (2) CAG-mRuby3	0.468	2×10^{13}	31
Conan	2.8	Male	Intravenous	(1) AAV.CAP-Mac (2) AAV9	(1) CAG-eGFP (2) CAG-mRuby3	0.386	2×10^{13}	31

All experiments were performed in the Cortical Systems and Behavior Laboratory at UCSD.
**Numbers in "Capsid" and "Cargo" column correspond to capsid-cargo pairs for each dual injection.*

Induced pluripotent stem cell (iPSC) experiments

Neuronal cultures were produced by differentiating and maturing iPSC-derived neural progenitor cells with Stemdiff™ Forebrain Differentiation and Maturation kits (StemCell #08600, #08605 respectively), according to their manufacturer's protocols.

Neural progenitor cells were produced by differentiation of the foreskin fibroblast-derived iPSC line: ACS™-1019 (ATCC# DYS-0100), with Stemdiff™ SMADi Neural Induction kits (StemCell l#08581), selection with Stemdiff™ Neural Rosette Selection Reagent (StemCell l#05832), and expansion in Stemdiff™ Neural Progenitor Media (StemCell l#05833), according to their manufacturer's protocols. Neurons were matured a minimum of 8 days prior to replating for transduction.

Mature neuronal cultures, seeded 15,000 cells/well in polyornithine and laminin coated black-walled 96 well optical plates, were cultured an additional 4 days prior to transduction. Replicate wells were transduced with virus serially diluted across six orders of magnitude in 90% maturation media and 10% OptiproSFM. 4 days post-transduction, cultures were fixed with 4% paraformaldehyde and counterstained with 1 ug/ml Hoechst 33322. Identification of transduced cells was determined by imaging 60 fields/well, using two channel fluorescence detection (Hoechst at ex386/em440, eGFP ex485/em521) on a CellInsight CX5 HCS Platform. Individual cells were identified by Hoechst detection of their nuclei and applying size and contact constrained ring masks to each cell. Cell transduction was determined by measuring eGFP fluorescence above a threshold level within an individual ring mask. For each population, the percentage of transduced cells was plotted vs the applied dose. Curve-fits and EC_{50} values were determined with a Prism GraphPad [agonist] vs response (three parameter) regression method. To report per-cell eGFP expression efficiencies, the eGFP spot fluorescence intensities were averaged from

each ring mask across a minimum of 5,000 cells/well. Curve fits were obtained using the Prism GraphPad Biphasic, X as concentration regression method.

Adult rhesus macaque slice characterization experiments

One adult rhesus macaque (14 years and 1 month; 10.83 kg) from the Washington National Primate Research Center was planned for routine euthanasia, and the brain was collected as part of the facility's Tissue Distribution Program. A block of the superior temporal gyrus was sectioned into 300 μm slices and slices were recovered[109] and cultured on an air-liquid membrane interface[128] as previously described. Approximately 30 minutes after plating slices, we administered 1-2 μL of AAV (5 x 10^{13} vg/mL of AAV9 or AAV.CAP-Mac packaging either ssCAG-FXN-HA or ssCAG-eGFP). Experiments were performed in biological triplicates for each condition and culture medium was refreshed every 48 hours until tissue collection at 8 days post-transduction. On the day of tissue collection, the slices were imaged to confirm transduction, slices were cut in half, and each half-slice was flash-frozen in a dry ice-ethanol bath. Samples were stored at -20 ˚C until further processing.

Each half-slice was processed (one each for DNA and RNA recovery). DNA was isolated using the Qiagen DNeasy Blood and Tissue Kit (Qiagen, catalog # 69504) and RNA was recovered using TRIzol (Thermo Fisher Scientific, catalog #15596026) and the PureLink RNA Mini Kit (Thermo Fisher Scientific, catalog # 12183018A). DNA was

removed from the RNA sample by modifying the first wash of the PureLink RNA Mini Kit as follows: wash with 350 uL of Wash Buffer 1, then add 80 uL of RNase-Free DNaseI in RDD buffer (Qiagen catalog # 79254) and incubate the column at room temperature for 15 minutes, then wash again with 350 uL of Wash Buffer 1 before proceeding with the protocol. We performed first-strand cDNA synthesis from 400 ng total RNA in 20 uL reactions using Promega GoScript Reverse Transcription Kit (Promega, catalog # A5000).

We then evaluated vector genomes and viral transcripts found in each sample using quantitative qPCR on a Roche Lightcycler II. 100 ng of DNA was used in a 20 uL amplification reaction using TaqMan probes from Thermo Fisher Scientific (EGFP-FAM probe, Assay ID Mr04097229_mr, catalog #4331182; custom genomic reference probe CN2386-2-VIC, Assay ID ARH6DUK, catalog #4448512, designed to target both *Macaca mulatta* and *Macaca nemestrina*).

Chapter 5

CONCLUSIONS

We describe here the identification and characterization of AAV.CAP-Mac, an AAV9-derived capsid that is biased towards neurons in infant Old World primates after systemic, intravenous administration. This neuronal tropism is conserved in two Old World primate species, the rhesus macaque (*Macaca mulatta*) and green monkey (*Chlorocebus sabaeus*), and we leverage CAP-Mac's ability to cross the BBB in infant Old World primates for non-invasive delivery of genetically encoded sensors. Namely, we used CAP-Mac to deliver a cocktail of fluorescent reporters for Brainbow-like, morphological labeling of neurons as well as delivery of GCaMP8s to record intracellular calcium gradients in macaque neurons *ex vivo*. This represents one of the first known instances of non-invasive, somatic cell gene delivery to the non-human primate brain for functional interrogation.

Up until the writing of this dissertation, few options existed for genetic perturbation of Old World primates, such as the rhesus macaque. While recent advances in gene-editing technologies have simplified germline engineering, the long gestational periods and lifespans of macaques have made it difficult to generate entire colonies of transgenic animals. Several groups have developed genetically engineered NHPs, however none have

been generated past the F1 offspring[129,130]. Additionally, while the clinical benefit of germline gene-editing is clear, many concerns still exist regarding the ethical use of germline editing. Any technological and methodological advances that bring germline modifications closer to human patients (i.e., genetically modified NHPs) need to be approached with cautious optimism, prudent oversight, and consensus within the scientific community[131,132]. Given the lack of options for and the ethical concerns of germline engineering in NHPs, AAV-mediated somatic cell gene-delivery offers an attractive alternative to genetically perturb more complex animal models. The success of CAP-Mac and other capsids that show efficacy in the NHP brain provide a blueprint for developing a toolbox of novel viral vectors that access a variety of cell-types in the NHP with genetic precision. To maximize the scientific community's ability to study the NHP brain, future AAV engineering efforts should focus on optimizing the following properties: (1) shared mechanism of crossing the BBB across mice and NHP, (2) increased efficiency in the brain and de-targeting from peripheral tissue (e.g., liver and DRG), and (3) access to additional cell-types in the brain.

By comprehensively characterizing CAP-Mac in various species, across developmental states, and via multiple routes of administration, we found that CAP-Mac tropism in the brain is highly dependent on all three variables. Importantly, intravenous CAP-Mac tropism was consistently neuronal in infants of two Old World primate species but was biased towards astrocytes in the adult macaque. Additionally, CAP-Mac tropism

shifted towards brain vasculature in the adult mouse and the adult marmoset. In lieu of a readily available transgenic NHPs, mouse transgenic lines will remain a vital tool to understanding the innerworkings of the brain, especially as it pertains to understanding disease biology. As such, future capsids should strive to be true "translational" AAV vectors with conserved mechanism of crossing the BBB across species.

Despite CAP-Mac's neuronal bias, it still only transduces a low percentage of neurons (approximately 1%). As such, there is still much work to be done to increase the efficiency of gene transfer in the brain—in both infant and adult NHPs. In the case of the CAP-Mac biological recording demonstrations shown here, sparse gene expression in neurons was a feature, as both two-photon microscopy and morphological reconstructions benefit from non-overlapping expression of transgene to identify single cells for recording or tracing, respectively. However, in addition to *ex vivo* single-cell methods of measuring biological activity that we used in the CAP-Mac experiments, many insights can be drawn from population level recordings and perturbations of the brain *in vivo*. For example, optogenetic studies that modulate animal behavior will require dense, widespread opsin expression in a specific brain region to observe the behavior-level changes that are commonly observed in rodent optogenetics experiments. In addition to increasing transduction efficiency in the brain, engineering efforts should focus on simultaneously de-targeting AAV capsids from non-target tissue, especially those that are known to be susceptible to vector-associated toxicity (i.e., the liver and the DRGs). While strategies

exist to reduce transgene expression in these tissues using micro-RNA targeting sites, long-term solutions should focus on developing highly specific vectors that only enter a defined cell-type of interest, as there AAVs have limited packaging capacity and not every off-target tissue may have a well-defined and specific micro-RNA to reduce transgene expression.

While neurons are known to be the primary functional unit of the brain for information processing, non-neuronal subtypes are known to play a critical role in the pathogenesis of disease, highlighting just one justification to target non-neuronal subtypes[133]. Again, cell-type specificity may be partially addressed using cell-type specific promoter and enhancer elements, with the same drawbacks as micro-RNA targeting sites (i.e., AAVs have limited packaging capacity and not every tissue and cell-type has well-defined enhancers to perfectly restrict expression).

To achieve these future engineering goals, several strategies exist that build on the first iteration of engineered capsids. While the earliest selection methodologies select for capsid library variants using DNA as the surrogate output, several strategies now exist that probe library variants on the level of RNA expression[77,134]. Recently, several groups have also done significant work to identify the specific receptors that are mechanistically responsible for the neurotropic properties of engineered variants[88,135]. Given the need for a conserved mechanism across species, this is an attractive method for further engineering.

Additionally, some groups have begun to use machine learning to identify interesting regions of the capsids that are amenable to further evolution[136,137]. Given the current revolution of AI and machine learning, applying these computational methods for AAV development is an appealing strategy. One potential avenue of engineering that has yet to be explored may combine computational methods with receptor-guided engineering methods by designing *de novo* protein-protein interactions between AAVs and receptors[138]. Nonetheless, AAV.CAP-Mac and similar capsids represent the pivotal first step of engineered gene-delivery carriers that are both vital tools that inform our understanding of the inner workings of the mammalian brain and vital therapies that hold the power to completely cure genetic disorders. It is thus imperative that capsid development continues to build on the body of work of today, to help make the future tools and therapies of tomorrow a reality.

BIBLIOGRAPHY

1. Rogers S. Induction of arginase in rabbit epithelium by the Shope rabbit papilloma virus. Nature. 1959 Jun 27;183(4678):1815–6. PMID: 14438381
2. Rogers S. Shope papilloma virus: A passenger in man and its significance to the potential control of the host genome. Nature. 1966 Dec 10;212(5067):1220–2. PMID: 21090446
3. Terheggen HG, Schwenk A, Lowenthal A, Van Sande M, Colombo JP. Argininemia with arginase deficiency. Lancet. 1969 Oct 4;294(7623):748–749. PMID: 4186193
4. Friedmann T, Roblin R. Gene therapy for human genetic disease? Science. 1972 Mar 3;175(4025):949–55. PMID: 5061866
5. Satoh PS, Yoshida TO, Ito Y. Studies on the arginase activity of Shope papilloma: possible presence of isozymes. Virology. 1967 Oct;33(2):354–6. PMID: 6053146
6. Orth G, Vielle F, Changeux JP. On the arginase of the Shope papillomas. Virology. 1967 Apr;31(4):729–32. PMID: 6022698
7. Terheggen HG, Lowenthal A, Lavinha F, Colombo JP, Rogers S. Unsuccessful trial of gene replacement in arginase deficiency. Zeitschrift fur Kinderheilkunde. 1975;119(1):1–3. PMID: 164740
8. Friedmann T. Gene Therapy: Fact and Fiction in Biology's New Approaches to Disease. Friedmann T, editor. 1982.
9. Blaese RM, Culver KW, Miller AD, Carter CS, Fleisher T, Clerici M, Shearer G, Chang L, Chiang Y, Tolstoshev P, Greenblatt JJ, Rosenberg SA, Klein H, Berger M, Mullen CA, Ramsey WJ, Muul L, Morgan RA, Anderson WF. T lymphocyte-directed gene therapy for ADA- SCID: Initial trial results after 4 years. Science. 1995 Oct 20;270(5235):475–80. PMID: 7570001
10. Gene Therapy Clinical Trials Worldwide [Internet]. The Journal of Gene Medicine. 2022. Available from: https://a873679.fmphost.com/fmi/webd/GTCT
11. Mendell JR, Al-Zaidy S, Shell R, Arnold WD, Rodino-Klapac LR, Prior TW, Lowes L, Alfano L, Berry K, Church K, Kissel JT, Nagendran S, L'Italien J, Sproule DM, Wells C, Cardenas JA, Heitzer MD, Kaspar A, Corcoran S, Braun L, Likhite S, Miranda C, Meyer K, Foust KD, Burghes AHM, Kaspar BK. Single-dose gene-replacement therapy for spinal muscular atrophy. The New England Journal of Medicine. 2017 Nov 2;377(18):1713–1722. PMID: 29091557

12. Russell S, Bennett J, Wellman JA, Chung DC, Yu ZF, Tillman A, Wittes J, Pappas J, Elci O, McCague S, Cross D, Marshall KA, Walshire J, Kehoe TL, Reichert H, Davis M, Raffini L, George LA, Hudson FP, Dingfield L, Zhu X, Haller JA, Sohn EH, Mahajan VB, Pfeifer W, Weckmann M, Johnson C, Gewaily D, Drack A, Stone E, Wachtel K, Simonelli F, Leroy BP, Wright JF, High KA, Maguire AM. Efficacy and safety of voretigene neparvovec (AAV2-hRPE65v2) in patients with RPE65-mediated inherited retinal dystrophy: A randomised, controlled, open-label, phase 3 trial. Lancet. 2017 Aug 26;390(10097):849–860. PMID: 28712537
13. Harrison C. High-dose AAV gene therapy deaths. Nature Biotechnology. 2020 Aug;38(8):910–910. PMID: 32760027
14. Morales L, Gambhir Y, Bennett J, Stedman HH. Broader implications of progressive liver dysfunction and lethal sepsis in two boys following systemic high-dose AAV. Molecular Therapy. 2020 Aug 5;28(8):1753–1755. PMID: 32710826
15. Verma IM. A tumultuous year for gene therapy. Molecular Therapy. 2000 Nov;2(5):415–6. PMID: 11082313
16. Enquist LW, Card JP. Recent advances in the use of neurotropic viruses for circuit analysis. Current Opinion in Neurobiology. 2003 Oct;13(5):603–6. PMID: 14630225
17. Loewy AD. Viruses as transneuronal tracers for defining neural circuits. Neuroscience and Biobehavioral Reviews. 1998 Oct;22(6):679–84. PMID: 9809303
18. Davidson BL, Breakefield XO. Viral vectors for gene delivery to the nervous system. Nature Reviews Neuroscience. 2003 May;4(5):353–64. PMID: 12728263
19. Lentz TB, Gray SJ, Samulski RJ. Viral vectors for gene delivery to the central nervous system. Neurobiology of Disease. 2012 Nov;48(2):179–88. PMID: 22001604
20. Rose JA, Berns KI, Hoggan MD, Koczot FJ. Evidence for a single-stranded adenovirus-associated virus genome: Formation of a DNA density hybrid on release of viral DNA. Proceedings of the National Academy of Sciences. 1969 Nov 1;64(3):863–9. PMID: 5264145
21. Atchison RW, Casto BC, Hammon WM. Adenovirus-associated defective virus particles. Science. 1965 Aug 13;149(3685):754–756. PMID: 14325163
22. Hoggan MD, Blacklow NR, Rowe WP. Studies of small DNA viruses found in various adenovirus preparations: physical, biological, and immunological characteristics. Proceedings of the National Academy of Sciences. 1966 Jun 1;55(6):1467–1474. PMID: 5227666
23. Maes ME, Colombo G, Schulz R, Siegert S. Targeting microglia with lentivirus and AAV: Recent advances and remaining challenges. Neuroscience Letters. 2019 Aug 10;707:134310. PMID: 31158432

24. Campos LJ, Arokiaraj CM, Chuapoco MR, Chen X, Goeden N, Gradinaru V, Fox AS. Advances in AAV technology for delivering genetically encoded cargo to the nonhuman primate nervous system. Current Research in Neurobiology. 2023 Apr;4:100086.
25. Betley JN, Sternson SM. Adeno-associated viral vectors for mapping, monitoring, and manipulating neural circuits. Human Gene Therapy. 2011 Jun;22(6):669–77. PMID: 21319997
26. Bedbrook CN, Deverman BE, Gradinaru V. Viral strategies for targeting the central and peripheral nervous systems. Annual Review of Neuroscience. 2018;41:323–348. PMID: 29709207
27. Deverman BE, Ravina BM, Bankiewicz KS, Paul SM, Sah DWY. Gene therapy for neurological disorders: Progress and prospects. Nature Reviews Drug Discovery. 2018 Sep;17(9):641–659. PMID: 30093643
28. Hudry E, Vandenberghe LH. Therapeutic AAV gene transfer to the nervous system: A clinical reality. Neuron. 2019 Mar 6;101(5):839–862. PMID: 30844402
29. Wang D, Tai PWL, Gao G. Adeno-associated virus vector as a platform for gene therapy delivery. Nature Reviews Drug Discovery. 2019;18(5):358–378. PMID: 30710128
30. Meyer NL, Chapman MS. Adeno-associated virus (AAV) cell entry: Structural insights. Trends in Microbiology. 2022 May;30(5):432–451. PMID: 34711462
31. Pillay S, Meyer NL, Puschnik AS, Davulcu O, Diep J, Ishikawa Y, Jae LT, Wosen JE, Nagamine CM, Chapman MS, Carette JE. An essential receptor for adeno-associated virus infection. Nature. 2016;530(7588):108–112. PMID: 26814968
32. Pillay S, Zou W, Cheng F, Puschnik AS, Meyer NL, Ganaie SS, Deng X, Wosen JE, Davulcu O, Yan Z, Engelhardt JF, Brown KE, Chapman MS, Qiu J, Carette JE. Adeno-associated virus (AAV) serotypes have distinctive Interactions with domains of the cellular AAV receptor. Journal of Virology. 2017 Sep 15;91(18). PMID: 28679762
33. Xie Q, Bu W, Bhatia S, Hare J, Somasundaram T, Azzi A, Chapman MS. The atomic structure of adeno-associated virus (AAV-2), a vector for human gene therapy. Proceedings of the National Academy of Sciences. 2002 Aug 6;99(16):10405–10. PMID: 12136130
34. DiMattia MA, Nam HJ, Van Vliet K, Mitchell M, Bennett A, Gurda BL, McKenna R, Olson NH, Sinkovits RS, Potter M, Byrne BJ, Aslanidi G, Zolotukhin S, Muzyczka N, Baker TS, Agbandje-McKenna M. Structural insight into the unique properties of adeno-associated virus serotype 9. Journal of Virology. 2012 Jun;86(12):6947–58. PMID: 22496238
35. Li C, Samulski RJ. Engineering adeno-associated virus vectors for gene therapy. Nature Reviews Genetics. 2020 Apr;21(4):255–272. PMID: 32042148

36. Kotterman MA, Schaffer D V. Engineering adeno-associated viruses for clinical gene therapy. Nature Reviews Genetics. 2014 Jul;15(7):445–51. PMID: 24840552
37. Challis RC, Ravindra Kumar S, Chen X, Goertsen D, Coughlin GM, Hori AM, Chuapoco MR, Otis TS, Miles TF, Gradinaru V. Adeno-associated virus toolkit to target diverse brain cells. Annual Review of Neuroscience. 2022 Jul 8;45(1):447–469. PMID: 35440143
38. Foust KD, Nurre E, Montgomery CL, Hernandez A, Chan CM, Kaspar BK. Intravascular AAV9 preferentially targets neonatal neurons and adult astrocytes. Nature Biotechnology. 2009;27(1):59–65. PMID: 19098898
39. Deverman BE, Pravdo PL, Simpson BP, Kumar SR, Chan KY, Banerjee A, Wu WL, Yang B, Huber N, Pasca SP, Gradinaru V. Cre-dependent selection yields AAV variants for widespread gene transfer to the adult brain. Nature Biotechnology. 2016 Feb 1;34(2):204–209. PMID: 26829320
40. Chan KY, Jang MJ, Yoo BB, Greenbaum A, Ravi N, Wu WL, Sánchez-Guardado L, Lois C, Mazmanian SK, Deverman BE, Gradinaru V. Engineered AAVs for efficient noninvasive gene delivery to the central and peripheral nervous systems. Nature Neuroscience. 2017 Jun 26;20(8):1172–1179. PMID: 28671695
41. Ravindra Kumar S, Miles TF, Chen X, Brown D, Dobreva T, Huang Q, Ding X, Luo Y, Einarsson PH, Greenbaum A, Jang MJ, Deverman BE, Gradinaru V. Multiplexed Cre-dependent selection yields systemic AAVs for targeting distinct brain cell types. Nature Methods. 2020;17(5):541–550. PMID: 32313222
42. Goertsen D, Flytzanis NC, Goeden N, Chuapoco MR, Cummins A, Chen Y, Fan Y, Zhang Q, Sharma J, Duan Y, Wang L, Feng G, Chen Y, Ip NY, Pickel J, Gradinaru V. AAV capsid variants with brain-wide transgene expression and decreased liver targeting after intravenous delivery in mouse and marmoset. Nature Neuroscience. 2022 Jan 9;25(1):106–115. PMID: 34887588
43. Chen X, Wolfe DA, Sivadasan Bindu D, Zhang M, Taskin N, Goertsen D, Shay TF, Sullivan E, Huang SF, Ravindra Kumar S, Arokiaraj CM, Plattner V, Campos LJ, Mich J, Monet D, Ngo V, Ding X, Omstead V, Weed N, Bishaw Y, Gore B, Lein ES, Akrami A, Miller C, Levi BP, Keller A, Ting JT, Fox AS, Eroglu C, Gradinaru V. Functional gene delivery to and across brain vasculature of systemic AAVs with endothelial-specific tropism in rodents and broad tropism in primates. bioRxiv. 2023 Jan 13;2023.01.12.523844. PMID: 36711773
44. Bell CL, Gurda BL, Van Vliet K, Agbandje-McKenna M, Wilson JM. Identification of the galactose binding domain of the adeno-associated virus serotype 9 capsid. Journal of Virology. 2012;86(13):7326–7333. PMID: 22514350
45. Jang S, Shen HK, Ding X, Miles TF, Gradinaru V. Structural basis of receptor usage by the engineered capsid AAV-PHP.eB. Molecular Therapy - Methods & Clinical Development. 2022 Sep 8;26:343–354. PMID: 36034770

46. Xu G, Zhang R, Li H, Yin K, Ma X, Lou Z. Structural basis for the neurotropic AAV9 and the engineered AAVPHP.eB recognition with cellular receptors. Molecular Therapy - Methods & Clinical Development. 2022 Sep 8;26:52–60. PMID: 35755945
47. Liguore WA, Domire JS, Button D, Wang Y, Dufour BD, Srinivasan S, McBride JL. AAV-PHP.B administration results in a differential pattern of CNS biodistribution in non-human primates compared with mice. Molecular Therapy. 2019;27(11):2018–2037. PMID: 31420242
48. Hordeaux J, Wang Q, Katz N, Buza EL, Bell P, Wilson JM. The Neurotropic Properties of AAV-PHP.B Are Limited to C57BL/6J Mice. Molecular Therapy. 2018;26(3):664–668. PMID: 29428298
49. Mitchell JF, Leopold DA. The marmoset monkey as a model for visual neuroscience. Neuroscience Research. 2015 Apr;93:20–46. PMID: 25683292
50. Phillips KA, Bales KL, Capitanio JP, Conley A, Czoty PW, 't Hart BA, Hopkins WD, Hu S lok, Miller LA, Nader MA, Nathanielsz PW, Rogers J, Shively CA, Voytko M Lou. Why primate models matter. American Journal of Primatology. 2014 Sep;76(9):801–27. PMID: 24723482
51. Preuss TM. Critique of pure marmoset. Brain, Behavior and Evolution. 2019;93(2–3):92–107. PMID: 31416070
52. Tarantal AF, Noctor SC, Hartigan-O'Connor DJ. Nonhuman primates in translational research. Annual Review of Animal Biosciences. 2022 Feb 15;10(1):441–468. PMID: 35167321
53. De A, El-Shamayleh Y, Horwitz GD. Fast and reversible neural inactivation in macaque cortex by optogenetic stimulation of GABAergic neurons. eLife. 2020;9:1–21. PMID: 32452766
54. Galvan A, Hu X, Smith Y, Wichmann T. Effects of optogenetic activation of corticothalamic terminals in the motor thalamus of awake monkeys. Journal of Neuroscience. 2016;36(12):3519–3530. PMID: 27013680
55. El-Shamayleh Y, Kojima Y, Soetedjo R, Horwitz GD. Selective Optogenetic Control of Purkinje Cells in Monkey Cerebellum. Neuron. 2017;95(1):51-62.e4. PMID: 28648497
56. Watanabe H, Sano H, Chiken S, Kobayashi K, Fukata Y, Fukata M, Mushiake H, Nambu A. Forelimb movements evoked by optogenetic stimulation of the macaque motor cortex. Nature Communications. 2020;11(1):1–9. PMID: 32591505
57. Oguchi M, Jiasen J, Yoshioka TW, Tanaka YR, Inoue K, Takada M, Kikusui T, Nomoto K, Sakagami M. Microendoscopic calcium imaging of the primary visual cortex of behaving macaques. Scientific Reports. 2021;11(1):1–15. PMID: 34426639

58. Bollimunta A, Santacruz SR, Eaton RW, Xu PS, Morrison JH, Moxon KA, Carmena JM, Nassi JJ. Head-mounted microendoscopic calcium imaging in dorsal premotor cortex of behaving rhesus macaque. Cell Reports. 2021;35(11):109239. PMID: 34133921
59. Weiss AR, Liguore WA, Domire JS, Button D, McBride JL. Intra-striatal AAV2.retro administration leads to extensive retrograde transport in the rhesus macaque brain: implications for disease modeling and therapeutic development. Scientific Reports. 2020;10(1):1–14. PMID: 32332773
60. Yazdan-Shahmorad A, Diaz-Botia C, Hanson TL, Kharazia V, Ledochowitsch P, Maharbiz MM, Sabes PN. A large-scale interface for optogenetic stimulation and recording in nonhuman primates. Neuron. 2016;89(5):927–939. PMID: 26875625
61. Bankiewicz KS, Eberling JL, Kohutnicka M, Jagust W, Pivirotto P, Bringas J, Cunningham J, Budinger TF, Harvey-White J. Convection-enhanced delivery of AAV vector in Parkinsonian monkeys; in vivo detection of gene expression and restoration of dopaminergic function using pro-drug approach. Experimental Neurology. 2000;164(1):2–14. PMID: 10877910
62. Kells AP, Hadaczek P, Yin D, Bringas J, Varenika V, Forsayeth J, Bankiewicz KS. Efficient gene therapy-based method for the delivery of therapeutics to primate cortex. Proceedings of the National Academy of Sciences. 2009;106(7):2407–2411. PMID: 19193857
63. Yazdan-Shahmorad A, Tian N, Kharazia V, Samaranch L, Kells A, Bringas J, He J, Bankiewicz K, Sabes PN. Widespread optogenetic expression in macaque cortex obtained with MR-guided, convection enhanced delivery (CED) of AAV vector to the thalamus. Journal of Neuroscience Methods. 2018;293:347–358. PMID: 29042259
64. Salegio EA, Samaranch L, Kells AP, Forsayeth J, Bankiewicz K. Guided delivery of adeno-associated viral vectors into the primate brain. Advanced Drug Delivery Reviews. 2012 May;64(7):598–604. PMID: 1000000221
65. Fetsch CR, Odean NN, Jeurissen D, El-Shamayleh Y, Horwitz GD, Shadlen MN. Focal optogenetic suppression in macaque area MT biases direction discrimination and decision confidence, but only transiently. eLife. 2018;7:1–23. PMID: 30051817
66. Stauffer WR, Lak A, Yang A, Borel M, Paulsen O, Boyden ES, Schultz W. Dopamine neuron-specific optogenetic stimulation in rhesus macaques. Cell. 2016;166(6):1564-1571.e6. PMID: 27610576
67. Gray SJ, Nagabhushan Kalburgi S, McCown TJ, Jude Samulski R. Global CNS gene delivery and evasion of anti-AAV-neutralizing antibodies by intrathecal AAV administration in non-human primates. Gene Therapy. 2013;20(4):450–459. PMID: 23303281

68. Samaranch L, Salegio EA, San Sebastian W, Kells AP, Foust KD, Bringas JR, Lamarre C, Forsayeth J, Kaspar BK, Bankiewicz KS. Adeno-associated virus serotype 9 transduction in the central nervous system of nonhuman primates. Human Gene Therapy. 2011;23(4):382–389. PMID: 22201473
69. Arotcarena ML, Dovero S, Biendon N, Dutheil N, Planche V, Bezard E, Dehay B. Pilot study assessing the impact of intrathecal administration of variants AAV-PHP.B and AAV-PHP.eB on brain transduction in adult rhesus macaques. Frontiers in Bioengineering and Biotechnology. 2021;9:1–10. PMID: 34869273
70. Hinderer C, Bell P, Vite CH, Louboutin JP, Grant R, Bote E, Yu H, Pukenas B, Hurst R, Wilson JM. Widespread gene transfer in the central nervous system of cynomolgus macaques following delivery of AAV9 into the cisterna magna. Molecular Therapy - Methods & Clinical Development. 2014;1(September):14051. PMID: 26052519
71. Bey K, Deniaud J, Dubreil L, Joussemet B, Cristini J, Ciron C, Hordeaux J, Le Boulc'h M, Marche K, Maquigneau M, Guilbaud M, Moreau R, Larcher T, Deschamps JY, Fusellier M, Blouin V, Sevin C, Cartier N, Adjali O, Aubourg P, Moullier P, Colle MA. Intra-CSF AAV9 and AAVrh10 administration in nonhuman primates: Promising routes and vectors for which neurological diseases? Molecular Therapy - Methods & Clinical Development. 2020;17(June):771–784. PMID: 32355866
72. Meseck EK, Guibinga G, Wang S, McElroy C, Hudry E, Mansfield K. Intrathecal sc-AAV9-CB-GFP: Systemic distribution predominates following single-dose administration in cynomolgus macaques. Toxicologic Pathology. 2022 Jun;50(4):415–431. PMID: 35658751
73. Hordeaux J, Hinderer C, Goode T, Katz N, Buza EL, Bell P, Calcedo R, Richman LK, Wilson JM. Toxicology study of intra-cisterna magna adeno-associated virus 9 expressing human alpha-L-iduronidase in rhesus macaques. Molecular Therapy - Methods & Clinical Development. 2018;10(September):79–88. PMID: 30073179
74. Hordeaux J, Hinderer C, Goode T, Buza EL, Bell P, Calcedo R, Richman LK, Wilson JM. Toxicology study of intra-cisterna magna adeno-associated virus 9 expressing iduronate-2-sulfatase in rhesus macaques. Molecular Therapy - Methods & Clinical Development. 2018;10(September):68–78. PMID: 30073178
75. Hinderer C, Katz N, Buza EL, Dyer C, Goode T, Bell P, Richman LK, Wilson JM. Severe toxicity in nonhuman primates and piglets following high-dose intravenous administration of an adeno-associated virus vector expressing human SMN. Human Gene Therapy. 2018;29(3):285–298. PMID: 29378426

76. Choudhury SR, Harris AF, Cabral DJ, Keeler AM, Sapp E, Ferreira JS, Gray-Edwards HL, Johnson JA, Johnson AK, Su Q, Stoica L, DiFiglia M, Aronin N, Martin DR, Gao G, Sena-Esteves M. Widespread central nervous system gene transfer and silencing after systemic delivery of novel AAV-AS vector. Molecular Therapy. 2016;24(4):726–735. PMID: 26708003
77. Nonnenmacher M, Wang W, Child MA, Ren XQ, Huang C, Ren AZ, Tocci J, Chen Q, Bittner K, Tyson K, Pande N, Chung CHY, Paul SM, Hou J. Rapid evolution of blood-brain-barrier-penetrating AAV capsids by RNA-driven biopanning. Molecular Therapy - Methods & Clinical Development. 2021;20(March):366–378. PMID: 33553485
78. Hanlon KS, Meltzer JC, Buzhdygan T, Cheng MJ, Sena-Esteves M, Bennett RE, Sullivan TP, Razmpour R, Gong Y, Ng C, Nammour J, Maiz D, Dujardin S, Ramirez SH, Hudry E, Maguire CA. Selection of an Efficient AAV Vector for Robust CNS Transgene Expression. Molecular Therapy - Methods & Clinical Development. 2019 Dec;15(December):320–332. PMID: 31788496
79. Basso MA. Monkey neurophysiology to clinical neuroscience and back again. Proceedings of the National Academy of Sciences. 2016;113(24):6591–3. PMID: 27226305
80. Gray DT, Barnes CA. Experiments in macaque monkeys provide critical insights into age-associated changes in cognitive and sensory function. Proceedings of the National Academy of Sciences. 2019;116(52):26247–26254. PMID: 31871147
81. Goertsen D, Goeden N, Flytzanis NC, Gradinaru V. Targeting the lung epithelium after intravenous delivery by directed evolution of underexplored sites on the AAV capsid. Molecular Therapy - Methods & Clinical Development. 2022;26(September):331–342. PMID: 35990749
82. Sasaki E, Suemizu H, Shimada A, Hanazawa K, Oiwa R, Kamioka M, Tomioka I, Sotomaru Y, Hirakawa R, Eto T, Shiozawa S, Maeda T, Ito M, Ito R, Kito C, Yagihashi C, Kawai K, Miyoshi H, Tanioka Y, Tamaoki N, Habu S, Okano H, Nomura T. Generation of transgenic non-human primates with germline transmission. Nature. 2009;459(7246):523–527. PMID: 19478777
83. Park JE, Zhang XF, Choi SH, Okahara J, Sasaki E, Silva AC. Generation of transgenic marmosets expressing genetically encoded calcium indicators. Scientific Reports. 2016;6(October):1–12. PMID: 27725685
84. Okano H, Sasaki E, Yamamori T, Iriki A, Shimogori T, Yamaguchi Y, Kasai K, Miyawaki A. Brain/MINDS: A Japanese national brain project for marmoset neuroscience. Neuron. 2016;92(3):582–590. PMID: 27809998
85. Challis RC, Ravindra Kumar S, Chan KY, Challis C, Beadle K, Jang MJ, Kim HM, Rajendran PS, Tompkins JD, Shivkumar K, Deverman BE, Gradinaru V. Systemic AAV vectors for widespread and targeted gene delivery in rodents. Nature Protocols. 2019;14(2):379–414. PMID: 30626963

86. Bargmann C, Newsome W, Anderson D, Brown E, Deisseroth K, Donoghue J, MacLeish P, Marder E, Normann R, Sanes J, Schnitzer M, Sejnowski T, Tank D, Tsien R, Ugurbil K. Brain 2025: A Scientific Vision. National Institutes of Health; 2014.
87. Hordeaux J, Yuan Y, Clark PM, Wang Q, Martino RA, Sims JJ, Bell P, Raymond A, Stanford WL, Wilson JM. The GPI-linked protein LY6a drives AAV-PHP.B transport across the blood-brain barrier. Molecular Therapy. 2019;27(5):912–921. PMID: 30819613
88. Huang Q, Chan KY, Tobey IG, Chan YA, Poterba T, Boutros CL, Balazs AB, Daneman R, Bloom JM, Seed C, Deverman BE. Delivering genes across the blood-brain barrier: LY6a, a novel cellular receptor for AAV-PHP.B capsids. PLoS ONE. 2019;14(11):1–17. PMID: 31725765
89. Batista AR, King OD, Reardon CP, Davis C, Shankaracharya, Philip V, Gray-Edwards H, Aronin N, Lutz C, Landers J, Sena-Esteves M. Ly6a differential expression in blood-brain barrier is responsible for strain specific central nervous system transduction profile of AAV-PHP.B. Human gene therapy. 2020;31(1–2):90–102. PMID: 31696742
90. Bevan AK, Duque S, Foust KD, Morales PR, Braun L, Schmelzer L, Chan CM, McCrate M, Chicoine LG, Coley BD, Porensky PN, Kolb SJ, Mendell JR, Burghes AHM, Kaspar BK. Systemic gene delivery in large species for targeting spinal cord, brain, and peripheral tissues for pediatric disorders. Molecular Therapy. 2011;19(11):1971–1980. PMID: 21811247
91. Gray SJ, Matagne V, Bachaboina L, Yadav S, Ojeda SR, Samulski RJ. Preclinical differences of intravascular AAV9 delivery to neurons and glia: a comparative study of adult mice and nonhuman primates. Molecular Therapy. 2011 Jun;19(6):1058–69. PMID: 21487395
92. Herculano-Houzel S, Ribeiro P, Campos L, Valotta da Silva A, Torres LB, Catania KC, Kaas JH. Updated neuronal scaling rules for the brains of Glires (rodents/lagomorphs). Brain, Behavior and Evolution. 2011;78(4):302–14. PMID: 21985803
93. Keller D, Erö C, Markram H. Cell densities in the mouse brain: A systematic review. Frontiers in Neuroanatomy. 2018;12(October). PMID: 30405363
94. Brandt L, Cristinelli S, Ciuffi A. Single-cell analysis reveals heterogeneity of virus infection, pathogenicity, and host responses: HIV as a pioneering example. Annual Review of Virology. 2020;7:333–350. PMID: 32991268
95. Suomalainen M, Greber UF. Virus infection variability by single-cell profiling. Viruses. 2021;13(8). PMID: 34452433

96. Brown D, Altermatt M, Dobreva T, Chen S, Wang A, Thomson M, Gradinaru V. Deep parallel characterization of AAV tropism and AAV-mediated transcriptional changes via single-cell RNA sequencing. Frontiers in Immunology. 2021;12(October):1–24. PMID: 34759919
97. Ngai J. BRAIN 2.0: Transforming neuroscience. Cell. 2022;185(1):4–8. PMID: 34995517
98. Cai D, Cohen KB, Luo T, Lichtman JW, Sanes JR. Improved tools for the Brainbow toolbox. Nature Methods. 2013;10(6):540–547. PMID: 23866336
99. Livet J, Weissman TA, Kang H, Draft RW, Lu J, Bennis RA, Sanes JR, Lichtman JW. Transgenic strategies for combinatorial expression of fluorescent proteins in the nervous system. Nature. 2007;450(7166):56–62. PMID: 17972876
100. Ramsingh AI, Gray SJ, Reilly A, Koday M, Bratt D, Koday MT, Munson P, Murnane R, Smedley J, Hu Y, Messer A, Fuller DH. Correction: Sustained AAV9-mediated expression of a non-self protein in the CNS of non-human primates after immunomodulation. PloS one. 2018;13(11):e0207077. PMID: 30383837
101. Hadaczek P, Forsayeth J, Mirek H, Munson K, Bringas J, Pivirotto P, McBride JL, Davidson BL, Bankiewicz KS. Transduction of nonhuman primate brain with adeno-associated virus serotype 1: vector trafficking and immune response. Human gene therapy. 2009 Mar;20(3):225–37. PMID: 19292604
102. Samaranch L, Sebastian WS, Kells AP, Salegio EA, Heller G, Bringas JR, Pivirotto P, DeArmond S, Forsayeth J, Bankiewicz KS. AAV9-mediated expression of a non-self protein in nonhuman primate central nervous system triggers widespread neuroinflammation driven by antigen-presenting cell transduction. Molecular Therapy. 2014 Feb;22(2):329–337. PMID: 24419081
103. Golebiowski D, van der Bom IMJ, Kwon CS, Miller AD, Petrosky K, Bradbury AM, Maitland S, Kühn AL, Bishop N, Curran E, Silva N, GuhaSarkar D, Westmoreland S V., Martin DR, Gounis MJ, Asaad WF, Sena-Esteves M. Direct intracranial injection of AAVrh8 encoding monkey β-N-acetylhexosaminidase causes neurotoxicity in the primate brain. Human Gene Therapy. 2017 Jun;28(6):510–522. PMID: 28132521
104. Klink PC, Aubry JF, Ferrera VP, Fox AS, Froudist-Walsh S, Jarraya B, Konofagou EE, Krauzlis RJ, Messinger A, Mitchell AS, Ortiz-Rios M, Oya H, Roberts AC, Roe AW, Rushworth MFS, Sallet J, Schmid MC, Schroeder CE, Tasserie J, Tsao DY, Uhrig L, Vanduffel W, Wilke M, Kagan I, Petkov CI. Combining brain perturbation and neuroimaging in non-human primates. NeuroImage. 2021 Jul 23;235(6):118017. PMID: 33080229

105. Tremblay S, Acker L, Afraz A, Albaugh DL, Amita H, Andrei AR, Angelucci A, Aschner A, Balan PF, Basso MA, Benvenuti G, Bohlen MO, Caiola MJ, Calcedo R, Cavanaugh J, Chen Y, Chen S, Chernov MM, Clark AM, Dai J, Debes SR, Deisseroth K, Desimone R, Dragoi V, Egger SW, Eldridge MAG, El-Nahal HG, Fabbrini F, Federer F, Fetsch CR, Fortuna MG, Friedman RM, Fujii N, Gail A, Galvan A, Ghosh S, Gieselmann MA, Gulli RA, Hikosaka O, Hosseini EA, Hu X, Hüer J, Inoue K ichi, Janz R, Jazayeri M, Jiang R, Ju N, Kar K, Klein C, Kohn A, Komatsu M, Maeda K, Martinez-Trujillo JC, Matsumoto M, Maunsell JHR, Mendoza-Halliday D, Monosov IE, Muers RS, Nurminen L, Ortiz-Rios M, O'Shea DJ, Palfi S, Petkov CI, Pojoga S, Rajalingham R, Ramakrishnan C, Remington ED, Revsine C, Roe AW, Sabes PN, Saunders RC, Scherberger H, Schmid MC, Schultz W, Seidemann E, Senova YS, Shadlen MN, Sheinberg DL, Siu C, Smith Y, Solomon SS, Sommer MA, Spudich JL, Stauffer WR, Takada M, Tang S, Thiele A, Treue S, Vanduffel W, Vogels R, Whitmire MP, Wichmann T, Wurtz RH, Xu H, Yazdan-Shahmorad A, Shenoy K V., DiCarlo JJ, Platt ML. An open resource for non-human primate optogenetics. Neuron. 2020;108(6):1075-1090.e6. PMID: 33080229
106. Yardeni T, Eckhaus M, Morris HD, Huizing M, Hoogstraten-Miller S. Retro-orbital injections in mice. Lab Animal. 2011;40(5):155–160. PMID: 21508954
107. Treweek JB, Chan KY, Flytzanis NC, Yang B, Deverman BE, Greenbaum A, Lignell A, Xiao C, Cai L, Ladinsky MS, Bjorkman PJ, Fowlkes CC, Gradinaru V. Whole-body tissue stabilization and selective extractions via tissue-hydrogel hybrids for high-resolution intact circuit mapping and phenotyping. Nature Protocols. 2015;10(11):1860–1896. PMID: 26492141
108. Stringer C, Wang T, Michaelos M, Pachitariu M. Cellpose: A generalist algorithm for cellular segmentation. Nature Methods. 2021;18(1):100–106. PMID: 33318659
109. Ting JT, Kalmbach B, Chong P, De Frates R, Keene CDi, Gwinn RP, Cobbs C, Ko AL, Ojemann JG, Ellenbogen RG, Koch C, Lein E. A robust ex vivo experimental platform for molecular-genetic dissection of adult human neocortical cell types and circuits. Scientific Reports. 2018;8(1):1–13. PMID: 29849137
110. Ting JT, Lee BR, Chong P, Soler-Llavina G, Cobbs C, Koch C, Zeng H, Lein E. Preparation of acute brain slices using an optimized N-methyl-D-glucamine protective recovery method. Journal of visualized experiments : JoVE. 2018;(132):1–13. PMID: 29553547
111. Ek CJ, Dziegielewska KM, Stolp H, Saunders NR. Functional effectiveness of the blood-brain barrier to small water-soluble molecules in developing and adult opossum (Monodelphis domestica). The Journal of Comparative Neurology. 2006 May 1;496(1):13–26. PMID: 16528724

112. Daneman R, Zhou L, Agalliu D, Cahoy JD, Kaushal A, Barres BA. The mouse blood-brain barrier transcriptome: A new resource for understanding the development and function of brain endothelial cells. Ikezu T, editor. PLoS ONE. 2010 Oct 29;5(10):e13741. PMID: 21060791
113. Daneman R, Zhou L, Kebede AA, Barres BA. Pericytes are required for blood–brain barrier integrity during embryogenesis. Nature. 2010 Nov 13;468(7323):562–566. PMID: 20944625
114. Saunders NR, Liddelow SA, Dziegielewska KM. Barrier mechanisms in the developing brain. Frontiers in Pharmacology. 2012;3(March):1–18. PMID: 22479246
115. Giger T, Khaitovich P, Somel M, Lorenc A, Lizano E, Harris LW, Ryan MM, Lan M, Wayland MT, Bahn S, Pääbo S. Evolution of neuronal and endothelial transcriptomes in primates. Genome Biology and Evolution. 2010;2(1):284–292. PMID: 20624733
116. Song HW, Foreman KL, Gastfriend BD, Kuo JS, Palecek SP, Shusta E V. Transcriptomic comparison of human and mouse brain microvessels. Scientific Reports. 2020;10(1):1–14. PMID: 32704093
117. Schaffenrath J, Huang SF, Wyss T, Delorenzi M, Keller A. Characterization of the blood–brain barrier in genetically diverse laboratory mouse strains. Fluids and Barriers of the CNS. 2021;18(1):1–15. PMID: 34321020
118. Chen X, Ravindra Kumar S, Adams CD, Yang D, Wang T, Wolfe DA, Arokiaraj CM, Ngo V, Campos LJ, Griffiths JA, Ichiki T, Mazmanian SK, Osborne PB, Keast JR, Miller CT, Fox AS, Chiu IM, Gradinaru V. Engineered AAVs for non-invasive gene delivery to rodent and non-human primate nervous systems. Neuron. 2022 Jul 20;110(14):2242-2257.e6. PMID: 35643078
119. Stanton AC, Lagerborg KA, Tellez L, Krunnfusz A, King EM, Ye S, Solomon IH, Tabebordbar M, Sabeti PC. Systemic administration of novel engineered AAV capsids facilitates enhanced transgene expression in the macaque CNS. Med. 2022 Nov;1–20. PMID: 36417917
120. Zinn E, Unzu C, Schmit PF, Turunen HT, Zabaleta N, Sanmiguel J, Fieldsend A, Bhatt U, Diop C, Merkel E, Gurrala R, Peacker B, Rios C, Messemer K, Santos J, Estelien R, Andres-Mateos E, Wagers AJ, Tipper C, Vandenberghe LH. Ancestral library identifies conserved reprogrammable liver motif on AAV capsid. Cell Reports Medicine. 2022;3(11):100803. PMID: 36327973
121. McBride JL, Neuringer M, Ferguson B, Kohama SG, Tagge IJ, Zweig RC, Renner LM, McGill TJ, Stoddard J, Peterson S, Su W, Sherman LS, Domire JS, Ducore RM, Colgin LM, Lewis AD. Discovery of a CLN7 model of Batten disease in non-human primates. Neurobiology of Disease. 2018;119(July):65–78. PMID: 30048804

122. Lallani SB, Villalba RM, Chen Y, Smith Y, Chan AWS. Striatal interneurons in transgenic nonhuman primate model of Huntington's disease. Scientific Reports. 2019;9(1):1–9. PMID: 30837611
123. Chand D, Mohr F, McMillan H, Tukov FF, Montgomery K, Kleyn A, Sun R, Tauscher-Wisniewski S, Kaufmann P, Kullak-Ublick G. Hepatotoxicity following administration of onasemnogene abeparvovec (AVXS-101) for the treatment of spinal muscular atrophy. Journal of Hepatology. 2021 Mar;74(3):560–566. PMID: 33186633
124. Harrison C. High-dose AAV gene therapy deaths. Nature Biotechnology. 2020 Aug 5;38(8):910–910. PMID: 32760027
125. Hordeaux J, Buza EL, Dyer C, Goode T, Mitchell TW, Richman L, Denton N, Hinderer C, Katz N, Schmid R, Miller R, Choudhury GR, Horiuchi M, Nambiar K, Yan H, Li M, Wilson JM. Adeno-associated virus-induced dorsal root ganglion pathology. Human Gene Therapy. 2020;31(15–16):808–818. PMID: 32845779
126. Madisen L, Zwingman TA, Sunkin SM, Oh SW, Zariwala HA, Gu H, Ng LL, Palmiter RD, Hawrylycz MJ, Jones AR, Lein ES, Zeng H. A robust and high-throughput Cre reporting and characterization system for the whole mouse brain. Nature Neuroscience. 2010 Jan;13(1):133–40. PMID: 20023653
127. Kauffman KJ, Oberli MA, Dorkin JR, Hurtado JE, Kaczmarek JC, Bhadani S, Wyckoff J, Langer R, Jaklenec A, Anderson DG. Rapid, single-cell analysis and discovery of vectored mRNA transfection in vivo with a loxP-flanked tdTomato reporter mouse. Molecular Therapy - Nucleic Acids. 2018 Mar 2;10:55–63. PMID: 29499956
128. Mich JK, Graybuck LT, Hess EE, Mahoney JT, Kojima Y, Ding Y, Somasundaram S, Miller JA, Kalmbach BE, Radaelli C, Gore BB, Weed N, Omstead V, Bishaw Y, Shapovalova N V., Martinez RA, Fong O, Yao S, Mortrud M, Chong P, Loftus L, Bertagnolli D, Goldy J, Casper T, Dee N, Opitz-Araya X, Cetin A, Smith KA, Gwinn RP, Cobbs C, Ko AL, Ojemann JG, Keene CD, Silbergeld DL, Sunkin SM, Gradinaru V, Horwitz GD, Zeng H, Tasic B, Lein ES, Ting JT, Levi BP. Functional enhancer elements drive subclass-selective expression from mouse to primate neocortex. Cell Reports. 2021;34(13):108754. PMID: 33789096
129. Sato K, Sasaki E. Genetic engineering in nonhuman primates for human disease modeling. Journal of Human Genetics. 2018 Feb;63(2):125–131. PMID: 29203824
130. Park JE, Silva AC. Generation of genetically engineered non-human primate models of brain function and neurological disorders. American Journal of Primatology. 2019 Feb;81(2):e22931. PMID: 30585654
131. Halpern J, O'Hara SE, Doxzen KW, Witkowsky LB, Owen AL. Societal and ethical impacts of germline genome editing: how can we secure human rights? The CRISPR Journal. 2019 Oct;2(5):293–298. PMID: 31599687

132. Gyngell C, Douglas T, Savulescu J. The ethics of germline gene editing. Journal of Applied Philosophy. 2017 Aug;34(4):498–513. PMID: 28919655
133. Reynolds RH, Botía J, Nalls MA, Noyce AJ, Nicolas A, Cookson MR, Bandres-Ciga S, Gibbs JR, Hernandez DG, Singleton AB, Reed X, Leonard H, Blauwendraat C, Faghri F, Bras J, Guerreiro R, Tucci A, Kia DA, Houlden H, Plun-Favreau H, Mok KY, Wood NW, Lovering R, R'Bibo L, Rizig M, Chelban V, Trabzuni D, Tan M, Morris HR, Middlehurst B, Quinn J, Billingsley K, Holmans P, Kinghorn KJ, Lewis P, Escott-Price V, Williams N, Foltynie T, Brice A, Danjou F, Lesage S, Corvol JC, Martinez M, Giri A, Schulte C, Brockmann K, Simón-Sánchez J, Heutink P, Gasser T, Rizzu P, Sharma M, Shulman JM, Robak L, Lubbe S, Mencacci NE, Finkbeiner S, Lungu C, Scholz SW, Gan-Or Z, Rouleau GA, Krohan L, van Hilten JJ, Marinus J, Adarmes-Gómez AD, Bernal-Bernal I, Bonilla-Toribio M, Buiza-Rueda D, Carrillo F, Carrión-Claro M, Mir P, Gómez-Garre P, Jesús S, Labrador-Espinosa MA, Macias D, Vargas-González L, Méndez-del-Barrio C, Periñán-Tocino T, Tejera-Parrado C, Diez-Fairen M, Aguilar M, Alvarez I, Boungiorno MT, Carcel M, Pastor P, Tartari JP, Alvarez V, González MM, Blazquez M, Garcia C, Suarez-Sanmartin E, Barrero FJ, Rezola EM, Yarza JAB, Pagola AG, de Munain Arregui AL, Ruiz-Martínez J, Cerdan D, Duarte J, Clarimón J, Dols-Icardo O, Infante J, Marín J, Kulisevsky J, Pagonabarraga J, Gonzalez-Aramburu I, Rodriguez AS, Sierra M, Duran R, Ruz C, Vives F, Escamilla-Sevilla F, Mínguez A, Cámara A, Compta Y, Ezquerra M, Marti MJ, Fernández M, Muñoz E, Fernández-Santiago R, Tolosa E, Valldeoriola F, García-Ruiz P, Heredia MJG, Errazquin FP, Hoenicka J, Jimenez-Escrig A, Martínez-Castrillo JC, Lopez-Sendon JL, Torres IM, Tabernero C, Vela L, Zimprich A, Pihlstrom L, Koks S, Taba P, Majamaa K, Siitonen A, Okubadejo NU, Ojo OO, Pitcher T, Anderson T, Bentley S, Fowdar J, Mellick G, Dalrymple-Alford J, Henders AK, Kassam I, Montgomery G, Sidorenko J, Zhang F, Xue A, Vallerga CL, Wallace L, Wray NR, Yang J, Visscher PM, Gratten J, Silburn PA, Halliday G, Hickie I, Kwok J, Lewis S, Kennedy M, Pearson J, Hardy J, Gagliano Taliun SA, Ryten M. Moving beyond neurons: the role of cell type-specific gene regulation in Parkinson's disease heritability. npj Parkinson's Disease. 2019 Apr 17;5(1):6. PMID: 31016231
134. Tabebordbar M, Lagerborg KA, Stanton A, King EM, Ye S, Tellez L, Krunnfusz A, Tavakoli S, Widrick JJ, Messemer KA, Troiano EC, Moghadaszadeh B, Peacker BL, Leacock KA, Horwitz N, Beggs AH, Wagers AJ, Sabeti PC. Directed evolution of a family of AAV capsid variants enabling potent muscle-directed gene delivery across species. Cell. 2021 Sep;184(19):4919-4938.e22. PMID: 34506722

135. Shay TF, Sullivan EE, Ding X, Chen X, Ravindra Kumar S, Goertsen D, Brown D, Crosby A, Vielmetter J, Borsos M, Wolfe DA, Lam AW, Gradinaru V. Primate-conserved carbonic anhydrase IV and murine-restricted LY6C1 enable blood-brain barrier crossing by engineered viral vectors. Science Advances. 2023 Apr 21;9(16). PMID: 37075114
136. Ogden PJ, Kelsic ED, Sinai S, Church GM. Comprehensive AAV capsid fitness landscape reveals a viral gene and enables machine-guided design. Science. 2019 Nov 29;366(6469):1139–1143. PMID: 31780559
137. Bryant DH, Bashir A, Sinai S, Jain NK, Ogden PJ, Riley PF, Church GM, Colwell LJ, Kelsic ED. Deep diversification of an AAV capsid protein by machine learning. Nature Biotechnology. 2021 Jun 11;39(6):691–696. PMID: 33574611
138. Gainza P, Wehrle S, Van Hall-Beauvais A, Marchand A, Scheck A, Harteveld Z, Buckley S, Ni D, Tan S, Sverrisson F, Goverde C, Turelli P, Raclot C, Teslenko A, Pacesa M, Rosset S, Georgeon S, Marsden J, Petruzzella A, Liu K, Xu Z, Chai Y, Han P, Gao GF, Oricchio E, Fierz B, Trono D, Stahlberg H, Bronstein M, Correia BE. De novo design of protein interactions with learned surface fingerprints. Nature. 2023 May 4;617(7959):176–184. PMID: 37100904